

Multiuser MIMO Downlink Made Practical: Achievable Rates with Simple Channel State Estimation and Feedback Schemes

Giuseppe Caire, University of Southern California

Los Angeles CA, 90089 USA

Nihar Jindal, University of Minnesota

Minneapolis MN, 55455 USA

Mari Kobayashi, SUPELEC

Gif-sur-Yvette, France

Niranjay Ravindran, University of Minnesota

Minneapolis MN, 55455 USA

Abstract

We consider a MIMO fading broadcast channel and compute achievable ergodic rates when channel state information is acquired at the receivers via downlink training and explicit channel feedback is performed to provide transmitter channel state information (CSIT). Both “analog” and quantized (digital) channel feedback are analyzed, and digital feedback is shown to be potentially superior when the feedback *channel uses* per channel coefficient is larger than 1. Also, we show that by proper design of the digital feedback link, errors in the feedback have a relatively minor effect even if simple uncoded modulation is used on the feedback channel. We extend our analysis to the case of fading MIMO Multiaccess Channel (MIMO-MAC) in the feedback link, as well as to the case of a time-varying channel and feedback delay. We show that by exploiting the MIMO-MAC nature of the uplink channel, a fully scalable system with both downlink multiplexing gain and feedback redundancy proportional to the number of base station antennas can be achieved. Furthermore, the feedback strategy is optimized by a non-trivial combination of time-division and space-division multiple-access. For the case of delayed feedback, we show that in the realistic case where the fading process has (normalized) maximum Doppler frequency shift $0 \leq F < 1/2$, a fraction $1 - 2F$ of the optimal multiplexing gain is achievable. The general conclusion of this work is that *very significant* downlink throughput is achievable with *simple and efficient* channel state feedback, provided that the feedback link is properly designed.

I. INTRODUCTION

Multiple antenna downlink channels have been the subject of a great deal of research for a number of years now, primarily motivated by the very significant capacity increase associated with multi-user MIMO techniques. In the downlink of a cellular-like system, a base station equipped with multiple antennas wishes to communicate with a number of terminals, each possibly equipped with multiple receive antennas. If a traditional orthogonalization technique such as TDMA is used, the base station transmits to a single receiver on each time-frequency resource and thus is limited to point-to-point MIMO techniques [1], [2]. Alternatively, the base station can use multi-user MIMO (also commonly referred to as SDMA, or space-division multiple access) to *simultaneously* transmit to multiple receivers on the same time-frequency resource by appropriate utilization of spatial dimensions.

Under the assumption of perfect channel state information (CSI) at the transmitter and receivers, multi-user MIMO in the form of linear beamforming plus interference pre-cancellation (based on dirty-paper coding) is now known to achieve the capacity of the MIMO downlink channel [3], [4], [5], [6], [7]. Furthermore, the capacity of the MIMO downlink channel is significantly larger than the rates achievable with point-to-point MIMO techniques [3], [8], [9]. Intuitively, the multi-user MIMO benefit comes from being able to use the transmit antenna array and knowledge of the instantaneous channel to efficiently direct signals/energy towards different receivers. To emphasize the importance of CSI, note that in the extreme case of no CSI at the base station and identical fading statistics at all receivers, the multi-user MIMO benefit is completely lost and point-to-point MIMO is optimal [3].

Given the widespread applicability of the MIMO downlink channel model to wireless systems (e.g., cellular, WiFi) as well as to some wireline systems (e.g., DSL), there has been a remarkable flurry of research activity, both in academia and industry, with the goal of designing practical systems that can operate near the capacity limits of

the MIMO downlink channel. In the process, two fundamental challenges to making multi-user MIMO "practical" have emerged: (a) design practical transceiver structures, including coding and decoding schemes, that approach the capacity limit, and (b) devise mechanisms that allow for accurate CSI to be obtained at the transmitter and receivers in a resource-efficient manner.

The optimal coding strategy in the case of perfect CSI has been shown to be a combination of linear beamforming and dirty paper pre-coding (DPC), but developing reasonable complexity implementations of DPC that approach capacity still remains a formidable challenge (see for example [10], [11], [12]). However, simpler schemes such as linear beamforming, Tomlinson-Harashima precoding [13], [14] or vector precoding [15], [16], combined with single user coding and decoding, have emerged as a low-complexity, near-capacity transceiver design options. In this work we focus on linear beamforming, because of its analytical tractability. With this strategy the transmitted vector is a linear combination of the data symbols intended for different receivers, where the combining weights (i.e., beamforming vectors) are chosen on the basis of the current channel conditions. Although not optimal, this technique performs quite close to capacity (assuming perfect CSI) when combined with user selection algorithms that determine which of the receivers are to be transmitted to in a particular frame. This is true for systems with a moderate number of receivers as well as for systems with a very large user population [17]. Although linear beamforming is certainly not the only low complexity architecture for the MIMO broadcast [13], [14], [15], [16], its low complexity and near-capacity performance make it a very strong candidate for future implementation.

A. Contribution of Work

The focus of this paper is the design and analysis of mechanisms that allow for CSI to be efficiently obtained at receivers and the transmitter, and the evaluation of such mechanisms in the context of the rates achievable with linear beamforming for a system with multiple transmit antennas and a single antenna per receiver. We study a frequency-division duplexed system where no channel reciprocity can be exploited and thus feedback is required in order to provide the transmitter with CSI; note, however, that our analysis applies straightforwardly to the case of time-division duplexing as a special case (Remark 4.2). We consider a very general channel estimation and feedback model that treats the realistic scenario where user terminals (UT) first estimate their own channel (to obtain imperfect CSIR), then feed this information back over a generalized feedback channel, based on which the base station (BS) performs zero-forcing beamforming.

Although there has been quite a bit of work on limited feedback systems, especially for point-to-point MIMO systems (see for example [18], [19], [20], [21], [22], [23], [24]) as well as more recent work on MIMO broadcast channels (see for example [25], [26], [27], [28], [29], [30], [31]), our work presents a number of novelties relative to prior work:

- Rather than assuming perfect CSIR at the UT's, we consider the realistic scenario where UT's have imperfect CSIR (obtained via downlink training); since the imperfect CSIR is the basis of the channel feedback from UT's, this further degrades the quality of the CSI provided to the BS and is shown to have a non-negligible effect.
- We explicitly consider transmission over the feedback channel from each UT to the BS, which allows us to meaningfully measure the system resources dedicated to channel feedback and also allows for a comparison between analog (unquantized) and digital (quantized) feedback techniques. We began by modeling the feedback channel as an AWGN channel (orthogonal across UTs), and later generalize to a multiple-antenna fading uplink channel that is possibly shared by the UTs.
- We consider delayed feedback and quantify the loss of degrees of freedom in terms of the fading channel Doppler bandwidth, which is ultimately related to the UTs speed.

Perhaps the most significant outcome of our analysis is that for sufficiently fast feedback (more specifically, when the feedback delay is considerably less than the channel coherence time), the full multiplexing gain promised by the ideal MIMO broadcast channel can be achieved with very simple pilot-based channel estimation and feedback schemes that consume a relatively small fraction of system resources. Indeed, a fundamental property of the MIMO broadcast channel is that the quality of the CSIT must increase with SNR (regardless of what coding strategy is used) in order for the full multiplexing gain to be achievable [32], [33]. Under the reasonable assumption that the uplink channel quality is in some sense proportional to the downlink channel, our work shows that this requirement can be met using a fixed number of downlink and uplink channel symbols (i.e., estimation and feedback resources

need not increase with SNR) if the capacity of the uplink feedback channel is used appropriately. In addition to achieving the full multiplexing gain, these strategies also guarantee a bounded and quite reasonable throughput degradation relative to a similar system with perfect CSI (at the BS and UT's) at all SNR's.

We consider analog and digital feedback. Analog refers to the case where the estimated channel coefficients at the UTs are sent unquantized onto the feedback link by using quadrature-amplitude modulation. Digital refers to the case where the UTs make use of a specific vector quantization scheme, and send back a suitably encoded and modulated quantization index. In both cases, the full multiplexing gain can be achieved by using a fixed number of feedback channel uses per downlink channel coefficient.

The simple analog feedback suffices when one feedback channel use per channel coefficient is used (this is essentially the minimum feedback resource necessary to achieve full multiplexing gain). However, digital is preferred when more channel uses are dedicated to feedback, even when errors on the feedback link are accounted for. We explain this fact in light of well-known results on sending a Gaussian source through a Gaussian channel with "bandwidth expansion" under a mean-square distortion criterion [34], [35].

With both analog and digital feedback, we show that the MIMO multiple-access nature of the feedback link can be exploited in order to greatly improve the efficiency of the feedback. In particular, by using a combination of time-division and space-division multiple access in the feedback link, we can achieve full multiplexing gain with a total number of feedback channel uses that scales linearly with the number of BS antennas. For example, if the BS uses the same array for transmitting and receiving and the uplink and downlink channels have the same fading statistics, a spectral efficiency reduction (relative to a perfect CSI system) of at most 1 bps/Hz per UT (i.e., a 3 dB power loss) is achieved by transmitting $3M$ downlink pilot symbols (shared) and using a total of $2M$ uplink channel symbols for analog channel feedback, where M is the number of BS antennas with $M \geq 4$.

When the feedback requires significant delay, the simple scheme analyzed in this paper does not attain full multiplexing gain. However, for fading processes with normalized Doppler bandwidth F strictly less than $1/2$, we can show the achievability of a multiplexing gain equal to $M(1 - 2F)$, where M is the number of base station antennas. This result relates directly the achievable multiplexing gain with the UTs speed (quantified by their Doppler bandwidth) and may be useful for some system level design that handle users in different ways depending on their mobility. We also discuss the performance in the case of fading processes with non-bandlimited Doppler spectrum (e.g., Gauss-Markov AR-1 processes). Although the physical justification of such processes is questionable, they have been widely used in the wireless communication literature for their analytical tractability. We show that very attractive spectral efficiencies can be achieved in this case too for practical SNRs and relatively slowly-varying channel statistics, although the rate gap from the ideal case becomes unbounded as SNR increases.

Before continuing, it is worth contrasting our system setup with a rather different approach to beamforming with non-perfect CSIT based on random beams and multiuser-diversity scheduling. In [36], [37], as well as in several other follow-up works, a scheme where the beamforming matrix is chosen randomly over the set of unitary matrices and users are scheduled opportunistically, according to their signal-to-interference plus noise ratio (SINR), was proposed and analyzed. In this scheme, each UT feeds back only one analog number (SINR) and $\log_2 M$ bits to indicate its preferred beam. Assuming no feedback errors and no delay, this scheme is shown to achieve an ergodic sum rate that scales like $M \log \log K$ for fixed SNR, fixed BS antennas M and number of users $K \rightarrow \infty$. On the contrary, for any fixed K and increasing SNR, the scheme achieves a bounded sum rate, unless a single user per frame is scheduled. We argue here that the regime of large number of users K over a fixed system bandwidth is actually the opposite of what next generation (so-called 4th generation) wireless systems aim at. In fact, the goal of these systems is to provide very high rates to individual users, while in the random beamforming setting the rate per user would vanish very rapidly, as $\frac{\log \log K}{K}$. Therefore, if a system designer has to allocate a given number of uplink channel uses to CSIT feedback, instead of serving a large number of users with very coarse CSIT it is preferable to serve a small number of users K with very accurate (channel vector directions) channel state information. A recent result has in fact shown precisely this: given a total feedback budget and a large user population, considerably higher throughput is achieved by obtaining very accurate channel feedback from a relatively small number of users (selected according to some criterion that is independent of instantaneous channel conditions or channel quantization) and performing user selection in conjunction with naive zero-forcing beamforming rather than obtaining coarse feedback from many users as done in random beamforming [38].

The paper is organized as follows. The remainder of this section introduces the system model and discusses the optimal scheme versus the linear beamforming scheme in the case of perfect CSI. Section II defines the baseline

channel estimation, channel state feedback and zero-forcing beamforming strategy based on training symbols analyzed in this paper. Section III develops bounds on the ergodic rates achievable by the baseline scheme. Sections IV and V particularize the bounds of Section III to the case of analog and digital channel state feedback, and Section VI provides a detailed comparison, under several operating conditions. In Section VII we consider the effect of decoding errors on the digital feedback performance, and show that, somehow surprisingly, the impact of errors can be made negligible with a careful design of the digital feedback system parameters. Section VIII considers explicitly the fact that the feedback link is a MIMO multiple-access channel with fading, and characterizes the performance of the baseline system with analog or digital feedback when the feedback link operates with a combination of space-division and time-division multiple access. Finally, in Section IX we introduce the time-correlation of the fading process and consider the effect of delay in the feedback link. We make the connection between the rate gap bounds developed in Section III and the noisy MMSE prediction error of the fading process, and compute the achievable multiplexing gain in terms of the normalized channel Doppler bandwidth. Some concluding remarks are outlined in Section X.

B. Model setup

We consider a multi-input multi-output (MIMO) Gaussian broadcast channel modeling the downlink of a system where a Base Station (BS) has M antennas and K User Terminals (UT) have one antenna each.¹

A channel use of such channel is described by

$$y_k = \mathbf{h}_k^H \mathbf{x} + z_k, \quad k = 1, \dots, K \quad (1)$$

where y_k is the channel output at UT k , $z_k \sim \mathcal{CN}(0, N_0)$ is the corresponding Additive White Gaussian Noise (AWGN), $\mathbf{h}_k \in \mathbb{C}^M$ is the vector of channel coefficients from the k -th UT antenna to the BS antenna array and \mathbf{x} is the vector of channel input symbols transmitted by the BS. The channel input is subject to the average power constraint $\mathbb{E}[|\mathbf{x}|^2] \leq P$.

We assume that the channel *state*, given by the collection of all channel vectors $\mathbf{H} = [\mathbf{h}_1, \dots, \mathbf{h}_K] \in \mathbb{C}^{M \times K}$, varies in time according to a block-fading model, where \mathbf{H} is constant over each *frame* of length T channel uses, and evolves from frame to frame according to an ergodic stationary spatially white jointly Gaussian process, where the entries of \mathbf{H} are Gaussian i.i.d. with elements $\sim \mathcal{CN}(0, 1)$.

A word of caution should be spent about the block-fading model. Despite the fact that we consider ergodic rates, we nevertheless assume the regime of very large fading blocks relative to the number of symbols used for channel estimation and feedback, namely, $T \gg M$. This assumption is reasonable, based on practical wireless communication channel parameters. For example, a channel with coherence bandwidth of 500 kHz and Doppler bandwidth of 6.66 Hz (corresponding to a walking speed of 1m/s at 2GHz carrier frequency) remains approximately constant for blocks of $\approx 500 \cdot 10^3 \times \frac{1}{4 \times 6.66} = 18770$ channel uses [39], [40]. Even assuming a BS with a large number of antennas (say, $M = 16$) the ratio T/M is still larger than three orders of magnitude. For this reason, we shall neglect in the degrees of freedom count (pre-log factor of sum rate) factors of the type $1 - M/T$.

An interesting extension of the results of this paper would consider T of the same order of M , and pursue the achievable pre-log factor by taking into account the dimensionality loss due to training, along the lines of what done in [41] for the point-to-point MIMO case. We do not treat this case here for simplicity of exposition, although our analysis can handle this case in a rather straightforward manner.

C. Optimal coding versus linear beamforming

As said before, if \mathbf{H} is perfectly and instantaneously known to all terminals (perfect CSIT and CSIR), the capacity region of the channel (1) is obtained by MMSE-DFE beamforming and Gaussian DPC (see [3], [4], [5], [6], [42]).

Because of simplicity and robustness to non-perfect CSIT, simple *linear precoding* schemes with standard Gaussian coding have been extensively considered: the transmit signal is formed as $\mathbf{x} = \mathbf{Vu}$, such that $\mathbf{V} \in \mathbb{C}^{M \times K}$ is a *linear beamforming* matrix and $\mathbf{u} \in \mathbb{C}^K$ contains the symbols from K independently generated Gaussian codewords. In particular, for $K \leq M$ the Zero-Forcing (ZF) beamforming chooses the k -th column \mathbf{v}_k of \mathbf{V} to be a unit vector orthogonal to the subspace $\mathcal{S}_k = \text{span}\{\mathbf{h}_j : j \neq k\}$.

¹Since this work consider explicit channel state feedback schemes where the role of the transmitter and of the receiver are reversed, we borrow some terminology from wireless local area networks and refer to the terminals in the system as BS and UTs.

In this paper we focus on the achievable *ergodic* rates under ZF beamforming and Gaussian coding. For what is said at the beginning of this section, this strategy under perfect CSIT and CSIR appears to provide a good tradeoff between performance and implementation simplicity. In this case, the achievable rate-sum is given by

$$R^{\text{ZF}} = \max_{\sum_k \mathbb{E}[\mathcal{P}_k(\mathbf{H})] \leq P} \sum_{k=1}^K \mathbb{E} \left[\log \left(1 + \frac{|\mathbf{h}_k^H \mathbf{v}_k|^2 \mathcal{P}_k(\mathbf{H})}{N_0} \right) \right]. \quad (2)$$

where the optimal power allocation is obtained by waterfilling over the set of channel gains $\{|\mathbf{h}_k^H \mathbf{v}_k|^2 : k = 1, \dots, K\}$. If $K > M$, a *user scheduling* algorithm should be used in order to select in each frame an *active* user subset not larger than M . Schemes for user scheduling have been extensively discussed, for example in [43], [31], [44], [45]. In this work we are mainly interested in the high-spectral efficiency regime, where the achievable sum rate behaves as $\kappa \log P/N_0 + O(1)$, and κ is the system *multiplexing gain* or “pre-log factor” of the ergodic sum rate. We shall exclusively focus on the case of $K = M$ users.² This restriction is dictated by two reasons: on one hand, the case $K = M$ and i.i.d. fading makes closed-form analysis possible; on the other hand, the maximum possible system multiplexing gain is $\kappa = M$ for all $K \geq M$. Hence, the case $K = M$ suffices to capture the fundamental aspects of the problem.

It is well-known that using uniform power $\mathcal{P}_k = P/M$ for all $k = 1, \dots, M$, rather using optimal water-filling, incurs a loss only in the $O(1)$ term, and we shall restrict to this choice in the rest of this paper. Under perfect CSIT and CSIR, the optimal DPC sum-rate C and the ZF sum-rate R^{ZF} are given by $M \log P/N_0 + O(1)$ and differ only in the constant term. On the contrary, under non-perfect CSIT the rate sum may behave in a radically different way. For example, under perfect CSIR and no CSIT, when \mathbf{H} has i.i.d. Gaussian entries, the sum rate is equal to $\log P/N_0 + O(1)$ [3], [46]. These two extremes clearly point out the key role of CSIT in the MIMO broadcast channel. In the rest of this paper we show that full multiplexing gain can be indeed achieved or closely approached by very simple channel state estimation and feedback schemes, thus providing a very strong argument for the practical feasibility of multiuser MIMO downlink.

Remark 1.1: A slightly different form of ZF beamforming is commonly used in the literature:

$$\mathbf{x} = \sqrt{\frac{P}{\gamma}} \mathbf{H}^{-1} \mathbf{u} \quad (3)$$

where \mathbf{u} is the vector of equal-power, independently generated data symbols (i.i.d. complex Gaussian), with the normalization constant γ chosen either as $\gamma = \mathbb{E} \left[\text{tr} \left((\mathbf{H} \mathbf{H}^H)^{-1} \right) \right]$ (long-term power constraint, i.e., $\mathbb{E} [|\mathbf{x}|^2] = P$ where the expectation is over the Gaussian inputs as well as the distribution of \mathbf{H}), or $\gamma = \text{tr} \left((\mathbf{H} \mathbf{H}^H)^{-1} \right)$ (short-term power constraint, i.e., $\mathbb{E} [|\mathbf{x}|^2] = P$ for each \mathbf{H} where the expectation is only over the Gaussian inputs but not over the distribution of \mathbf{H}).

The beamforming vectors are clearly the same as our version of ZF beamforming, but the power allocation differs significantly from our choice $\mathcal{P}_k = P/M$. With the choice $\mathcal{P}_k = P/M$, the received SNR at UT k is $\frac{|\mathbf{h}_k^H \mathbf{v}_k|^2 P}{N_0 M}$. As we explain in more details later, the quantity $\mathbf{h}_k^H \mathbf{v}_k$ is complex Gaussian with unit variance and thus each user experiences Rayleigh fading with average SNR $\frac{P}{N_0 M}$. Furthermore, received SNR's differ across UT's and also across fading realizations.

On the other hand, if power allocation is performed according to (3), the received SNR is $\frac{P}{N_0 \gamma}$. In the case of the long-term power constraint, this corresponds to a received SNR of $\frac{P}{N_0} \frac{1}{\mathbb{E}[\text{tr}((\mathbf{H} \mathbf{H}^H)^{-1})]}$ for all UT's in all channel realizations, and thus *fairness* across users and across channel realizations. In terms of the notation used earlier, this corresponds to choosing $\mathcal{P}_k(\mathbf{H}) = \frac{P}{|\mathbf{h}_k^H \mathbf{v}_k|^2 \mathbb{E}[\text{tr}((\mathbf{H} \mathbf{H}^H)^{-1})]}$. However, because $\text{tr} \left((\mathbf{H} \mathbf{H}^H)^{-1} \right)$ does not have a finite mean, this policy cannot satisfy an average power constraint and thus provides zero rate. The short-term power constraint provides fairness across UT's but not across channel realizations and leads to a received SNR of $\frac{P}{N_0} \frac{1}{\text{tr}((\mathbf{H} \mathbf{H}^H)^{-1})}$. This policy does produce a positive ergodic rate, but a relatively small one because the received SNR of all UT's is quite small whenever $\text{tr} \left((\mathbf{H} \mathbf{H}^H)^{-1} \right)$ is large. This occurs whenever \mathbf{H} is not well-conditioned and

² Because of the symmetry of the user channel statistics, our analysis directly applies to the case where $K > M$ and a subset of M UTs is selected in each frame by some scheduling algorithm that does not take into account the channel state information.

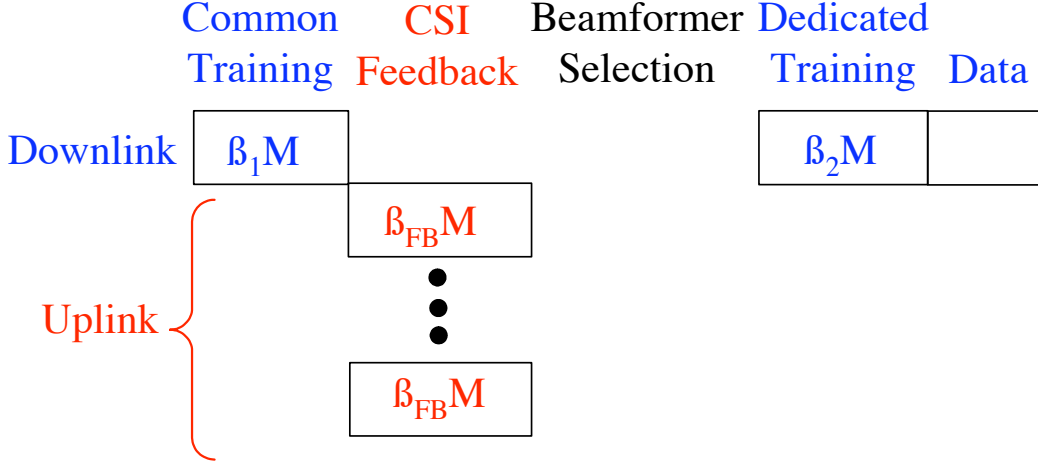


Fig. 1. Channel estimation and feedback model

thus occurs fairly frequently because \mathbf{H} is square. Although fairness may be desirable for certain applications, using only power allocation to achieve this outcome and not utilizing the other degrees of freedom typically available (e.g., user selection, bandwidth) does not appear to be particularly efficient. \diamond

II. CHANNEL STATE ESTIMATION AND FEEDBACK

We assume that each UT estimates its channel vector from *downlink training symbols* and then feeds this information back to the BS. This scenario, referred to as “closed-loop” CSIT estimation, applies to the case of Frequency-Division Duplexing (FDD), where uplink and downlink are assigned to different frequency bands with separation significantly larger than the channel coherence bandwidth, such that the uplink and downlink channel coefficients are essentially statistically independent. Our goal is to study channel estimation and feedback schemes, evaluated in terms of achievable ergodic rates, in FDD systems.

An alternative to FDD is Time-Division Duplexing (TDD), where uplink and downlink share in time-division the same frequency band. In this case, provided that the channel coherence time is significantly larger than the concatenation of an uplink and downlink slot and that hardware is appropriately calibrated, the downlink channel can be learned by the BS in an “open-loop” mode, from the training symbols inserted in the uplink slots [27]. The feedback implicitly provided by the uplink training symbols essentially come for free, at no additional system cost³, and thus explicit feedback from UTs to BS does not make much sense. The case of TDD with open-loop channel state estimation is discussed in [27], [47]. Although our focus is exclusively on FDD systems, it is interesting to note that our analysis of analog channel feedback schemes trivially extends to open-loop TDD systems (Section IV, Remark 4.2).

We hasten to say that the choice of FDD versus TDD involves many other system aspects, perhaps even more fundamental than CSIT estimation, such as inter-cell interference management, handoff schemes, cell synchronization, and implementation and power-efficiency of the terminals. While TDD is widespread in wireless LANs [48], FDD is by far the most common choice in wireless cellular networks [49]. Hence, our detailed analysis of FDD systems is very relevant.

We analyze the case when the BS employs a simple *naive* ZF beamforming scheme, that computes a mismatched beamforming matrix from the CSIT fed back from the UTs.

Our baseline system is depicted in Fig. 1 and consists of the following phases:

- 1) **Common Training:** In order to allow for channel estimation, $\beta_1 M$ shared pilots ($\beta_1 \geq 1$ symbols per

³All current and future proposals for wireless systems physical layers make use of training symbols for coherent detection [39], [40].

antenna) are transmitted on the downlink⁴. Each UT k estimates its channel from the observation

$$\mathbf{s}_k = \sqrt{\beta_1 P} \mathbf{h}_k + \mathbf{z}_k \quad (4)$$

corresponding to the common training (downlink) channel output, where $\mathbf{z}_k \sim \mathcal{CN}(0, N_0 \mathbf{I})$. The MMSE estimate $\tilde{\mathbf{h}}_k$ of \mathbf{h}_k given the observation \mathbf{s}_k (as in (4)) is given by [50]:

$$\tilde{\mathbf{h}}_k = \mathbb{E}[\mathbf{h}_k \mathbf{s}_k^H] \mathbb{E}[\mathbf{s}_k \mathbf{s}_k^H]^{-1} \mathbf{s}_k = \frac{\sqrt{\beta_1 P}}{N_0 + \beta_1 P} \mathbf{s}_k \quad (5)$$

Note that \mathbf{h}_k can be written in terms of the estimate $\tilde{\mathbf{h}}_k$ and independent additive white Gaussian estimation noise \mathbf{n}_k as:

$$\mathbf{h}_k = \tilde{\mathbf{h}}_k + \mathbf{n}_k, \quad (6)$$

where \mathbf{n}_k is Gaussian with covariance [50]:

$$\mathbb{E}[\mathbf{n}_k \mathbf{n}_k^H] = \mathbb{E}[\mathbf{h}_k \mathbf{h}_k^H] - \mathbb{E}[\mathbf{h}_k \mathbf{s}_k^H] \mathbb{E}[\mathbf{s}_k \mathbf{s}_k^H]^{-1} \mathbb{E}[\mathbf{s}_k \mathbf{h}_k^H] = \sigma_1^2 \mathbf{I}$$

with

$$\sigma_1^2 = \frac{1}{1 + \beta_1 P / N_0} \quad (7)$$

2) **Channel State Feedback:** Each UT feeds back its channel estimate $\tilde{\mathbf{h}}_k$ to the BS immediately after completion of the common training phase. We use $\hat{\mathbf{H}} = [\hat{\mathbf{h}}_1, \dots, \hat{\mathbf{h}}_K] \in \mathbb{C}^{M \times K}$ to denote the (imperfect) channel information available at the BS corresponding to true channel state \mathbf{H} (which is constant for each frame). The feedback method is thus a mapping (possibly probabilistic) from $\tilde{\mathbf{h}}_k$ to $\hat{\mathbf{h}}_k$, or alternatively from \mathbf{h}_k to $\hat{\mathbf{h}}_k$ (where the second interpretation follows from the representation (6)). For now we leave the feedback scheme unspecified to allow development of general achievability bounds in Section III, and particularize to specific feedback schemes from Section IV onwards.

The uplink channel is a MIMO Multiple Access Channel (MIMO-MAC) with fading. For simplicity, we start by considering the case of orthogonal access without fading and SNR $\frac{P}{N_0}$ for the channel state feedback channel. Furthermore, the baseline model of Fig. 1 assumes no delay in the feedback. Later, we shall remove these simplifying assumptions and address the full MIMO-MAC with fading (see Section VIII), discuss the design tradeoffs for the channel state feedback and consider the case where feedback has delay and the channel state changes from slot to slot (see Section IX). In general, we measure the *amount* of feedback by the number of channel uses or the number of feedback symbols as opposed to feedback bits; in our case we assume each UT transmits its feedback over $\beta_{fb} M$ feedback channel symbols.

3) **Beamformer Selection:** The BS selects the beamforming vectors by treating the estimated CSIT $\hat{\mathbf{H}}$ as if it was the true channel (this is why we refer to this approach as “naive”). Following the ZF recipe, $\hat{\mathbf{v}}_k$ is a unit vector orthogonal to the subspace $\mathcal{S}_k = \text{span}\{\hat{\mathbf{h}}_j : j \neq k\}$. We use the notation $\hat{\mathbf{V}} = [\hat{\mathbf{v}}_1, \dots, \hat{\mathbf{v}}_K]$. Because $K = M$ and the BS channel estimates $\hat{\mathbf{h}}_1, \dots, \hat{\mathbf{h}}_M$ are independent, the subspace \mathcal{S}_k is $M - 1$ dimensional (with probability one) and is independent of $\hat{\mathbf{h}}_k$. The beamforming vector $\hat{\mathbf{v}}_k$ is chosen in the one-dimensional nullspace of \mathcal{S}_k (with arbitrary absolute phase); as a result $\hat{\mathbf{v}}_k$ is independent of the channel estimate $\hat{\mathbf{h}}_k$ and thus is also independent of the true channel vector \mathbf{h}_k .

4) **Dedicated Training:** Once the BS has computed the beamforming vectors $\hat{\mathbf{V}}$, coherent detection of data at each UT is enabled by an additional round of downlink training transmitted along each beamforming vector. This additional round of training is required because the beamforming vectors $\{\hat{\mathbf{v}}_k\}$ are functions of the channel state information $\{\hat{\mathbf{h}}_1, \dots, \hat{\mathbf{h}}_K\}$ at the BS, while UT k at best knows only \mathbf{h}_k (in the case of noiseless digital feedback, but not in the case of analog feedback). Therefore, the coupling coefficients between the beamforming vectors and the UT channel vector are unknown.

⁴If β_1 is an integer, pilot symbols can be orthogonal in time, i.e., β_1 pilots are successively transmitted from each of the M BS antennas for a total of $\beta_1 M$ channel uses. More generally, it is sufficient for $\beta_1 M$ to be an integer and to use a unitary $M \times \beta_1 M$ spreading matrix as described in [27]. Regardless of the particular spreading matrix used, it is easy to see that the received observations are equivalent to that written in (4), and that the received (average) SNR is precisely $\beta_1 \frac{P}{N_0}$.

Let the set of the coefficients affecting the signal received by UT k be denoted by

$$\mathcal{A}_k \triangleq \{a_{k,j} : j = 1, \dots, M\}$$

where $a_{k,j} = \mathbf{h}_k^H \hat{\mathbf{v}}_j$ is the coupling coefficient between the k -th channel and the j -th beamforming vector. The received signal at the k -th UT is given by

$$\begin{aligned} y_k &= \mathbf{h}_k^H \hat{\mathbf{V}} \mathbf{u} + z_k \\ &= a_{k,k} u_k + \sum_{j \neq k} a_{k,j} u_j + z_k \\ &= a_{k,k} u_k + I_k + z_k \end{aligned} \quad (8)$$

where $I_k = \sum_{j \neq k} a_{k,j} u_j$ is the interference at UT k and $a_{k,k}$ is the *useful signal* coefficient. The dedicated training is intended to allow the estimation of the coefficients in \mathcal{A}_k at each UT k . This is accomplished by transmitting β_2 orthogonal training symbols along each of the beamforming vectors on the downlink, thus requiring a total of $\beta_2 M$ downlink channel uses.⁵ The relevant observation model for the estimation of \mathcal{A}_k is given by

$$r_{k,j} = \sqrt{\beta_2 P} a_{k,j} + z_{k,j}, \quad j = 1, \dots, M \quad (9)$$

We denote the full set of observations available to UT k as:

$$\mathcal{R}_k \triangleq \{r_{k,j} : j = 1, \dots, M\}.$$

In particular, we shall consider explicitly the case where UT k estimates its useful signal coefficient using linear MMSE estimation based on $r_{k,k}$, i.e.,

$$\hat{a}_{k,k} = \frac{\sqrt{\beta_2 P}}{N_0 + \beta_2 P} r_{k,k}. \quad (10)$$

Because $\hat{\mathbf{v}}_k$ is a unit vector independent of \mathbf{h}_k , the useful signal coefficient $a_{k,k} = \mathbf{h}_k^H \hat{\mathbf{v}}_k$ is complex Gaussian with unit variance. As a result we have the representation

$$a_{k,k} = \hat{a}_{k,k} + f_k \quad (11)$$

where $\hat{a}_{k,k}$ and f_k are independent and Gaussian with variance

$$\sigma_2^2 = \frac{1}{1 + \beta_2 P / N_0} \quad (12)$$

and $1 - \sigma_2^2$, respectively.

5) **Data Transmission:** After the dedicated downlink training phase, the BS sends the coded data symbols u_1, \dots, u_K for the rest of the frame duration. The effective channel output for this phase is therefore given by the sequence of corresponding channel output symbols y_k given by (8), and by the observation of the dedicated training phase \mathcal{R}_k given by (9). A simpler receiver scheme takes into account only the useful signal coefficient and does not try to estimate the interference coupling coefficients $a_{k,j}$ for $j \neq k$. In this case, the relevant channel output is formed by the sequence of symbols y_k and by $\hat{a}_{k,k}$, given by (10).

When considering the *ergodic* rates achievable by the proposed scheme, we implicitly assume that coding is performed over a long sequence of frames, each frame comprising a common training phase, channel state feedback phase, dedicated training phase and data transmission.

We conclude this section with two remarks. First, we would like to observe that two phases of training, a common “pilot channel” and dedicated per-user training symbols is common practice in some wireless cellular systems, as for example in the downlink of the 3rd generation Wideband CDMA standard [51] and in the MIMO component of future 4th generation systems [52].

Second, we notice here that imperfect CSIR has two effects: it further degrades the CSIT because channel feedback is performed on the basis of a noisy estimate of the true channel, and it also introduces additional uncertainty at the UT receivers and thereby reduces the downlink mutual information. We shall quantify these effects in the next section.

⁵If $\beta_2 M$ is an integer but β_2 is not, the unitary spreading approach used for common training can also be used here.

III. ACHIEVABLE RATE BOUNDS

We are interested in the achievable rates using naive beamforming performed on the basis of a particular feedback mechanism (to be specified later) and assuming equal power per user. With independent coding for each user, one very reasonable choice consists of letting all codebooks be Gaussian independently generated, i.e., the input symbols are $u_k \sim \mathcal{CN}(0, P/M)$. The remainder of this section is dedicated to deriving upper and lower bounds on the mutual information achieved for Gaussian inputs, indicated by R_k :

$$R_k \triangleq I(u_k; y_k, \mathcal{R}_k). \quad (13)$$

A. Lower Bounds

We begin by deriving a lower bound on R_k using techniques similar to those in [53], [41], [54].

Theorem 1: The achievable rate for ZF beamforming with Gaussian inputs and CSI training and feedback as described in Section II can be bounded from below by:

$$R_k \geq \mathbb{E} \left[\log \left(1 + \frac{|\hat{a}_{k,k}|^2 P / (N_0 M)}{1 + \sigma_2^2 P / (N_0 M) + \mathbb{E} [|I_k|^2 |\hat{a}_{k,k}|] / N_0} \right) \right] \quad (14)$$

Proof: The proof is closely inspired by that of Lemma B.0.1 of [54]. First, notice that since $\hat{a}_{k,k}$ is a function of \mathcal{R}_k , by the data-processing inequality we have that

$$I(u_k; y_k, \mathcal{R}_k) \geq I(u_k; y_k, \hat{a}_{k,k})$$

Then, because $I(u_k; y_k, \hat{a}_{k,k}) = h(u_k) - h(u_k | y_k, \hat{a}_{k,k})$ and $h(u_k) = \log(\pi e \frac{P}{M})$, a lower bound on mutual information is derived by upper bounding $h(u_k | y_k, \hat{a}_{k,k})$ as follows:

$$\begin{aligned} h(u_k | y_k, \hat{a}_{k,k}) &\stackrel{(a)}{=} h(u_k - \alpha y_k | y_k, \hat{a}_{k,k}) \\ &\stackrel{(b)}{\leq} h(u_k - \alpha y_k | \hat{a}_{k,k}) \\ &\stackrel{(c)}{\leq} \mathbb{E} [\log (\pi e \cdot \mathbb{E} [|u_k - \alpha y_k|^2 | \hat{a}_{k,k}])] \end{aligned} \quad (15)$$

where (a) holds for any deterministic function α of y_k and $\hat{a}_{k,k}$, (b) follows from the fact that conditioning reduces entropy and (c) follows by the fact that differential entropy is maximized by a Gaussian RV with the same second moment. Substituting (11) in (8) we have

$$y_k = (\hat{a}_{k,k} + f_k)u_k + I_k + z_k \quad (16)$$

where $\hat{a}_{k,k}u_k$ and $f_ku_k + I_k + z_k$ are *uncorrelated* and zero-mean, even if we condition on $\hat{a}_{k,k}$, because $\hat{a}_{k,k}, f_k, u_1, \dots, u_K, z_k$ are independent, zero-mean Gaussian's. Thus, we have

$$\mathbb{E} [|y_k|^2 | \hat{a}_{k,k}] = |\hat{a}_{k,k}|^2 \mathbb{E} [|u_k|^2] + \sigma_2^2 \mathbb{E} [|u_k|^2] + \mathbb{E} [|I_k|^2 | \hat{a}_{k,k}] + N_0, \quad (17)$$

Choosing α that minimizes $\mathbb{E} [|u_k - \alpha y_k|^2 | \hat{a}_{k,k}]$ tightens the bound. This corresponds to setting α y_k equal to the linear MMSE estimate of u_k given y_k and $\hat{a}_{k,k}$, i.e.,

$$\alpha = \frac{\mathbb{E} [u_k y_k^* | \hat{a}_{k,k}]}{\mathbb{E} [|y_k|^2 | \hat{a}_{k,k}]} = \frac{\mathbb{E} [|u_k|^2] \hat{a}_{k,k}^*}{\mathbb{E} [|y_k|^2 | \hat{a}_{k,k}]} \quad (18)$$

Using (17), the corresponding MMSE is given by

$$\mathbb{E} [|u_k - \alpha y_k|^2 | \hat{a}_{k,k}] = \mathbb{E} [|u_k|^2] \left(1 - \frac{\mathbb{E} [|u_k|^2] |\hat{a}_{k,k}|^2}{\mathbb{E} [|y_k|^2 | \hat{a}_{k,k}]} \right) \quad (19)$$

$$= \frac{P}{M} \frac{1 + \sigma_2^2 \frac{P}{N_0 M} + \mathbb{E} [|I_k|^2 | \hat{a}_{k,k}] / N_0}{|\hat{a}_{k,k}|^2 \frac{P}{N_0 M} + 1 + \sigma_2^2 \frac{P}{N_0 M} + \mathbb{E} [|I_k|^2 | \hat{a}_{k,k}] / N_0} \quad (20)$$

Replacing (20) into (15) and using $h(u_k) = \log(\pi e \frac{P}{M})$, we obtain (14). \square

The conditional interference second moment $\mathbb{E} [|I_k|^2 | \hat{a}_{k,k}]$ in (14) may be difficult to compute due to the dependency of I_k , which contains the coefficients $a_{k,j}$ for $j \neq k$, on $\hat{a}_{k,k}$. However, we will not need to compute this explicitly, as is seen in our next results.

A very useful measure of the performance of the channel estimation/feedback scheme is the difference between R_k and the achievable rate with ZF beamforming and ideal CSIT and CSIR. We denote this rate as R_k^{ZF} , which is precisely the rate of user k with uniform (across users) and constant (in time) power allocation $\mathcal{P}_k(\mathbf{H}) = \frac{P}{M}$ in (2). Thus, we define the rate gap as follows:

$$\Delta R \triangleq R_k^{\text{ZF}} - R_k. \quad (21)$$

We now provide an upper bound on the rate gap incurred under channel estimation and feedback with respect to ideal CSI under ZF beamforming.

Theorem 2: The rate gap incurred by ZF beamforming with CSIT training and feedback as described in Section II with respect to ideal ZF with equal power allocation is upperbounded by:

$$\boxed{\Delta R \leq \log \left(1 + \sigma_2^2 \frac{P}{N_0 M} + \frac{\mathbb{E} [|I_k|^2]}{N_0} \right)} \quad (22)$$

Proof: From (2), using $\mathcal{P}_k(\mathbf{H}) = \frac{P}{M}$, we have:

$$R^{\text{ZF}}(P) = \mathbb{E} \left[\log \left(1 + \frac{|\mathbf{h}_k^H \mathbf{v}_k|^2 P}{N_0 M} \right) \right]. \quad (23)$$

Using the lower bound on R_k from Theorem 1, we obtain:

$$\begin{aligned} \Delta R &= R_k^{\text{ZF}} - R_k \\ &\leq \mathbb{E} \left[\log \left(1 + \frac{|\mathbf{h}_k^H \mathbf{v}_k|^2 P}{N_0 M} \right) \right] - \mathbb{E} \left[\log \left(1 + \frac{|\hat{a}_{k,k}|^2 P / (N_0 M)}{1 + \sigma_2^2 P / (N_0 M) + \mathbb{E} [|I_k|^2 | \hat{a}_{k,k}] / N_0} \right) \right] \\ &= \mathbb{E} \left[\log \left(1 + \frac{|\mathbf{h}_k^H \mathbf{v}_k|^2 P}{N_0 M} \right) \right] - \mathbb{E} \left[\log \left(1 + |\hat{a}_{k,k}|^2 \frac{P}{N_0 M} + \sigma_2^2 \frac{P}{N_0 M} + \frac{\mathbb{E} [|I_k|^2 | \hat{a}_{k,k}]}{N_0} \right) \right] \\ &\quad + \mathbb{E} \left[\log \left(1 + \sigma_2^2 \frac{P}{N_0 M} + \frac{\mathbb{E} [|I_k|^2 | \hat{a}_{k,k}]}{N_0} \right) \right] \\ &\stackrel{(a)}{\leq} \mathbb{E} \left[\log \left(1 + \frac{|\mathbf{h}_k^H \mathbf{v}_k|^2 P}{N_0 M} \right) \right] - \mathbb{E} \left[\log \left(1 + \frac{P}{N_0 M} (|\hat{a}_{k,k}|^2 + \sigma_2^2) \right) \right] \\ &\quad + \mathbb{E} \left[\log \left(1 + \sigma_2^2 \frac{P}{N_0 M} + \frac{\mathbb{E} [|I_k|^2 | \hat{a}_{k,k}]}{N_0} \right) \right] \\ &\stackrel{(b)}{\leq} \mathbb{E} \left[\log \left(1 + \sigma_2^2 \frac{P}{N_0 M} + \frac{\mathbb{E} [|I_k|^2 | \hat{a}_{k,k}]}{N_0} \right) \right] \end{aligned} \quad (24)$$

$$\stackrel{(c)}{\leq} \log \left(1 + \sigma_2^2 \frac{P}{N_0 M} + \frac{\mathbb{E} [|I_k|^2]}{N_0} \right) \quad (25)$$

where (a) follows by dropping the non-negative interference term $\mathbb{E} [|I_k|^2 | \hat{a}_{k,k}] / N_0$ and using the monotonicity of the $\log(\cdot)$ function. Using the fact that \mathbf{h}_k is spatially white and \mathbf{v}_k is selected independent of \mathbf{h}_k (by the ZF procedure), it follows that $\mathbf{h}_k^H \mathbf{v}_k \sim \mathcal{CN}(0, 1)$ and $\hat{a}_{k,k} \sim \mathcal{CN}(0, 1 - \sigma_2^2)$. Direct application of Lemma 1 with $A = P / (N_0 M)$, $\lambda = \sigma_2^2$ and X distributed as $|\mathbf{h}_k^H \mathbf{v}_k|^2$ (i.e., central chi-squared with mean 1 and two degrees of freedom), thus proves (b). Finally, (c) follows from the concavity of $\log(\cdot)$ and Jensen's inequality. \square

Lemma 1: Let X denote a non-negative random variable with $\mathbb{E}[X] = 1$ and A be a positive constant, then

$$\mathbb{E} [\log (1 + XA)] \leq \mathbb{E} [\log (1 + (\lambda + (1 - \lambda)X) A)] \quad (26)$$

for any $0 \leq \lambda \leq 1$.

Proof: For all $0 \leq z \leq 1$, define the function

$$\psi(z) = \mathbb{E}[\log(1 + zA + (1 - z)XA)] \quad (27)$$

Then (26) is equivalent to the inequality $\psi(0) \leq \psi(\lambda)$. By the concavity of $\log(\cdot)$ and Jensen's inequality we have

$$\begin{aligned} \psi(z) &\leq \log(1 + zA + (1 - z)\mathbb{E}[X]A) \\ &= \log(1 + A) \\ &= \psi(1) \end{aligned} \quad (28)$$

In particular, $\psi(0) \leq \psi(1)$. Moreover, $\psi(z)$ is an expectation of the composition of a concave function and a linear function of z , and is hence concave [55]. Thus, the concave function $\psi(z)$ for $z \in [0, 1]$ lies above the line joining the points $(0, \psi(0))$ and $(1, \psi(1))$. Hence, we have $\psi(0) \leq \psi(\lambda)$ for $\lambda \in [0, 1]$, which proves (26). \square

For clarity of notation, we denote the rate gap upper bound as $\overline{\Delta R}$:

$$\overline{\Delta R} \triangleq \log \left(1 + \sigma_2^2 \frac{P}{N_0 M} + \frac{\mathbb{E}[|I_k|^2]}{N_0} \right) \quad (29)$$

Interestingly, the rate gap upper bound captures the dependence on the two phases of training and on the channel state feedback through the downlink useful signal coefficient estimation variance σ_2^2 and the residual interference variance $\mathbb{E}[|I_k|^2]$. Because $I_k = \sum_{j \neq k} a_{k,j} u_j$ with the u_j 's chosen independently as $\mathcal{CN}(0, P/M)$, we have:

$$\mathbb{E}[|I_k|^2] = \frac{P}{M} \sum_{j \neq k} \mathbb{E}[|a_{k,j}|^2] = \frac{P}{M} \sum_{j \neq k} \mathbb{E}[|\mathbf{h}_k^H \hat{\mathbf{v}}_j|^2]. \quad (30)$$

The beamforming vector $\hat{\mathbf{v}}_j$ is chosen orthogonal to the BS's channel estimate $\hat{\mathbf{h}}_k$, and thus $|\mathbf{h}_k^H \hat{\mathbf{v}}_j|^2$ is proportional to the mismatch between the true channel \mathbf{h}_k and $\hat{\mathbf{h}}_k$. Recall that this mismatch is due to common training, which causes mismatch between \mathbf{h}_k and the UT estimate $\hat{\mathbf{h}}_k$, as well as the channel feedback mechanism, which further corrupts the UT estimate $\hat{\mathbf{h}}_k$ to ultimately provide the BS with $\hat{\mathbf{h}}_k$. On the other hand, the useful signal coefficient estimation error (of variance σ_2^2) depends only on the dedicated training phase. In the following sections, we shall compute these terms and particularize the above results for specific feedback schemes, i.e., specific schemes that map $\tilde{\mathbf{h}}_k$ to $\hat{\mathbf{h}}_k$.

An obvious result of the rate gap upper bound is the following lower bound to R_k :

Corollary 3.1: The achievable rate for ZF beamforming with Gaussian inputs and CSIT training and feedback as described in Section II can be bounded from below by:

$$R_k \geq R_k^{\text{ZF}} - \overline{\Delta R} \quad (31)$$

By studying (23) we see that R_k^{ZF} is precisely the ergodic capacity of a point-to-point channel in Rayleigh fading with average SNR $\frac{P}{N_0 M}$, and thus can be written in closed form in terms of the exponential integral as [56]:

$$R_k^{\text{ZF}} = \exp \left(\frac{N_0 M}{P} \right) \text{E}_i \left(1, \frac{N_0 M}{P} \right) \quad (32)$$

where $\text{E}_i(n, x) = \int_1^\infty \frac{e^{-xt}}{t^n} dt$, $x > 0$ [57]. Since the rate gap upper bound in Theorem 2 is derived by further lower bounding the achievable rate lower bound from Theorem 1, it is clear that the lower bound of Corollary 3.1 is no larger than the lower bound of Theorem 1. Furthermore, it is also clear that only the estimation of $a_{k,k}$ in the derivation of the bound is relevant, and therefore Corollary 3.1 also provides a lower bound to the achievable rate for a system where the dedicated training phase is used only to estimate the useful signal coefficients $a_{k,k}$ at each UT rather than the full set of coefficients \mathcal{A}_k .

B. Upper Bounds

A useful upper bound to R_k is reached by providing each UT k with exact knowledge of the signal and interference coefficients \mathcal{A}_k , and thus this bound is referred to as the “genie-aided upper-bound”.

Theorem 3: Consider a ZF beamforming system with CSIT feedback as described in Section II but assume that once the beamforming matrix $\widehat{\mathbf{V}}$ is chosen, a genie provides the k -th UT with perfect knowledge of the coefficients $\mathcal{A}_k = \{a_{k,j} = \mathbf{h}_k^H \widehat{\mathbf{V}}_j : j = 1, \dots, M\}$. Then, the achievable rate for Gaussian inputs is upperbounded by:

$$R_k \leq \mathbb{E} \left[\log \left(1 + \frac{|a_{k,k}|^2 P / (N_0 M)}{1 + \sum_{j \neq k} |a_{k,j}|^2 P / (N_0 M)} \right) \right]. \quad (33)$$

Proof: Since \mathcal{R}_k is a noisy version of \mathcal{A}_k , the data-processing inequality yields

$$R_k = I(u_k; y_k, \mathcal{R}_k) \leq I(u_k; y_k, \mathcal{A}_k) \quad (34)$$

Noticing that y_k conditioned on \mathcal{A}_k is complex Gaussian with variance $N_0 + \sum_{j=1}^M |a_{k,j}|^2 P / M$ while y_k conditioned on (\mathcal{A}_k, u_k) is complex Gaussian with variance $N_0 + \sum_{j \neq k} |a_{k,j}|^2 P / M$, we immediately obtain that $I(u_k; y_k, \mathcal{A}_k)$, with Gaussian inputs, is equal to the RHS of (33). \square

In several previous works, achievable rates for Gaussian inputs have been studied while *implicitly* making the above genie-aided assumption [25], [29], [58], [59]. However, this is not necessarily a trivial assumption, particularly given that the interference coefficients are (by design) very small (i.e., approximately at or near the noise floor). The practical relevance of Theorem 3 is then justified by the fact that it yields an easily computable expression and, for large β_2 , the genie-aided upper bound can be closely approached by a receiver that estimates all interference coupling coefficients and not only the useful signal coefficient. In this work we are able to test the validity of this genie-aided assumption by comparing the lower bound of Corollary 3.1 to this upper bound.

C. Summary of Bounds

Before particularizing the bounds to various feedback strategies, it is useful to first summarize the various achievability bounds to the primary quantity of interest R_k :

$$\begin{aligned} & R_k^{\text{ZF}}(P) - \log \left(1 + \sigma_2^2 \frac{P}{N_0 M} + \frac{\mathbb{E}[|I_k|^2]}{N_0} \right) && \text{[Corollary 3.1]} \\ & \leq \mathbb{E} \left[\log \left(1 + \frac{|\widehat{a}_{k,k}|^2 P / (N_0 M)}{1 + \sigma_2^2 P / (N_0 M) + \mathbb{E}[|I_k|^2 | \widehat{a}_{k,k}] / N_0} \right) \right] && \text{[Theorem 1]} \\ & \leq R_k = I(u_k; y_k, \mathcal{R}_k) \\ & \leq I(u_k; y_k, \mathcal{A}_k) = \mathbb{E} \left[\log \left(1 + \frac{|a_{k,k}|^2 P / (N_0 M)}{1 + \sum_{j \neq k} |a_{k,j}|^2 P / (N_0 M)} \right) \right] && \text{[Theorem 3]} \end{aligned}$$

Because the joint distribution of $(I_k, \widehat{a}_{k,k})$ is not known, the computation of the lower bound from Theorem 1 appears to be difficult, even by Monte Carlo simulation. Hence, we shall use Corollary 3.1, which can be computed analytically for the cases considered here. In this lower bound, the effect of common training and channel feedback are reflected in the quantity $\mathbb{E}[|I_k|^2]$, while σ_2^2 reflects the effect of (imperfect) dedicated training. The upper bound of Theorem 3 assumes perfect dedicated training (i.e., perfect knowledge of all coefficients), but the effects of common training and channel feedback are still captured by the interference terms $\{|a_{k,j}|^2\}_{j \neq k}$; this bound shall be computed via Monte Carlo simulation because again the joint distribution of the coefficients \mathcal{A}_k is unknown.

IV. ANALOG CHANNEL FEEDBACK

We now particularize our results to an “analog” channel state feedback scheme, assuming no feedback delay. The estimated downlink channel coefficients are explicitly transmitted on the uplink (feedback link) by each UT using unquantized quadrature-amplitude modulation [27], [31], [60], [61]. We make the simplifying assumption that the feedback channel is unfaded AWGN, with the same downlink SNR, P/N_0 , and that the UTs make use of orthogonal signaling (e.g., TDMA, FDMA or orthogonal CDMA). Each UT transmits over $\beta_{\text{fb}} M$ channel symbols, for a total of $\beta_{\text{fb}} M^2$ symbols.

Recall that each UT receives $\mathbf{s}_k = \sqrt{\beta_1 P} \mathbf{h}_k + \mathbf{z}_k$ during the common training phase. Then, each UT transmits a scaled version of \mathbf{s}_k during the channel feedback phase (each UT scales \mathbf{s}_k to arrive at its MMSE estimate $\hat{\mathbf{h}}_k$, but it is more convenient to work directly with \mathbf{s}_k in this context) and the resulting BS observation is given by:

$$\mathbf{g}_k = \frac{\sqrt{\beta_{\text{fb}} P}}{\sqrt{\beta_1 P + N_0}} \mathbf{s}_k + \tilde{\mathbf{w}}_k \quad (35)$$

$$= \frac{\sqrt{\beta_{\text{fb}} \beta_1} P}{\sqrt{\beta_1 P + N_0}} \mathbf{h}_k + \frac{\sqrt{\beta_{\text{fb}} P}}{\sqrt{\beta_1 P + N_0}} \mathbf{z}_k + \tilde{\mathbf{w}}_k \quad (36)$$

$$= \frac{\sqrt{\beta_{\text{fb}} \beta_1} P}{\sqrt{\beta_1 P + N_0}} \mathbf{h}_k + \mathbf{w}_k \quad (37)$$

where $\tilde{\mathbf{w}}_k$ represents the AWGN noise on the uplink feedback channel (variance N_0) and \mathbf{z}_k is the noise during the common training phase. The power scaling β_{fb} corresponds to the number of channel uses per channel coefficient, assuming that transmission in the feedback channel has per-symbol power P (averaged over frames) and that the channel state vector is modulated by a $\beta_{\text{fb}} M \times M$ unitary spreading matrix [27]. Because $\tilde{\mathbf{w}}_k$ and \mathbf{z}_k are independent, spatially white complex Gaussian's with per-component variance N_0 , \mathbf{w}_k is a spatially white Gaussian process with components distributed as $\mathcal{CN}(0, \sigma_w^2)$ with:

$$\sigma_w^2 = N_0 \left(1 + \frac{\beta_{\text{fb}} P / N_0}{1 + \beta_1 P / N_0} \right) \quad (38)$$

The BS then computes the MMSE estimate of the channel vector \mathbf{h}_k having received \mathbf{g}_k as:

$$\hat{\mathbf{h}}_k = \frac{\sqrt{\beta_{\text{fb}} \beta_1} P}{\sqrt{\beta_1 P + N_0} (\beta_{\text{fb}} P + N_0)} \mathbf{g}_k. \quad (39)$$

Notice that we can write \mathbf{h}_k in terms of $\hat{\mathbf{h}}_k$ using (37) as follows:

$$\mathbf{h}_k = \hat{\mathbf{h}}_k + \mathbf{e}_k \quad (40)$$

where $\hat{\mathbf{h}}_k$ and \mathbf{e}_k are mutually independent and \mathbf{e}_k has Gaussian i.i.d. components with mean zero and variance equal to the MMSE estimation error given by

$$\sigma_e^2 = \frac{\sigma_w^2}{\sigma_w^2 + \frac{\beta_{\text{fb}} \beta_1 P^2}{\beta_1 P + N_0}} = \frac{1}{1 + \beta_1 \frac{P}{N_0}} + \frac{\beta_1 \frac{P}{N_0}}{(1 + \beta_{\text{fb}} \frac{P}{N_0})(1 + \beta_1 \frac{P}{N_0})} \quad (41)$$

$$\leq \frac{1}{1 + \beta_1 \frac{P}{N_0}} + \frac{1}{1 + \beta_{\text{fb}} \frac{P}{N_0}} \leq \frac{1}{P/N_0} \left(\frac{1}{\beta_1} + \frac{1}{\beta_{\text{fb}}} \right). \quad (42)$$

where the upper bound (42) is tight for $\frac{P}{N_0} \rightarrow \infty$.

We can now use this characterization of $(\mathbf{h}_k, \hat{\mathbf{h}}_k)$ to derive the rate gap upper bound for analog feedback:

Theorem 4: If each UT feeds back its channel coefficients in analog fashion over $\beta_{\text{fb}} M$ channel uses of an AWGN uplink channel with SNR $\frac{P}{N_0}$, the rate gap upper bound is given by ("AF" standing for Analog Feedback):

$$\boxed{\overline{\Delta R}^{\text{AF}} = \log \left(1 + \frac{1}{M} \frac{\frac{P}{N_0}}{1 + \beta_2 \frac{P}{N_0}} + \frac{M-1}{M} \frac{P}{N_0} \frac{1 + (\beta_{\text{fb}} + \beta_1) \frac{P}{N_0}}{(1 + \beta_{\text{fb}} \frac{P}{N_0})(1 + \beta_1 \frac{P}{N_0})} \right)} \quad (43)$$

Proof: In order to compute $\overline{\Delta R}^{\text{AF}}$, we need to compute the variance of the interference term:

$$\begin{aligned}
\mathbb{E} [|I_k|^2] &= \sum_{j \neq k} \frac{P}{M} \mathbb{E} [|\mathbf{h}_k^H \hat{\mathbf{v}}_j|^2] \\
&\stackrel{(a)}{=} \sum_{j \neq k} \frac{P}{M} \left(\mathbb{E} [|\hat{\mathbf{h}}_k^H \hat{\mathbf{v}}_j + \mathbf{e}_k^H \hat{\mathbf{v}}_j|^2] \right) \\
&\stackrel{(b)}{=} \sum_{j \neq k} \frac{P}{M} \mathbb{E} [|\mathbf{e}_k^H \hat{\mathbf{v}}_j|^2] \\
&\stackrel{(c)}{=} \sum_{j \neq k} \frac{P}{M} \mathbb{E} [\hat{\mathbf{v}}_j^H \mathbb{E} [\mathbf{e}_k \mathbf{e}_k^H] \hat{\mathbf{v}}_j] \\
&= \sum_{j \neq k} \frac{P}{M} \sigma_e^2 \mathbb{E} [\hat{\mathbf{v}}_j^H \hat{\mathbf{v}}_j] \\
&= (M-1) \frac{P}{M} \sigma_e^2
\end{aligned} \tag{44}$$

where (a) follows from (40), where (b) follows from the fact that $\hat{\mathbf{h}}_k^H \hat{\mathbf{v}}_j = 0 \forall j \neq k$ by the naive ZF procedure, and (c) is obtained from the independence of \mathbf{e}_k and $\hat{\mathbf{v}}_j$, as $\hat{\mathbf{v}}_j$ is a deterministic function of $\{\hat{\mathbf{h}}_i\}_{i \neq j}$. Applying $\|\hat{\mathbf{v}}_j\| = 1$ and the fact that there are $M-1$ interference terms yield the remaining steps. By using (44) and (41) in the general expression for $\overline{\Delta R}$ we get the final result. \square

Using (42) it is easy to see that $\overline{\Delta R}^{\text{AF}}$ can be upper bounded by:

$$\overline{\Delta R}^{\text{AF}} \leq \log \left(1 + \frac{1}{M\beta_2} + \frac{M-1}{M} \left(\frac{1}{\beta_{\text{fb}}} + \frac{1}{\beta_1} \right) \right), \tag{45}$$

where both sides of (45) converge as $\frac{P}{N_0} \rightarrow \infty$. An *intuitive* understanding for this rate loss is obtained if one re-examines the UT received signal in the form used in Theorem 1:

$$y_k = \hat{a}_{k,k} u_k + \underbrace{f_k u_k^G}_{\text{Self Noise}} + \underbrace{\sum_{j \neq k} (\mathbf{h}_k^H \hat{\mathbf{v}}_j) u_j^G}_{\text{Interference}} + \underbrace{z_k}_{\text{Noise}} \tag{46}$$

The imperfect CSI (at the UT and BS) effectively increases the noise from the thermal noise level N_0 to the sum of the thermal noise, self-noise, and interference power, and the rate gap upper bound $\overline{\Delta R}^{\text{AF}}$ is precisely the logarithm of the ratio of the effective noise to the thermal noise power. Because f_k has variance σ_2^2 , the self-noise has power $\frac{P}{M} \sigma_2^2 = \frac{P}{M} \frac{1}{1+\beta_2 P/N_0} \approx \frac{N_0}{M\beta_2}$. Each of the interference coefficients $|\mathbf{h}_k^H \hat{\mathbf{v}}_j|^2$ has power σ_e^2 , and thus the total interference power from the other $M-1$ beams is $\frac{P}{M} (M-1) \sigma_e^2 \approx \frac{M-1}{M} N_0 \left(\frac{1}{\beta_1} + \frac{1}{\beta_{\text{fb}}} \right)$. Thus the effective noise power is approximately $N_0 \left(1 + \frac{1}{M\beta_2} + \frac{M-1}{M} \left(\frac{1}{\beta_1} + \frac{1}{\beta_{\text{fb}}} \right) \right)$, and dividing by N_0 and taking the logarithm yields (45). Furthermore, from this interpretation we can easily see that the rate gap is a factor of $M-1$ more dependent on β_1 (common training) than on β_2 (dedicated training) simply because the error due to dedicated training is only multiplied by one signal (the desired signal) while the error due to common training (which leads to imperfect CSIT) is multiplied by the signals of $M-1$ interferers.

Since the rate gap is bounded by a constant (as shown in (45)), we conclude that the multiplexing gain is preserved (i.e., $\lim_{P \rightarrow \infty} \frac{R_k}{\log_2 P} = 1$) in spite of the imperfect CSI. In general, the multiplexing gain of the analog CSIT feedback scheme depends critically on the behavior of the product $\sigma_e^2 P/N_0$ in the limit of large SNR $P/N_0 \rightarrow \infty$; in Section IX we will see that the behavior of this term critically depends on feedback delay as well as the channel process for the case of time-correlated fading.

The case of perfect CSIR corresponds to perfect channel estimation during the common training phase (i.e., $\beta_1 = \infty$) and perfect estimation of $a_{k,k}$ during the dedicated training phase (i.e., $\beta_2 = \infty$). Letting $\beta_1, \beta_2 \rightarrow \infty$ in

(45), we have the rate gap for perfect CSIR bounded as:

$$\Delta R_{\text{CSIR}}^{\text{AF}} \leq \log \left(1 + \frac{M-1}{M} \frac{1}{\beta_{\text{fb}}} \right) \quad (47)$$

$$\leq \log \left(1 + \frac{1}{\beta_{\text{fb}}} \right) \quad (48)$$

Remark 4.1: In many systems, the uplink SNR is smaller than the downlink SNR because UT's transmit with reduced power. If the uplink SNR is $\Gamma \frac{P}{N_0}$ rather than $\frac{P}{N_0}$, the rate gap upper bound is equal to the expression in Theorem 4 with β_{fb} replaced with $\Gamma \beta_{\text{fb}}$. This clearly does not change the multiplexing gain, but can have a significant effect on the rate gap. \diamond

Remark 4.2: It is easy to see that a TDD system with perfectly reciprocal uplink-downlink channels where each UT transmits β_{TDD} pilots (a single pilot trains all M BS antennas) in an orthogonal manner corresponds exactly to an FDD system with perfect feedback ($\beta_{\text{fb}} \rightarrow \infty$) and $\beta_1 = \beta_{\text{TDD}}$, because the downlink training in an FDD system is equivalent to the uplink training in a TDD system. Therefore, as a byproduct of our analysis, we obtain a result for the TDD open loop CSIT estimation:

$$\overline{\Delta R}^{\text{TDD}} = \log \left[1 + \left(\frac{1}{M} \frac{1}{1 + \beta_2 \frac{P}{N_0}} + \frac{M-1}{M} \frac{1}{1 + \beta_{\text{TDD}} \frac{P}{N_0}} \right) \frac{P}{N_0} \right] \quad (49)$$

$$\leq \log \left(1 + \frac{1}{M \beta_2} + \frac{M-1}{M} \frac{1}{\beta_{\text{TDD}}} \right). \quad (50)$$

Dedicated training is necessary even in TDD systems because UT's do not know the channels of other UT's and thus are not aware of the beamforming vectors used by the BS. Finally, note that a total of $M\beta_{\text{TDD}}$ uplink training symbols and $M\beta_2$ downlink (dedicated) training symbols are transmitted. \diamond

Orthogonal access in the channel state feedback link yields a feedback redundancy that increases like $O(M^2)$ while the downlink capacity increases only, at best, like $O(M)$. This may not be a big problem for practical finite M , provided that the channel coherence time T is much larger than M . However, it is clear that such a system is not scalable with the number of antennas. We shall see in Section VIII that, by exploiting the MIMO-MAC nature of the feedback channel, the feedback symbols need not be orthogonally multiplexed, and a more efficient use of the feedback channel can be achieved (see also [27], [26]).

We conclude this section by remarking that the various training and feedback phases can be optimized in order to minimize the rate gap bound (45), subject to a constraint on the total number T_r of uplink and downlink channel uses devoted to training and feedback. In the case of orthogonal access on the feedback channel, considered in this section, we have that $T_r = (\beta_1 + \beta_2)M + \beta_{\text{fb}}M^2$ and we require β_1, β_2 and β_{fb} to be ≥ 1 . The detailed optimization of the training and feedback parameters is beyond the scope of this paper and will be reported in a separate paper [62]. Here, we only provide an example. For $M = 4$ and $T_r = 45$ we find the optimized values:

$$\beta_1 M = 13, \quad \beta_2 M = 8, \quad \beta_{\text{fb}} M = 6.$$

We generally find that the optimal β_1^* is approximately a factor of \sqrt{M} larger than the optimal β_2^* , while $\beta_2^* \approx \beta_{\text{fb}}^*$. It should be noticed that with the UT speed, carrier frequency and coherence bandwidth parameters discussed in the Introduction, each fading frame spans a number of channel uses that is more than three orders of magnitude larger than $T_r = 45$. This confirms that training and feedback consume a relatively negligible fraction of the system degrees of freedom for slowly varying channels.

V. DIGITAL CHANNEL FEEDBACK

We now consider “digital” feedback, where the channel coefficients are quantized at each UT and represented by B bits. The packet of B bits is fed back by each UT to the BS. For the time being, we consider an *error-free* and *delay-free* channel state feedback. We begin by computing the rate gap upper bound in terms of *bits*, and later in the section relate this to feedback *channel uses*.

The quantization codebook $\mathcal{C} = \{\mathbf{p}_1, \dots, \mathbf{p}_{2^B}\}$ used to quantize the channel coefficients at each UT (known to the BS) consists of 2^B unit-norm vectors in \mathbb{C}^M . The quantization $\hat{\mathbf{h}}_k$ of the estimated channel vector $\tilde{\mathbf{h}}_k$ is selected

from \mathcal{C} according to the rule [20], [19], [18], [25]:

$$\hat{\mathbf{h}}_k = \arg \max_{\mathbf{p} \in \mathcal{C}} \frac{|\tilde{\mathbf{h}}_k^H \mathbf{p}|^2}{\|\tilde{\mathbf{h}}_k\|^2} \quad (51)$$

The corresponding quantization index, represented by B bits, is fed back to the BS. Notice that $\hat{\mathbf{h}}_k$ is of unit-norm and hence no channel magnitude information is fed back in this model.

In [25] it is shown that for a particular random ensemble of quantization codebooks referred to as *Random Vector Quantization* (RVQ)⁶, obtained by generating 2^B quantization vectors independently and uniformly distributed on the unit sphere in \mathbb{C}^M (see [25] and references therein), the average (angular) distortion is given by:

$$\mathbb{E} \left[\sin^2 \left(\tilde{\mathbf{h}}_k, \hat{\mathbf{h}}_k \right) \right] = 2^B \beta \left(2^B, \frac{M}{M-1} \right). \quad (52)$$

where $\beta(\cdot)$ is the beta function and $\sin^2 \left(\tilde{\mathbf{h}}_k, \hat{\mathbf{h}}_k \right) = 1 - \frac{|\tilde{\mathbf{h}}_k^H \hat{\mathbf{h}}_k|^2}{\|\tilde{\mathbf{h}}_k\|^2}$, and furthermore this quantity can be tightly bounded as:

$$\frac{M-1}{M} 2^{-\frac{B}{M-1}} \leq \mathbb{E} \left[\sin^2 \left(\tilde{\mathbf{h}}_k, \hat{\mathbf{h}}_k \right) \right] \leq 2^{-\frac{B}{M-1}}. \quad (53)$$

For analytical tractability we assume each UT uses an independently generated codebook (which prevents multiple users from feeding back the same quantization vector), and as a result we have [25]:

$$\mathbb{E} \left[\frac{|\tilde{\mathbf{h}}_k^H \hat{\mathbf{v}}_j|^2}{\|\tilde{\mathbf{h}}_k\|^2} \right] = \frac{1}{M-1} \mathbb{E} \left[\sin^2 \left(\tilde{\mathbf{h}}_k, \hat{\mathbf{h}}_k \right) \right], \quad (j \neq k). \quad (54)$$

For this particular choice of channel quantization, we can compute the rate gap upper bound in closed form:

Theorem 5: If each UT quantizes its channel to B bits (using RVQ) and conveys these bits noiselessly to the BS, the rate gap upper bound is given by (“DF” standing for Digital Feedback):

$$\overline{\Delta R}^{\text{DF}} = \log \left(1 + \frac{1}{M} \frac{\frac{P}{N_0}}{1 + \beta_2 \frac{P}{N_0}} + \frac{\frac{P}{N_0}}{1 + \beta_1 \frac{P}{N_0}} \left[\frac{\beta_1 P}{N_0} 2^B \beta \left(2^B, \frac{M}{M-1} \right) + \frac{M-1}{M} \right] \right)$$

and it is upper bounded as:

$$\boxed{\overline{\Delta R}^{\text{DF}} \leq \log \left(1 + \frac{1}{M} \frac{\frac{P}{N_0}}{1 + \beta_2 \frac{P}{N_0}} + \frac{\frac{P}{N_0}}{1 + \beta_1 \frac{P}{N_0}} \left[\frac{\beta_1 P}{N_0} 2^{-\frac{B}{M-1}} + \frac{M-1}{M} \right] \right)} \quad (55)$$

Proof: In order to compute the rate gap upper bound we compute the variance of the interference term for digital feedback by using the decomposition $\mathbf{h}_k = \tilde{\mathbf{h}}_k + \mathbf{n}_k$ from (6):

$$\begin{aligned} \mathbb{E}[|I_k|^2] &= \sum_{j \neq k} \frac{P}{M} \mathbb{E} \left[|\mathbf{h}_k^H \hat{\mathbf{v}}_j|^2 \right] \\ &\stackrel{(a)}{=} \sum_{j \neq k} \frac{P}{M} \left(\mathbb{E} \left[|\tilde{\mathbf{h}}_k^H \hat{\mathbf{v}}_j|^2 \right] + \mathbb{E} \left[|\mathbf{n}_k^H \hat{\mathbf{v}}_j|^2 \right] \right) \\ &\stackrel{(b)}{=} \sum_{j \neq k} \frac{P}{M} \left(\mathbb{E} \left[\|\tilde{\mathbf{h}}_k\|^2 \right] \mathbb{E} \left[\frac{|\tilde{\mathbf{h}}_k^H \hat{\mathbf{v}}_j|^2}{\|\tilde{\mathbf{h}}_k\|^2} \right] + \mathbb{E} \left[|\mathbf{n}_k^H \hat{\mathbf{v}}_j|^2 \right] \right) \\ &\stackrel{(c)}{=} \frac{P}{M} \mathbb{E} \left[\|\tilde{\mathbf{h}}_k\|^2 \right] 2^B \beta \left(2^B, \frac{M}{M-1} \right) + \sum_{j \neq k} \frac{P}{M} \mathbb{E} \left[\hat{\mathbf{v}}_j^H \mathbb{E}[\mathbf{n}_k \mathbf{n}_k^H] \hat{\mathbf{v}}_j \right] \\ &\stackrel{(d)}{=} \frac{\beta_1 P^2}{N_0 + \beta_1 P} 2^B \beta \left(2^B, \frac{M}{M-1} \right) + (M-1) \frac{P}{M} \sigma_1^2 \end{aligned} \quad (56)$$

⁶There are a number of reasons why we are well motivated to use RVQ for our analysis of digital feedback. First, note that RVQ is quite close to optimal vector quantization, particularly for moderate to large values of B . In [25] it is shown that the expected distortion (i.e., square of the sine of the angle between channel and quantization) of RVQ is no more than $\frac{M}{M-1}$ times larger than the distortion achieved with optimal vector quantization. Second, the isotropic and random nature of the ensemble of codebooks allows for analytical tractability. Finally, because the statistics of RVQ are known in closed form, RVQ can be exactly emulated by drawing only one scalar random variable and one random vector as described in [63]. For large B this is considerably simpler than actually performing brute-force quantization.

where (a) is obtained from the representation $\mathbf{h}_k = \tilde{\mathbf{h}}_k + \mathbf{n}_k$ and the fact that $\mathbb{E} \left[\tilde{\mathbf{h}}_k^H \hat{\mathbf{v}}_j \hat{\mathbf{v}}_j^H \mathbf{n}_k \right] = 0$ because \mathbf{n}_k is zero-mean Gaussian and is independent of $\tilde{\mathbf{h}}_k$ and $\hat{\mathbf{v}}_j$, (b) from the independence of the channel norm and direction of $\tilde{\mathbf{h}}_k$, (c) from (52) and finally, (d) by computing the expected norm of $\tilde{\mathbf{h}}_k = \frac{\sqrt{\beta_1 P}}{N_0 + \beta_1 P} \mathbf{s}_k$ using $\mathbf{s}_k = \sqrt{\beta_1 P} \mathbf{h}_k + \mathbf{z}_k$. The final result follows by using the above result in the expression (22) for the rate gap. \square

It is easy to see that we can further upper bound (55) as:

$$\overline{\Delta R}^{\text{DF}} \leq \log \left(1 + \frac{1}{M\beta_2} + \frac{M-1}{M} \frac{1}{\beta_1} + \left(\frac{P}{N_0} \right) 2^{-\frac{B}{M-1}} \right) \quad (57)$$

If we compare this to the rate gap upper bound for analog feedback given in (45), we notice that the dependence on β_1 and β_2 are precisely the same for both analog and digital feedback.

If $B = \alpha(M-1) \log_2 \frac{P}{N_0}$ for some $\alpha > 0$, then (57) becomes:

$$\overline{\Delta R}^{\text{DF}} \leq \log \left(1 + \frac{1}{M\beta_2} + \frac{M-1}{M} \frac{1}{\beta_1} + \left(\frac{P}{N_0} \right)^{1-\alpha} \right). \quad (58)$$

If $\alpha \geq 1$ this quantity is bounded and thus the full multiplexing gain is achieved. Furthermore for $\alpha > 1$ the effect of channel feedback completely vanishes. On the other hand, if $\alpha < 1$ the rate gap upper bound grows like $(1-\alpha) \log \frac{P}{N_0}$, and using [25, Theorem 4] it can be shown that both the genie-aided upper bound as well as R_k achieve a multiplexing gain of only α .

The case of perfect CSIR is again obtained by letting $\beta_1, \beta_2 \rightarrow \infty$, and from (57) we obtain

$$\Delta R_{\text{CSIR}}^{\text{DF}} \leq \log \left(1 + \frac{P}{N_0} 2^{-\frac{B}{M-1}} \right) \quad (59)$$

which recovers the result in [25, Theorem 1].

Remark 5.1: It is interesting to note that in the case of perfect CSIR, the lower bound of Corollary 3.1, the genie-aided upper bound, and R_k^{ZF} all coincide (in the sense that the absolute difference between them go to zero) at asymptotically high SNR, provided that $B = \alpha(M-1) \log_2 \frac{P}{N_0}$ with $\alpha > 1$. \diamond

In order to compare digital and analog feedback we need to meaningfully relate the number of feedback bits B with the number of channel uses in the feedback link (which is assumed to be unfaded AWGN with SNR $\frac{P}{N_0}$, as in the previous section). This can be done by assuming some coding scheme operating on the (noisy) feedback channel, and a simple scheme based on uncoded QAM modulation is described and analyzed in Section VII. For the time being, we shall make the very unrealistic assumption that the feedback link can operate error-free at capacity, i.e., it can reliably transmit $\log_2(1 + P/N_0)$ bits per symbol.⁷

The analog feedback considered before also provides a noisy version of the channel vector norm in addition to its direction. Although this information is irrelevant for the ZF beamforming considered here, it might be useful in some user selection algorithms such as those proposed in [43], [31], [44], [45]. In contrast, digital feedback based on Vector Quantization (with unit-norm quantization vectors) provides no norm information. Thus, for fair comparison, we assume that $\beta_{\text{fb}} M$ feedback symbols in the analog feedback scheme correspond to $\beta_{\text{fb}}(M-1)$ feedback symbols for the digital feedback scheme; i.e., a system using digital feedback could use one feedback symbol to transmit channel norm information. An alternative justification for this is to notice that the analog feedback system could be modified to operate in $\beta_{\text{fb}}(M-1)$ channel symbols by transmitting only the $M-1$ *relative* phases and amplitudes of the channel coefficients (relative to the first channel coefficient, without loss of generality) since the absolute channel norm and phase are irrelevant to the ZF beamforming considered here.

Thus, the number of feedback bits per mobile is $B = \beta_{\text{fb}}(M-1) \log_2(1 + P/N_0)$. Plugging this value of B into (57) gives:

$$\boxed{\overline{\Delta R}^{\text{DF}} \leq \log \left(1 + \frac{1}{M\beta_2} + \frac{M-1}{M} \frac{1}{\beta_1} + \frac{\frac{P}{N_0}}{\left(1 + \frac{P}{N_0} \right)^{\beta_{\text{fb}}}} \right)} \quad (60)$$

⁷Operating reliably at a rate close to capacity is not “unrealistic” by itself. However, this assumption is particularly unrealistic in the context of the considered model because the feedback channel coding block length is very small (of the order of the number of BS antennas) and because sensitivity to feedback delay (see Section IX) prevents grouping blocks of channel coefficients and using larger coding block length.

We note that the dependence on β_{fb} is approximately $\left(\frac{P}{N_0}\right)^{-\beta_{fb}}$, which is to be contrasted with a $\frac{1}{\beta_{fb}}$ dependence for the case of analog feedback. We defer the details of the comparison with analog feedback to Section VI.

We conclude this section with an example of the optimization of the training and feedback coefficients β_1, β_2 and β_{fb} that minimizes the rate gap (60) [62]. For $M = 4$, $P/N_0 = 10$ dB, and $T_r = 45$ we obtain

$$\beta_1 M = 11, \quad \beta_2 M = 6, \quad \beta_{fb} M = 7.$$

Similar to the case of analog feedback we generally find β_1^* to be approximately a factor of \sqrt{M} larger than β_2^* , but the optimal β_{fb} for digital feedback is generally smaller than for analog feedback for large values of T_r .

VI. COMPARISON BETWEEN ANALOG AND DIGITAL CHANNEL FEEDBACK

We compare analog and digital feedback under assumptions of no feedback errors (for digital feedback) and no feedback delay. In particular, the superiority of digital feedback is demonstrated and the role (often forgotten) of non-perfect CSIR is evidenced: in fact, under realistic non-perfect CSIR, the superiority of digital feedback is greatly reduced.

A. Perfect CSIR

We first compare the achievable rate lower bounds for analog and digital feedback under the assumption of perfect training, i.e., $\beta_1 = \beta_2 \rightarrow \infty$. From (48) and (60) we have:

$$\Delta R_{\text{CSIR}}^{\text{AF}} \leq \log \left(1 + \frac{1}{\beta_{fb}} \right) \quad (61)$$

$$\Delta R_{\text{CSIR}}^{\text{DF}} \leq \log \left(1 + \frac{\frac{P}{N_0}}{\left(1 + \frac{P}{N_0} \right)^{\beta_{fb}}} \right) \quad (62)$$

If $\beta_{fb} = 1$ then digital and analog feedback achieve essentially the same rate gap of at most 1 bit per channel use. However, if $\beta_{fb} > 1$, the rate gap of the quantized feedback vanishes for $\frac{P}{N_0} \rightarrow \infty$. For example, for $\beta_{fb} = 2$ the rate gap is upperbounded by $\log(1 + \frac{N_0}{P})$, which is quite small for even moderate values of P/N_0 (e.g., $P/N_0 = 10$ dB gives 0.13 bit per channel use). We conclude that, under the perfect CSIR assumption, digital is far superior to analog provided that $\beta_{fb} > 1$.

This conclusion finds an appealing interpretation in the context of rate-distortion theory. It is well-known (see for example [64] and references therein) that “analog transmission” (the source signal is input directly to the channel after suitable scaling in order to meet an average power constraint) is an optimal strategy to send an i.i.d. Gaussian source over a AWGN channel with the same bandwidth under quadratic distortion. In our case, the source vector is \mathbf{h}_k (Gaussian and i.i.d.) and the feedback channel is AWGN with SNR $\frac{P}{N_0}$. Hence, the fact that analog feedback cannot be essentially outperformed for $\beta_{fb} = 1$ is expected. However, it is also well-known that if the channel bandwidth is larger than the source bandwidth (which corresponds to the case where a block of M source coefficients are transmitted over $\beta_{fb} M$ channel uses with $\beta_{fb} > 1$), then analog transmission is strictly suboptimal with respect to a digital scheme operating at the rate-distortion bound, because the distortion with analog transmission is $O((P/N_0)^{-1})$ whereas it is $O((P/N_0)^{-\beta_{fb}})$ for digital transmission.

B. Imperfect CSIR

We now compare analog and digital feedback in the case of realistic (non-ideal) CSIR, obtained from the common and dedicated training schemes described in Section II. From (45) and (60) we have:

$$\overline{\Delta R}^{\text{AF}} \leq \log \left(1 + \frac{1}{M\beta_2} + \frac{M-1}{M} \left(\frac{1}{\beta_1} + \frac{1}{\beta_{fb}} \right) \right) \quad (63)$$

$$\begin{aligned} \overline{\Delta R}^{\text{DF}} &\leq \log \left(1 + \frac{1}{M\beta_2} + \frac{M-1}{M} \frac{1}{\beta_1} + \frac{\frac{P}{N_0}}{\left(1 + \frac{P}{N_0} \right)^{\beta_{fb}}} \right) \\ &\leq \begin{cases} \log \left(2 + \frac{1}{M\beta_2} + \frac{M-1}{M} \frac{1}{\beta_1} \right) & \text{for } \beta_{fb} = 1 \\ \log \left(1 + \frac{1}{M\beta_2} + \frac{M-1}{M} \frac{1}{\beta_1} \right) & \text{for } \beta_{fb} > 1 \end{cases} \end{aligned} \quad (64)$$

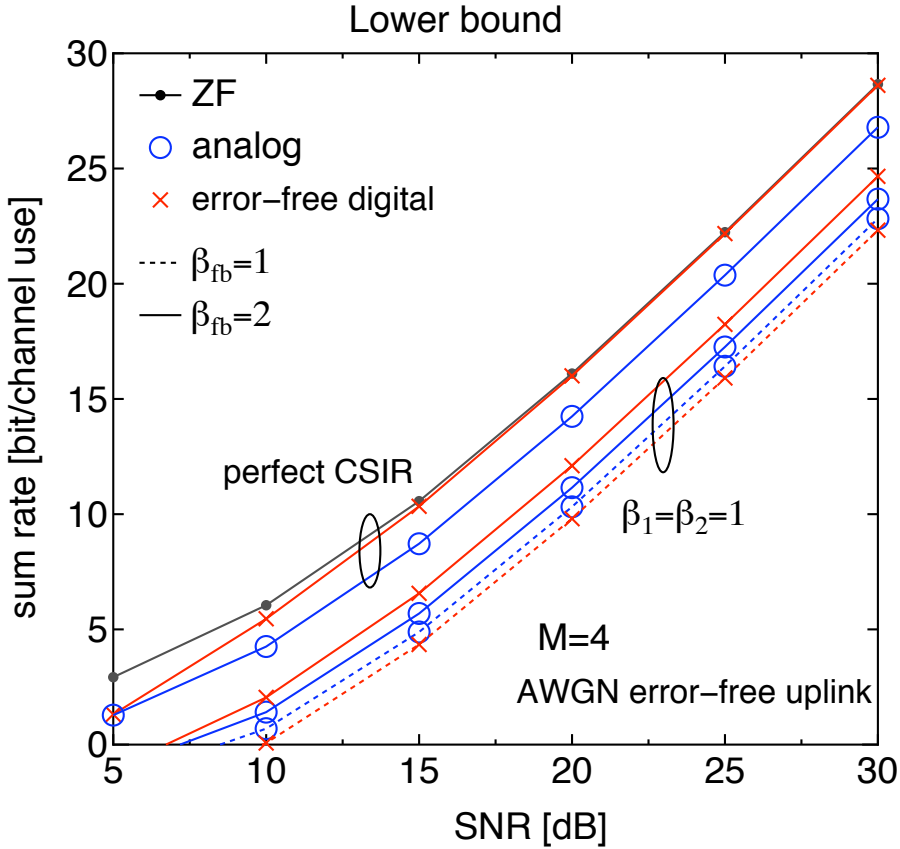


Fig. 2. Lower bounds over an error-free AWGN uplink

Comparing (45) and (64) we come to the same general conclusions as in Section VI-A: if $\beta_{\text{fb}} = 1$ then digital and analog are essentially equivalent, but if $\beta_{\text{fb}} > 1$ digital is superior to analog. However, notice that there are some important differences with the perfect CSIR scenario. First, the imperfect CSIR leads to residual interference that does not vanish with SNR; as a result, the rate gap for digital feedback is not driven to 0 even when $\beta_{\text{fb}} > 1$, for fixed β_1 and β_2 . For instance, even under perfect feedback (i.e., $\beta_{\text{fb}} = \infty$) with imperfect CSIR (β_1, β_2 finite), we have the following rate gap bound, that applies to either analog or digital feedback by letting $\beta_{\text{fb}} \rightarrow \infty$ in either (45) or (64):

$$\Delta R_{\text{CSIR}}^{\text{PERF. FB}} \leq \log \left(1 + \frac{1}{M\beta_2} + \frac{M-1}{M} \frac{1}{\beta_1} \right) \quad (65)$$

Another effect of realistic CSIR estimation is that, when $\beta_1 \approx \beta_2 \approx 1$, imperfect CSIR rather than the noise in the feedback channel or the quantization distortion is the dominating effect, thereby reducing digital feedback's advantage.

These effects are both visible in Fig. 2, where the lower bounds on the analog and digital feedback using the rate gap of (43) and (55) are plotted for $M = 4$ and $\beta_{\text{fb}} = 1, 2$, along with the throughput of zero-forcing (ZF) with perfect CSIT (32). The bottom four curves correspond to imperfect CSIR with $\beta_1 = \beta_2 = 1$. For $\beta_{\text{fb}} = 1$ (dotted lines), analog and digital feedback achieve essentially the same performance (as expected from (45) and (64)), while for $\beta_{\text{fb}} = 2$ (solid lines) digital feedback slightly outperforms analog feedback. The relative merit of digital versus analog becomes more and more significant as the quality of the CSIR improves. The upper curves correspond to perfect CSIR ($\beta_1 = \beta_2 \rightarrow \infty$), with $\beta_{\text{fb}} = 2$. Notice that the digital feedback scheme achieves the performance of ZF with perfect CSIT for $\text{SNR} \geq 15$ dB, and there is a rather substantial gap between analog and digital. In Fig. 3, we plot the genie-aided upper bound of Theorem 3 for analog and digital feedback for $M = 4$ and $\beta_{\text{fb}} = 1, 2$. Recall that the genie-aided upper bound assumes perfect knowledge of the coefficients A_k at each UT, which corresponds to letting $\beta_2 \rightarrow \infty$, but it is still meaningful to have imperfect common training (i.e., finite β_1) because this impacts the quality of the channel feedback. The bottom curves correspond to $\beta_1 = 1$ and $\beta_{\text{fb}} = 1, 2$, while the top curves are for $\beta_1 \rightarrow \infty$ and $\beta_{\text{fb}} = 2$ (i.e., imperfection in CSIT is due only to quantization

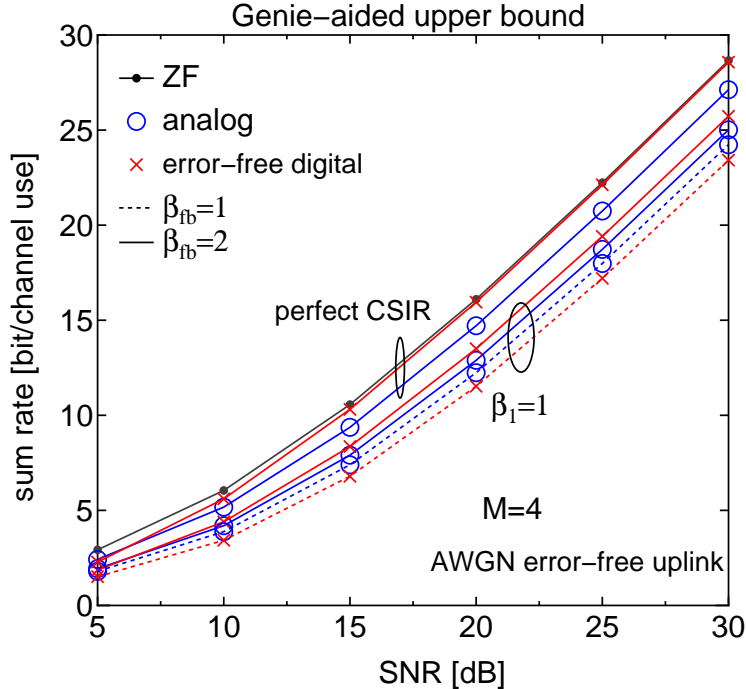


Fig. 3. Genie-aided upper bounds over an error-free AWGN uplink

error). Compared to Fig. 2, we remark that the genie-aided upper bound yields larger rates especially for small and moderate SNR regions, but the relationship between analog and digital feedback remains roughly the same: analog and digital are essentially equivalent for $\beta_{fb} = 1$, while digital has an advantage for $\beta_{fb} > 1$ that increases with the quality of the CSIR (i.e., with β_1 and β_2).

Finally, Fig. 4 compares analog and digital feedback over an error-free AWGN feedback channel with $M = 4$ as a function of the feedback redundancy β_{fb} for $\text{SNR} = 10, 20$ dB. We assume perfect CSIR ($\beta_1, \beta_2 \rightarrow \infty$). For each feedback scheme, the lower bound from Corollary 3.1 as well as the genie-aided bound of Theorem 3 are plotted. Notice that the lower bound and the genie-aided bound are generally quite close, and that the tightness of these bounds increases with SNR and β_{fb} . The superiority of digital feedback over analog feedback can be clearly observed for sufficiently large β_{fb} . At 10 dB, the genie-aided bound for digital crosses the genie-aided bound for analog at $\beta_{fb} = 1.5$, while the lower bounds cross at $\beta_{fb} \approx 2$. On the other hand, at 20 dB both bounds cross over at $\beta_{fb} \approx 1.25$. The fact that the crossover between digital and analog occurs at smaller values of β_{fb} when SNR is increased is to be expected by the fact that the both the lower bound and the genie-aided bound converge absolutely to R_k^{ZF} as $\text{SNR} \rightarrow \infty$ for any $\beta_{fb} > 2$.

VII. EFFECTS OF FEEDBACK ERRORS IN DIGITAL CSIT FEEDBACK

In this section we remove the optimistic assumption that the digital feedback channel can operate error-free at capacity. In general, coding for the channel state feedback should be regarded as a problem of joint source-channel coding, made particularly interesting by the non-standard distortion measure (that should be related to the residual interference of ZF beamforming) and by the fact that a very short block length is required. A thorough discussion of this subject is out of the scope of the present paper and is the matter of current investigation. Here, we restrict ourselves to the detailed analysis of a particularly simple scheme, based on uncoded QAM. Perhaps surprisingly, this scheme is *sufficient* to achieve a vanishing rate gap in the high SNR region, for an appropriate choice of the system parameters.

In the proposed scheme, the UTs perform quantization using RVQ and transmit the feedback bits using plain uncoded QAM. No intelligent bit-labeling of the quantization codebook or mapping of the quantization bits onto the QAM symbols is used (e.g., Gray labeling is used). Therefore, even a single erroneous feedback bit from UT k makes the BS's estimate $\hat{\mathbf{h}}_k$ essentially useless. To be more precise, if UT k 's feedback message is received in error then $\hat{\mathbf{h}}_k$ is not equal to the quantization vector that lies closest to \mathbf{h}_k (i.e., the quantization vector selected

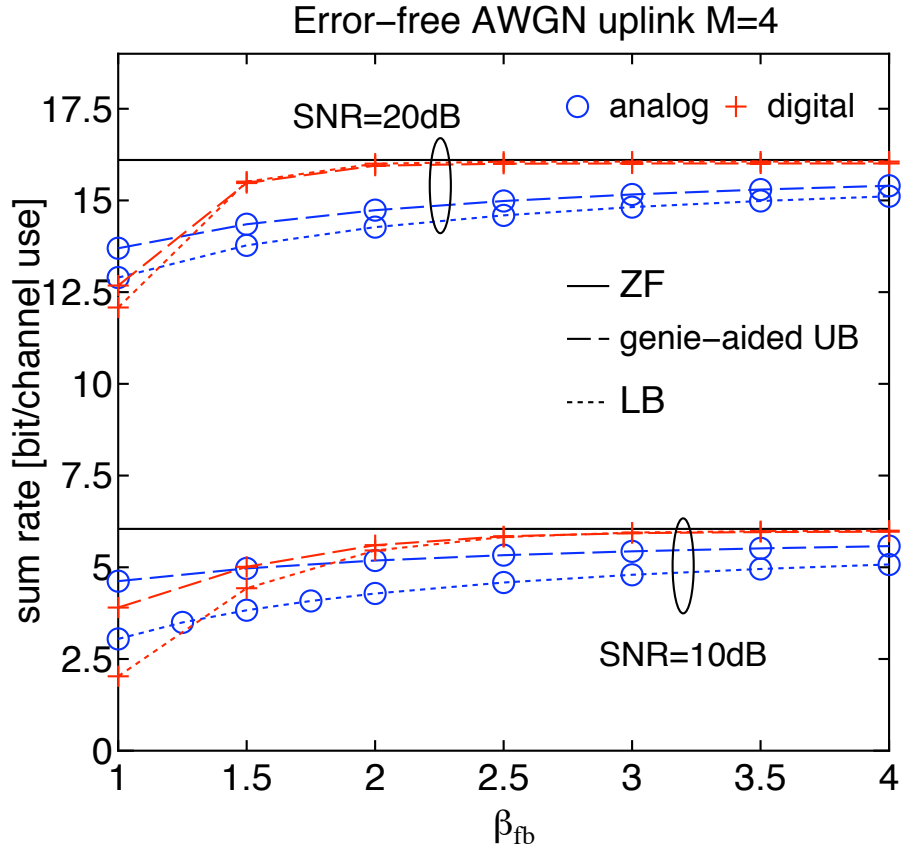


Fig. 4. Comparison as a function of β_{fb} over an error-free AWGN uplink.

by UT k) but is instead randomly chosen from the other $2^B - 1$ quantization vectors. Also, no particular error detection strategy is used and thus the BS computes the beamforming matrix on the basis of the received CSIT, although this may be in error.

Once again, we use $\beta_{fb}(M-1)$ channel uses to transmit the feedback bits. Interestingly, even for this very simple scheme there is a non-trivial tradeoff between quantization distortion and channel errors. In order to maintain a bounded rate gap, feedback must be scaled at least as $(M-1) \log_2 \left(1 + \frac{P}{N_0}\right) \approx (M-1) \log_2 \frac{P}{N_0}$. Therefore, we consider sending $B = \alpha(M-1) \log_2 \frac{P}{N_0}$ bits for $1 \leq \alpha \leq \beta_{fb}$ in $\beta_{fb}(M-1)$ channel uses, which corresponds to $\frac{\alpha}{\beta_{fb}} \log_2 \frac{P}{N_0}$ bits per QAM symbol.

In order to upper bound the probability of error, we note that the symbol error rate for square QAM with q constellation points is given by [40]:

$$P_s = 1 - \left(1 - 2 \left(1 - \frac{1}{\sqrt{q}}\right) Q\left(\frac{3(P/N_0)}{q-1}\right)\right)^2 \leq 2 \exp\left(-\frac{3}{2} \frac{P/N_0}{q-1}\right). \quad (66)$$

where $Q(x) = \int_x^\infty \frac{1}{\sqrt{2\pi}} e^{-t^2/2} dt$ is the Gaussian probability tail function. Using the fact that $q = (P/N_0)^{\frac{\alpha}{\beta_{fb}}}$, we have the following upper bound to the symbol error probability of QAM in AWGN:

$$P_s \leq 2 \exp\left(-\frac{3}{2} \left(\frac{P}{N_0}\right)^{1-\frac{\alpha}{\beta_{fb}}}\right) \quad (67)$$

If $\alpha = \beta_{fb}$ (which means trying to signal at capacity with uncoded modulation!) P_s does not decrease with SNR and system performance is very poor. However, for $\alpha < \beta_{fb}$, which corresponds to transmitting at a constant fraction (strictly less than one) of capacity, $P_s \rightarrow 0$ as $\frac{P}{N_0} \rightarrow \infty$. The error probability of the entire feedback message (transmitted in $\beta_{fb}(M-1)$ QAM symbols) is given by

$$\begin{aligned} P_{e,fb} &= 1 - (1 - P_s)^{\beta_{fb}(M-1)} \\ &\leq \beta_{fb}(M-1)P_s, \end{aligned} \quad (68)$$

where the inequality follows from the union bound. Note the tradeoff between distortion and feedback errors: α large corresponds to fine quantization but large $P_{e,fb}$, while α small corresponds to poorer quantization but reduced $P_{e,fb}$.

For simplicity, we first consider the perfect CSIR case (infinite β_1 and β_2) and decompose the interference variance term as

$$\mathbb{E}[|I_k|^2] = (1 - P_{e,fb})\mathbb{E}[|I_k|^2|\text{no fb. errors}] + P_{e,fb}\mathbb{E}[|I_k|^2|\text{fb. errors}]. \quad (69)$$

If the feedback message of the k -th UT is correctly received, then all beamforming vectors $\hat{\mathbf{v}}_j$ are in the orthogonal span of $\hat{\mathbf{h}}_k$ and therefore the analysis done previously for the error-free case applies, i.e., $\mathbb{E}[|I_k|^2|\text{no fb. errors}]$ is given by (56) with $\beta_1 = \beta_2 = \infty$. In the case of a feedback error, we can bound the variance as:

$$\begin{aligned} \mathbb{E}[|I_k|^2|\text{fb. errors}] &= \frac{P}{M} \sum_{j \neq k} \mathbb{E}[\|\mathbf{h}_k\|^2] \mathbb{E}\left[\frac{|\mathbf{h}_k^H \hat{\mathbf{v}}_j|^2}{\|\mathbf{h}_k\|^2}\right] \\ &= P(M-1)\mathbb{E}\left[\frac{|\mathbf{h}_k^H \hat{\mathbf{v}}_j|^2}{\|\mathbf{h}_k\|^2}\right] \\ &\stackrel{(a)}{=} P\mathbb{E}\left[\sin^2(\mathbf{h}_k, \hat{\mathbf{h}}_k)\right] \\ &\leq P, \end{aligned} \quad (70)$$

where (a) follows since the relationship in (54) holds because the channel estimates available to the BS are independent and isotropic even in the case of a feedback error. Putting these together yields:

$$\begin{aligned} \mathbb{E}[|I_k|^2] &= (1 - P_{e,fb})\mathbb{E}[|I_k|^2|\text{no fb. errors}] + P_{e,fb}\mathbb{E}[|I_k|^2|\text{fb. errors}] \\ &\leq (1 - P_{e,fb})P2^B\beta\left(2^B, \frac{M}{M-1}\right) + P_{e,fb}P \\ &\leq (1 - P_{e,fb})P2^{-\frac{B}{M-1}} + P_{e,fb}P. \end{aligned} \quad (71)$$

Using (71) in the rate gap upper bound expression, we have:

$$\begin{aligned} \overline{\Delta R}^{\text{DF-ERRORS}} &\leq \log\left(1 + (1 - P_{e,fb})\frac{P}{N_0}2^{-\frac{B}{M-1}} + \frac{P}{N_0}P_{e,fb}\right) \\ &= \log\left(1 + (1 - P_{e,fb})\left(\frac{P}{N_0}\right)^{1-\alpha} + \frac{P}{N_0}P_{e,fb}\right) \end{aligned} \quad (72)$$

where (72) is obtained by plugging in $B = \alpha(M-1)\log_2 \frac{P}{N_0}$ bits for quantization.

We notice that choosing $1 < \alpha < \beta_{\text{fb}}$ yields a vanishing rate gap for $\frac{P}{N_0} \rightarrow \infty$, as in the case of perfect CSIR and error-free feedback. This is because the feedback error probability decays exponentially with $(P/N_0)^{1-\frac{\alpha}{\beta_{\text{fb}}}}$ (see (67)), so that the term $\frac{P}{N_0}P_{e,fb}$ vanishes as $\frac{P}{N_0} \rightarrow \infty$ for all $\alpha < \beta_{\text{fb}}$, while obviously $(P/N_0)^{1-\alpha}$ vanishes for all $\alpha > 1$.

For the sake of completeness, the general expression for the rate gap upper bound for imperfect CSIR (finite β_1 and β_2) is given by:

$$\overline{\Delta R}^{\text{DF-ERRORS}} \leq \log\left(1 + \frac{1}{M\beta_2} + (1 - P_{e,fb})\left(\left(\frac{P}{N_0}\right)^{1-\alpha} + \frac{M-1}{M}\frac{1}{\beta_1}\right) + \frac{P}{N_0}P_{e,fb}\right). \quad (73)$$

Also in this case, the effect of channel feedback vanishes if we choose $1 < \alpha < \beta_{\text{fb}}$ but, as for error-free digital feedback, the rate gap does not vanish due to the imperfect CSIR.

A number of simple improvements are possible. For example, each UT may estimate its interference coefficients $\{a_{k,j} : j \neq k\}$ from the dedicated training phase, and decide if its feedback message was correctly received or was received in error by setting a threshold on the interference power: if the interference power is of the same order of $(M-1)P$, then it is likely that a feedback error occurred. If, on the contrary, it is of the order of $2^{-B/(M-1)}P$, then it is likely that the feedback message was correctly received. Interestingly, for $B = \alpha(M-1)\log_2 \frac{P}{N_0}$ with

$\alpha > 1$, detecting feedback error events becomes easier and easier as $\frac{P}{N_0}$ increases and/or as the number of antennas M increases. In brief, for a large number of antennas any terminal whose feedback message was received in error is completely drowned into interference and should be able to easily detect this fact. Assuming that the UTs can perfectly detect their own feedback error event, then they can simply discard the slots corresponding to feedback errors. The resulting achievable rate in this case is lowerbounded by

$$R_k^{\text{DF-ERRORS-DETECT}} \geq (1 - P_{e,fb}) \left[R_k^{\text{ZF}} - \log \left(1 + \frac{1}{M\beta_2} + \frac{M-1}{M} \frac{1}{\beta_1} + \left(\frac{P}{N_0} \right)^{1-\alpha} \right) \right] \quad (74)$$

in light of (58) and of Corollary 3.1. Note that this rate lies between the achievable rate lower bound in the case of no error detection (i.e., (73)) and the genie-aided upper bound from Theorem 3.

Remark 7.1: We notice here that the naive ZF strategy examined in this paper is *robust to feedback errors* in the following sense: the residual interference experienced by a given UT depends only on that particular UT feedback error probability. Therefore, a small number of users with poor feedback channel quality (very high feedback error probability) do not destroy the overall system performance. This observation goes against the conventional wisdom that feedback errors are “catastrophic”. Based on this wisdom, the feedback bits are heavily coded in current practice. On the contrary, our results show that very light coding is sufficient. \diamond

Remark 7.2: Although the rate gap vanishes as $\frac{P}{N_0} \rightarrow \infty$ for any $1 < \alpha < \beta_{\text{fb}}$, the asymptotics can set in very slowly and it is important to optimize α at finite SNR's. To minimize the rate gap bound in (72), we propose that the right hand side of the following be minimized:

$$(1 - P_{e,fb}) \left(\frac{P}{N_0} \right)^{-\alpha} + P_{e,fb} \leq \left(\frac{P}{N_0} \right)^{-\alpha} + 2\beta_{\text{fb}}(M-1) \exp \left(-\frac{3}{2} \left(\frac{P}{N_0} \right)^{1-\frac{\alpha}{\beta_{\text{fb}}}} \right) \quad (75)$$

Setting the derivative with respect to α equal to zero, we obtain the solution:

$$\alpha^* = \beta_{\text{fb}} \frac{W \left(\frac{1}{2(\beta_{\text{fb}}-1)} (3P/N_0)^{\frac{\beta_{\text{fb}}}{\beta_{\text{fb}}-1}} (M-1)^{1/(\beta_{\text{fb}}-1)} \right)}{\log(P/N_0)} - \frac{\beta_{\text{fb}}}{\beta_{\text{fb}}-1} \frac{\log(3(M-1)P/N_0)}{\log(P/N_0)} \quad (76)$$

where $W(\cdot)$ is the Lambert-W function [57], defined by $x = W(x)e^{W(x)}$ for $x \in [-1/e, +\infty)$. The choice $\alpha = \alpha^*$ can be confirmed to yield a near-optimal rate gap for large $\frac{P}{N_0}$. Moreover, taking the limit of (76) as $\frac{P}{N_0} \rightarrow \infty$ we have that $\alpha^* \uparrow \beta_{\text{fb}}$. This fact can be expected from the observation that, for sufficiently large SNR, the term $\left(\frac{P}{N_0} \right)^{1-\alpha}$ due to the quantization error dominates over the term $\frac{P}{N_0} P_{e,fb}$ due to channel feedback errors. Therefore, the optimal α is expected to grow towards β_{fb} as $\frac{P}{N_0}$ increases. On the contrary, as shown in the numerical results below, α^* must be significantly smaller than β_{fb} for practical (finite) $\frac{P}{N_0}$. This is due to the behavior of the term $\frac{P}{N_0} P_{e,fb}$ inside the $\log(\cdot)$ in the rate gap upper bound (72).

The optimization of α in the case of feedback error detection (the rate in (74)) yields rather different results. In fact, the factor $1 - P_{e,fb}$ converges very quickly to 1 for any fixed $\alpha < \beta_{\text{fb}}$ and for increasing SNR. Therefore, it is convenient to make α large but strictly smaller than β_{fb} in order to have the quantization error $\left(\frac{P}{N_0} \right)^{1-\alpha}$ vanish rapidly as SNR increases. \diamond

Fig. 5 shows the lower bounds based on (72) as well as the bound with ideal feedback error detection (74) of digital feedback with QAM feedback transmission for $M = 4$, $\beta_{\text{fb}} = 2$ for different values of α . For a reference, we also show the performance achieved by ZF with perfect CSIT (32). We assume perfect CSIR for all schemes. It is clear that the achievable rate lower bound (without error detection) depends critically on the value of α : choosing $\alpha \approx \beta_{\text{fb}}$ leads to a very large error probability and thus a very large rate gap, while choosing $\alpha = 1.1$ leads to a small error probability and reasonable performance. Note that for any $\alpha < \beta_{\text{fb}}$ (including $\alpha = 1.7$) the lower bound converges absolutely to the perfect CSI throughput as $\text{SNR} \rightarrow \infty$, but this convergence is clearly very slow. In contrast, the system is considerably less sensitive to the choice of α if ideal feedback error detection is assumed. This behavior is to be expected because the multi-user interference is essentially impulsive: with probability $1 - P_{e,fb}$ it has very small power (i.e., $\left(\frac{P}{N_0} \right)^{1-\alpha}$) while with probability $P_{e,fb}$ it has power of order P . The lower bound corresponds to the case where the receiver does not know where the impulses occur, while the error detection lower bound assumes that the impulses can be identified and the corresponding received symbols are discarded.

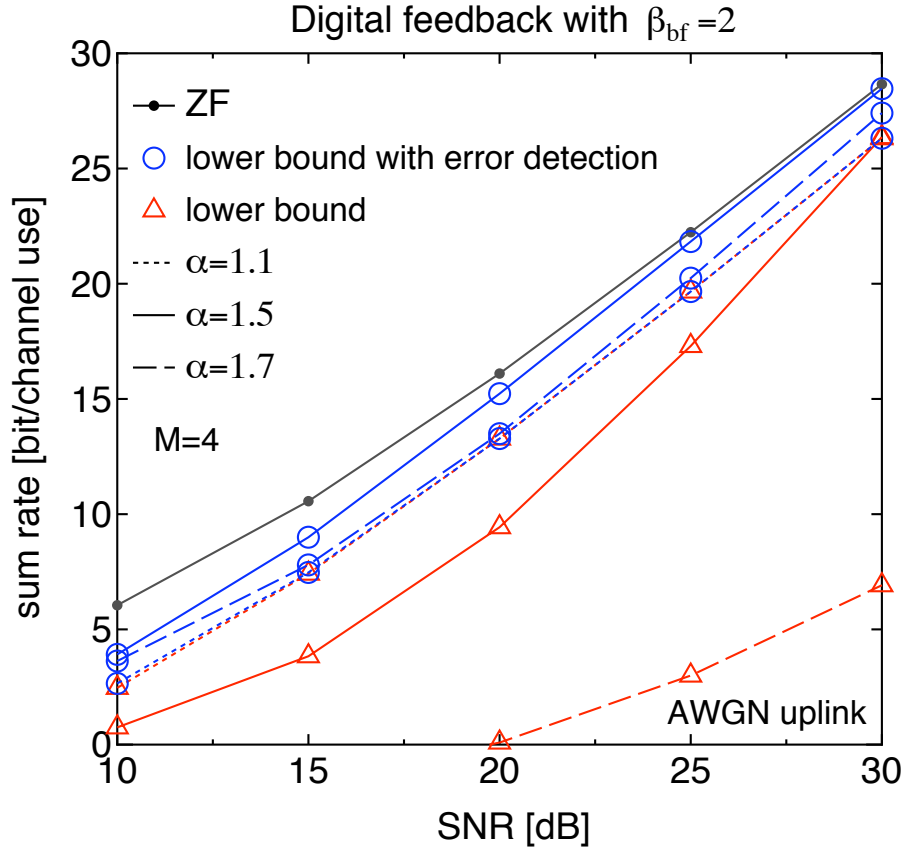


Fig. 5. Digital feedback with QAM modulation - Effect of α with $\beta_{fb} = 2$.

Fig. 6 compares analog feedback with digital feedback based on QAM modulation as a function of β_{fb} for $M = 4$ and $SNR = 10, 20$ dB by assuming perfect CSIR; this figure is analogous to Figure 4 except that we consider QAM-transmission over the feedback channel rather than assuming error-free digital feedback. For each feedback scheme, we plot the achievable rate lower bound (based on the rate gap expressions (43) and (72) for analog and digital respectively) as well as the genie-aided bound of Theorem 3 along with ZF with perfect CSIT (32). For digital feedback, we also show the lower bound with ideal feedback error detection (74). For each bound with digital feedback, the value of α is numerically optimized for each value of SNR and β_{fb} . The optimized values for the rate gap (72) agree well with those found analytically by (76).

At an SNR of 20dB, the genie-aided upper bound and the rate with error detection are virtually identical and cross the analog upper bound at $\beta_{fb} = 1.75$, while the digital feedback lower bound crosses over at $\beta_{fb} = 2$. Compared to error-free digital feedback (Fig. 4) at 20 dB, we notice that the introduction of feedback errors increase the crossover point slightly. Furthermore, while $\beta_{fb} \geq 2$ essentially corresponds to perfect feedback (i.e., a rate essentially equal to R_k^{ZF}) for error-free feedback, the introduction of feedback errors pushes this point to $\beta_{fb} \geq 3$. Generally speaking, feedback errors have a non-negligible but not overwhelming effect at 20 dB.

On the other hand, behavior is rather different at a moderate SNR of 10dB. Here we see that the genie-aided bound for digital feedback equals that for analog feedback at $\beta_{fb} = 3$, while the digital lower bound does not meet analog until $\beta_{fb} = 3.5$. In contrast, the cross-over points occur for β_{fb} between 1.5 and 2 for error-free digital feedback (Fig. 4). Furthermore, while $\beta_{fb} \geq 3$ corresponds to essentially perfect feedback in the case of no errors (for either the lower bound or the genie-aided upper bound), with errors there is still a gap between the perfect CSI rate and the genie-aided upper bound at $\beta_{fb} = 4$.

Feedback errors appear to have a considerably more significant effect at lower SNR's. There appear to be two fundamental reasons for this. First, note that uncoded QAM performs considerably better at higher SNR, in the sense that the symbol error probability decreases with SNR (and in fact goes to zero) for any $\alpha < \beta_{fb}$. For example, for $\alpha = .5\beta_{fb}$ the symbol error probability of QAM (with $.5\log_2 \frac{P}{N_0}$ bits per QAM symbol) is approximately 2×10^{-3} and 10^{-8} at SNR's of 10 and 20 dB, respectively. In addition, at higher SNR's choosing α only slightly larger than

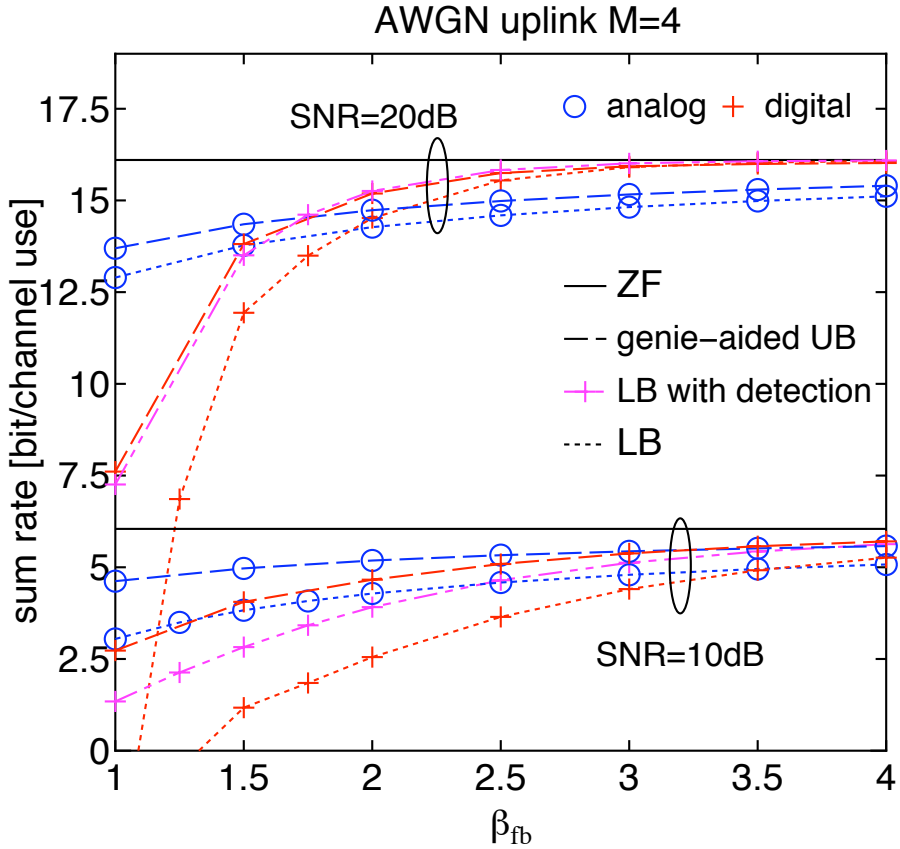


Fig. 6. Comparison as a function of β_{fb} over an AWGN feedback link with QAM transmission for $M = 4$.

1 almost completely eliminates distortion in the feedback link in the case of no feedback error, while a larger α is required at lower SNR's due to the $\left(\frac{P}{N_0}\right)^{1-\alpha}$ dependence. While these conclusions and interpretations have been drawn for the simple uncoded QAM scheme proposed here, it remains to be seen how these might change if more intelligent joint source-channel codes are used.

Finally we note that there is a substantial difference between the lower bound and the scheme incorporating some error detection mechanism for digital feedback and smaller values of β_{fb} . This is to be expected, given the impulse-noise interpretation given earlier.

VIII. CHANNEL STATE FEEDBACK ON THE MIMO-MAC

In this section we consider a more realistic and at the same time more efficient scheme for the channel state feedback channel. Although conceptually simple, orthogonal access in the feedback link requires $O(M^2)$ channel uses for the feedback, while the downlink capacity is at best $O(M)$. When the number of antennas M grows large, such a system would not scale well with M . On the other hand, the inherent MIMO-MAC nature of the physical uplink channel⁸ suggests an alternative approach, where multiple UT's simultaneously transmit on the MIMO uplink (feedback) channel and the spatial dimension is exploited for channel state feedback too. This idea was considered for an FDD system in [27] and analyzed in terms of the mean square error of the channel estimate provided to the BS.

As in [27], we partition the M users into $\frac{M}{L}$ groups of size L , and let UTs belonging to the same group transmit their feedback signal simultaneously, in the same time slot. Each UT transmits its M channel coefficients over $\beta_{fb}M$ channel uses, with $\beta_{fb} \geq 1$. Therefore, each group uses $\beta_{fb}M$ channel symbols and the total number of channel uses spent in the feedback is $\beta_{fb} \frac{M^2}{L}$. Clearly, by choosing $L \propto M$ (e.g., $L = M/2$) the resulting system is scalable with the number of antennas, and the feedback redundancy converges to a fixed fraction of the downlink capacity.

⁸From the UTs to the BS, assuming that the BS antennas are used for both transmission and reception.

We assume that the uplink feedback channel is affected by i.i.d. block fading (i.e., has the same distribution as the downlink channel) and that there is no feedback delay.

With respect to the analysis provided in [27], the present work differs in a few important aspects: 1) we consider both analog and digital feedback; 2) although our analog feedback model is essentially identical to the FDD scheme of [27], we consider optimal MMSE estimation rather than Least-Squares estimation (zero-forcing pseudo-inverse); 3) we put out results in the context of the rate gap framework, that yields directly fundamental lower bounds on achievable rates, rather than in terms of channel state estimation error.

A. Analog Feedback

In an analog feedback scheme, recall that each UT feeds back the noisy version of its downlink channel, given by $\frac{\sqrt{\beta_{\text{fb}}P}}{\sqrt{\beta_1P+N_0}} \mathbf{s}_k$ where $\mathbf{s}_k = \sqrt{\beta_1P}\mathbf{h}_k + \mathbf{z}_k$ is the observation provided by the common training phase, defined in (4). Given the symmetry of the problem, we can focus on the transmission of a single group of L UTs. Let $\mathbf{A} = [\mathbf{a}_1 \cdots \mathbf{a}_L] \in \mathbb{C}^{M \times L}$ be the uplink fading matrix for this group of UTs (with i.i.d. entries, $\sim \mathcal{CN}(0, 1)$) and let for $k = 1, \dots, L$

$$b_{k,j} = \frac{\sqrt{\beta_{\text{fb}}P}}{\sqrt{\beta_1P+N_0}} s_{k,j} = \frac{\sqrt{\beta_{\text{fb}}\beta_1P}}{\sqrt{\beta_1P+N_0}} h_{k,j} + \frac{\sqrt{\beta_{\text{fb}}P}}{\sqrt{\beta_1P+N_0}} z_{k,j} \quad (77)$$

denote the transmitted symbol by UT k for its j -th channel coefficient, where $s_{k,j}$ is the noisy observation of $h_{k,j}$ and $z_{k,j}$ is AWGN. For simplicity, we assume that the BS has perfect knowledge of the uplink channel state \mathbf{A} ; we later consider the more general case and see that the main conclusions are unchanged.

The M -dimensional received vector \mathbf{g}_j , upon which the BS estimates $h_{1,j}, \dots, h_{L,j}$, is given by:

$$\mathbf{g}_j = \sum_{i=1}^L \mathbf{a}_i b_{i,j} + \tilde{\mathbf{w}}_j = \mathbf{A}\mathbf{b}_j + \tilde{\mathbf{w}}_j \quad (78)$$

where $\tilde{\mathbf{w}}_j$ is an AWGN vector with i.i.d. elements $\sim \mathcal{CN}(0, N_0)$. Since both the UT downlink channels \mathbf{h}_j and the observation noises \mathbf{z}_j and $\tilde{\mathbf{w}}_j$ contain i.i.d. elements, it follows that the (optimal) MMSE estimator for the downlink channel coefficient $h_{k,j}$ (from BS antenna j to UT k) is given by

$$\hat{h}_{k,j} = \mathbb{E}[h_{k,j}\mathbf{g}_j^H]\mathbb{E}[\mathbf{g}_j\mathbf{g}_j^H]^{-1}\mathbf{g}_j = c \mathbf{a}_k^H \left[\beta_{\text{fb}}P\mathbf{A}\mathbf{A}^H + N_0\mathbf{I} \right]^{-1} \mathbf{g}_j \quad (79)$$

where we let, for brevity, $c = \frac{\sqrt{\beta_{\text{fb}}\beta_1P}}{\sqrt{\beta_1P+N_0}}$. The corresponding MMSE, for given feedback channel matrix \mathbf{A} , is given by

$$\sigma_k^2(\mathbf{A}) = 1 - c^2 \mathbf{a}_k^H \left[\beta_{\text{fb}}P\mathbf{A}\mathbf{A}^H + N_0\mathbf{I} \right]^{-1} \mathbf{a}_k \quad (80)$$

From the symmetry of the system we see that $\mathbb{E}[\sigma_k^2(\mathbf{A})]$ does not depend on k . Hence, after cumbersome but otherwise straightforward algebra, we obtain

$$\begin{aligned} \mathbb{E}[\sigma_k^2(\mathbf{A})] &= \mathbb{E} \left[\frac{1}{L} \text{tr} \left(\mathbf{I} - c^2 \mathbf{A}^H \left[\beta_{\text{fb}}P\mathbf{A}\mathbf{A}^H + N_0\mathbf{I} \right]^{-1} \mathbf{A} \right) \right] \\ &= \mathbb{E} \left[\frac{1}{L} \sum_{k=1}^L \frac{N_0 + (\beta_{\text{fb}}P - c^2)\lambda_k}{N_0 + \beta_{\text{fb}}P\lambda_k} \right] \\ &= \frac{1}{1 + \beta_1 \frac{P}{N_0}} + \frac{\beta_1 \frac{P}{N_0}}{1 + \beta_1 \frac{P}{N_0}} \text{mmse} \left(\beta_{\text{fb}} \frac{P}{N_0} \right) \end{aligned} \quad (81)$$

where we define the average channel state information estimation MMSE as

$$\text{mmse}(\rho) \triangleq \frac{1}{L} \sum_{k=1}^L \mathbb{E} \left[\frac{1}{1 + \rho\lambda_k} \right] \quad (82)$$

and where $\{\lambda_1, \dots, \lambda_L\}$ denote the eigenvalues of the $L \times L$ central Wishart matrix $\mathbf{A}\mathbf{A}^H$.

Using well-known results from multivariate statistics (see for example [65]), we can obtain the closed-form expression

$$\text{mmse}(\rho) = \frac{e^{1/\rho}}{\rho} \sum_{k=0}^{L-1} \sum_{\ell=0}^k \sum_{m=0}^{2\ell} X_{k,\ell,m} E_i(M-L+m+1, 1/\rho) \quad (83)$$

where the coefficients $X_{k,\ell,m}$ are given by

$$X_{k,\ell,m} = \frac{(-1)^m (2\ell)! (M-L+m)!}{L 2^{2k-m} \ell! m! (M-L+\ell)!} \binom{2(k-\ell)}{k-\ell} \binom{2(M-L+\ell)}{2\ell-m}$$

For later use, we provide here the asymptotic behavior of the product $\rho \text{mmse}(\rho)$ for $\rho \rightarrow \infty$. Using the asymptotic expansion of $e^{1/\rho} E_i(n, 1/\rho)$, we have

$$\rho \text{mmse}(\rho) = \begin{cases} \frac{1}{M-L} + o(1) & \text{for } L < M \\ -\gamma + \log \rho + \sum_{k=0}^{L-1} \sum_{\ell=0}^k \sum_{m=1}^{2\ell} \frac{X_{k,\ell,m}}{m} + o(1) & \text{for } L = M \end{cases} \quad (84)$$

where we used the facts:

$$E_i(1, 1/\rho) e^{1/\rho} = -\gamma + \log \rho + o(1), \quad \rho \rightarrow \infty \quad (85)$$

$$E_i(n, 1/\rho) e^{1/\rho} = \frac{1}{n-1} + o(1), \quad \text{for } n > 1, \rho \rightarrow \infty \quad (86)$$

$$\sum_{k=0}^{L-1} \sum_{\ell=0}^k \sum_{m=0}^{2\ell} \frac{X_{k,\ell,m}}{M-L+m} = \frac{1}{M-L}, \quad \text{for } L < M \quad (87)$$

$$\sum_{k=0}^{L-1} \sum_{\ell=0}^k X_{k,\ell,0} = 1, \quad \text{for } L = M \quad (88)$$

Following the same steps as in (44), we can write the interference power as

$$\begin{aligned} \mathbb{E}[|I_k|^2] &= \left(\frac{M-1}{M}\right) P \mathbb{E}[\sigma_k^2(\mathbf{A})] \\ &= \left(\frac{M-1}{M}\right) P \left[\frac{1}{1 + \frac{\beta_1 P}{N_0}} + \frac{\frac{\beta_1 P}{N_0}}{1 + \frac{\beta_1 P}{N_0}} \text{mmse}\left(\frac{\beta_{\text{fb}} P}{N_0}\right) \right] \end{aligned} \quad (89)$$

By using (89) in the rate gap expression of Theorem 2, we obtain

$$\overline{\Delta R}_{\text{MIMO-MAC}}^{\text{AF}} = \log \left(1 + \frac{1}{M} \frac{\frac{P}{N_0}}{1 + \beta_2 \frac{N_0}{P}} + \frac{M-1}{M} \frac{P}{N_0} \left[\frac{1}{1 + \frac{\beta_1 P}{N_0}} + \frac{\frac{\beta_1 P}{N_0}}{1 + \frac{\beta_1 P}{N_0}} \text{mmse}\left(\frac{\beta_{\text{fb}} P}{N_0}\right) \right] \right) \quad (90)$$

At this point, using the asymptotic expression (84), we obtain that for $L < M$ the rate gap is bounded and for high SNR converges to the constant

$$\lim_{P \rightarrow \infty} \overline{\Delta R}_{\text{MIMO-MAC}}^{\text{AF}} = \log \left(1 + \frac{1}{\beta_2 M} + \frac{M-1}{M} \left(\frac{1}{\beta_1} + \frac{1}{\beta_{\text{fb}}(M-L)} \right) \right) \quad (91)$$

Comparing this expression to the rate gap for analog feedback over an AWGN channel (45), we notice that an SNR (array) gain of $M-L$ is achieved (on the feedback channel) when the feedback is performed over the MIMO MAC because the feedback (of L users) is received over M antennas. In addition, a factor of L fewer feedback symbols are required when the feedback is performed over the MIMO MAC ($\beta_{\text{fb}} \frac{M^2}{L}$ vs. $\beta_{\text{fb}} M^2$). On the other hand, using the second line of the RHS of (84) it is immediate to show that for $L = M$ the rate gap grows unbounded as $\log \log \left(\frac{P}{N_0} \right)$.

From (91) we can optimize the value of L (assuming $L < M$) for a fixed number of feedback channel uses, which we denote by aM for some $a \geq 2$ (if $L < M$ there must be at least two groups and thus we must have at least $2M$ feedback symbols). Recall that the total number of channel uses, in terms of β_{fb} and group size L , is $\beta_{\text{fb}} \frac{M^2}{L}$. By letting $aM = \beta_{\text{fb}} \frac{M^2}{L}$ we obtain

$$\beta_{\text{fb}} = a \frac{L}{M}.$$

Using this expression in (91), we see that minimizing the rate gap bound is equivalent to maximizing the term $L(M - L)$ for fixed M and $L < M$. This is a parabola with downward concavity, whose maximum is reached at $L^* = \frac{M}{2}$. Substituting this value in (91) yields

$$\log \left(1 + \frac{1}{\beta_2 M} + \frac{2(M-1)}{M^2 \beta_{\text{fb}}} + \frac{M-1}{M} \frac{1}{\beta_1} \right) \quad (92)$$

where the total number of feedback symbols aM is $2\beta_{\text{fb}}$. Notice that the residual interference caused by channel estimation at the UTs (common training, β_1) is the most relevant among the three terms in (92).

In the case where the total number of feedback symbols is strictly smaller than $2M$ (i.e., $1 \leq a < 2$), choosing $L = M$ with $\beta_{\text{fb}} = a$ is the only option. Although this choice yields an unbounded rate gap, it does provide reasonable performance at finite SNR's. When $a \geq 2$ we could again choose $L = M$, but numerical results verify that also at finite SNR the choice $L^* = \frac{M}{2}$ outperforms $L = M$ in terms of the lower bound and the genie-aided upper bound. It follows that the optimal MIMO-MAC feedback strategy is a combination of TDMA and SDMA.

A legitimate question at this point is the following: is the condition $L < M$ a fundamental limit of the MIMO-MAC analog feedback in order to achieve a bounded rate gap, or is it due to the looseness of Theorem 2? In order to address this question, we examine the genie-aided rate upper bound of Theorem 3. Recall that the rate upper bound (33) is achievable under the assumption that the UTs have perfect knowledge of the interference coefficients.

From Theorem 3, and following steps similar to the proof of Theorem 2, we have that

$$\begin{aligned} I(u_k; y_k, \mathcal{A}_k) &= \mathbb{E} \left[\log \left(1 + \frac{|a_{k,k}|^2 P / (N_0 M)}{1 + \sum_{j \neq k} |a_{k,j}|^2 P / (N_0 M)} \right) \right] \\ &\geq R_k^{\text{ZF}} - \mathbb{E} \left[\log \left(1 + \sum_{j \neq k} |a_{k,j}|^2 \frac{P}{N_0 M} \right) \right] \end{aligned} \quad (93)$$

$$\geq R_k^{\text{ZF}} - \mathbb{E} \left[\log \left(1 + \sum_{j \neq k} \mathbb{E}[|a_{k,j}|^2 | \mathbf{A}] \frac{P}{N_0 M} \right) \right] \quad (94)$$

where (94) follows by conditioning with respect to the uplink channel matrix \mathbf{A} and then applying Jensen's inequality in the inner conditional expectation.

Using the decomposition $\mathbf{h}_k = \hat{\mathbf{h}}_k + \mathbf{n}_k$ following from MMSE channel estimation as given in (79), we arrive at the bound

$$R_k^{\text{ZF}} - I(u_k; y_k, \mathcal{A}_k) \leq \mathbb{E} \left[\log \left(1 + \frac{P}{N_0} \frac{M-1}{M} \sigma_k^2(\mathbf{A}) \right) \right] \quad (95)$$

where $\sigma_k^2(\mathbf{A})$ is defined in (80) and where now \mathbf{A} is an $M \times M$ matrix (we consider here the case $L = M$). By symmetry it is clear that the right-hand side of (95) is independent of k . Hence, using again Jensen's inequality, we have

$$\begin{aligned} R_k^{\text{ZF}} - I(u_k; y_k, \mathcal{A}_k) &\leq \frac{1}{M} \sum_{k=1}^M \mathbb{E} \left[\log \left(1 + \frac{P}{N_0} \frac{M-1}{M} \sigma_k^2(\mathbf{A}) \right) \right] \\ &\leq \mathbb{E} \left[\log \left(1 + \frac{P}{N_0} \frac{M-1}{M} \frac{1}{M} \sum_{k=1}^M \sigma_k^2(\mathbf{A}) \right) \right] \\ &\stackrel{(a)}{=} \mathbb{E} \left[\log \left(1 + \frac{P}{N_0} \frac{M-1}{M} \left(\frac{1}{1 + \beta_1 \frac{P}{N_0}} + \frac{\beta_1 \frac{P}{N_0}}{1 + \beta_1 \frac{P}{N_0}} \frac{1}{M} \sum_{k=1}^M \frac{1}{1 + \beta_{\text{fb}} \frac{P}{N_0} \lambda_k} \right) \right) \right] \\ &\leq \mathbb{E} \left[\log \left(1 + \frac{M-1}{M} \left(\frac{1}{\beta_1} + \frac{\frac{P}{N_0}}{1 + \beta_{\text{fb}} \frac{P}{N_0} \lambda_{\min}} \right) \right) \right] \end{aligned} \quad (96)$$

where (a) follows by using the same derivation that leads to (81) and (82), and the last line follows by monotonicity of the log, where λ_{\min} denotes the minimum eigenvalue of $\mathbf{A}^H \mathbf{A}$.

Our goal is to show that the bound in (96) is bounded. To this purpose, we write the last line of (96) as the sum of three terms,

$$\log \left(1 + \frac{M-1}{M\beta_1} + \frac{M-1}{M} \frac{P}{N_0} \right) + \mathbb{E} \left[\log \left(1 + \frac{\left(1 + \frac{M-1}{M\beta_1}\right) \frac{\beta_{\text{fb}} P}{N_0}}{1 + \frac{M-1}{M} \left(\frac{1}{\beta_1} + \frac{P}{N_0} \right)} \lambda_{\min} \right) \right] - \mathbb{E} \left[\log \left(1 + \beta_{\text{fb}} \frac{P}{N_0} \lambda_{\min} \right) \right] \quad (97)$$

For \mathbf{A} $M \times M$, complex Gaussian with i.i.d. zero-mean components, it is well-known that λ_{\min} is chi-squared with 2 degrees of freedom and mean 1 [66]. Hence, the third term in (97) yields

$$\mathbb{E} \left[\log \left(1 + \beta_{\text{fb}} \frac{P}{N_0} \lambda_{\min} \right) \right] = e^{\frac{N_0}{\beta_{\text{fb}} P}} \text{E}_i \left(1, \frac{N_0}{\beta_{\text{fb}} P} \right) = -\gamma + \log \frac{\beta_{\text{fb}} P}{N_0} + o(1)$$

The second term in (97) is bounded by a constant, independent of P/N_0 , and finally the first term in (97), for high SNR, can be written as $\log \frac{P}{N_0} + O(1)$. It follows that the $\log(P/N_0)$ terms in the first and the third terms of the the upper bound cancel, so that (97) is bounded.

This suggests that if the UTs are able to obtain an estimate of their *instantaneous* residual interference level in each slot, up to M UTs can feedback their channel state information at the same time.

Remark 8.1: It is also possible to analyze the more realistic scenario where the uplink channel matrix is known imperfectly at the BS. We consider the following simple training-based scheme: the L UTs within a feedback group transmit a preamble of $\beta_{\text{up}} L$ training symbols, where $\beta_{\text{up}} \geq 1$ defines the uplink training length (per UT). Without repeating all steps in the details, the uplink channel \mathbf{A} admits the following decomposition:

$$\mathbf{A} = \widehat{\mathbf{A}} + \widetilde{\mathbf{A}} \quad (98)$$

where $\widehat{\mathbf{A}}$ is the MMSE channel estimate and $\widetilde{\mathbf{A}}$ is the estimation error, with i.i.d. components $\sim \mathcal{CN}(0, \sigma_{\text{up}}^2)$ matrix where

$$\sigma_{\text{up}}^2 = \frac{1}{1 + \beta_{\text{up}} \frac{P}{N_0}}.$$

Furthermore, $\widehat{\mathbf{A}}$ and $\widetilde{\mathbf{A}}$ are jointly Gaussian and independent, and $\widehat{\mathbf{A}}$ has i.i.d. components $\sim \mathcal{CN}(0, 1 - \sigma_{\text{up}}^2)$.

Now, the MMSE estimation of the downlink channel coefficients $h_{k,\ell}$ is conditional with respect to $\widehat{\mathbf{A}}$. By repeating all previous steps, after a cumbersome calculation that we do not report here for the sake of brevity, we obtain the average estimation error in the form

$$\mathbb{E}[\sigma_k^2(\widehat{\mathbf{A}})] = \frac{1}{1 + \beta_1 \frac{P}{N_0}} + \frac{\beta_1 \frac{P}{N_0}}{1 + \beta_1 \frac{P}{N_0}} \text{mmse} \left(\frac{\beta_{\text{up}} \frac{P}{N_0}}{1 + \beta_{\text{up}} \frac{P}{N_0} + L \beta_{\text{fb}} \frac{P}{N_0}} \frac{\beta_{\text{fb}} P}{N_0} \right) \quad (99)$$

where $\text{mmse}(\cdot)$ was defined in (82). By comparing (99) with (81), we notice that they differ only in the argument of the function $\text{mmse}(\cdot)$. The two expressions coincide for $\beta_{\text{up}} \rightarrow \infty$, consistent with the fact that $\beta_{\text{up}} \rightarrow \infty$ corresponds to perfect estimation of the channel matrix \mathbf{A} . Furthermore, for large SNR, the two arguments differ by a constant multiplicative factor. Hence, apart from this constant factor that depends on the uplink training parameter β_{up} , the conclusions about the rate gap obtained for the case of perfect uplink channel knowledge also hold for the case of training-based uplink channel estimation. \diamond

Remark 8.2: In [27], the same model in (77) for analog channel state feedback over the MIMO-MAC uplink channel is considered. Instead of the linear MMSE estimator considered here, a zero-forcing approach (via the pseudo-inverse of the matrix \mathbf{A}) is examined. In the case of $L = M$ this yields an infinite error variance, which does not make sense in light of the fact that each channel coefficient has unity variance. This odd behavior can be avoided by performing an additional component-wise MMSE step. As a matter of fact, performance very similar to what we have found for the full MMSE estimator can be obtained for $L < M$ by using a zero-forcing receiver for the channel state feedback, followed by individual (componentwise) MMSE scaling. We omit the analysis of this simplified channel state information estimator for the sake of brevity. \diamond

Fig. 7 shows both the genie-aided upper bound of Theorem 3 and the lower bound based on (90) of analog feedback over a fading MIMO-MAC for $M = 4$ and $L = 2, 4$. We assume perfect CSIR. We notice that for $L = 2$, the lower bound coincides with the genie-aided upper bound and comes very close to the performance of ZF with ideal CSIT. For $L = M$, the rate gap of the lower bound (90) is unbounded but the double logarithmic growth

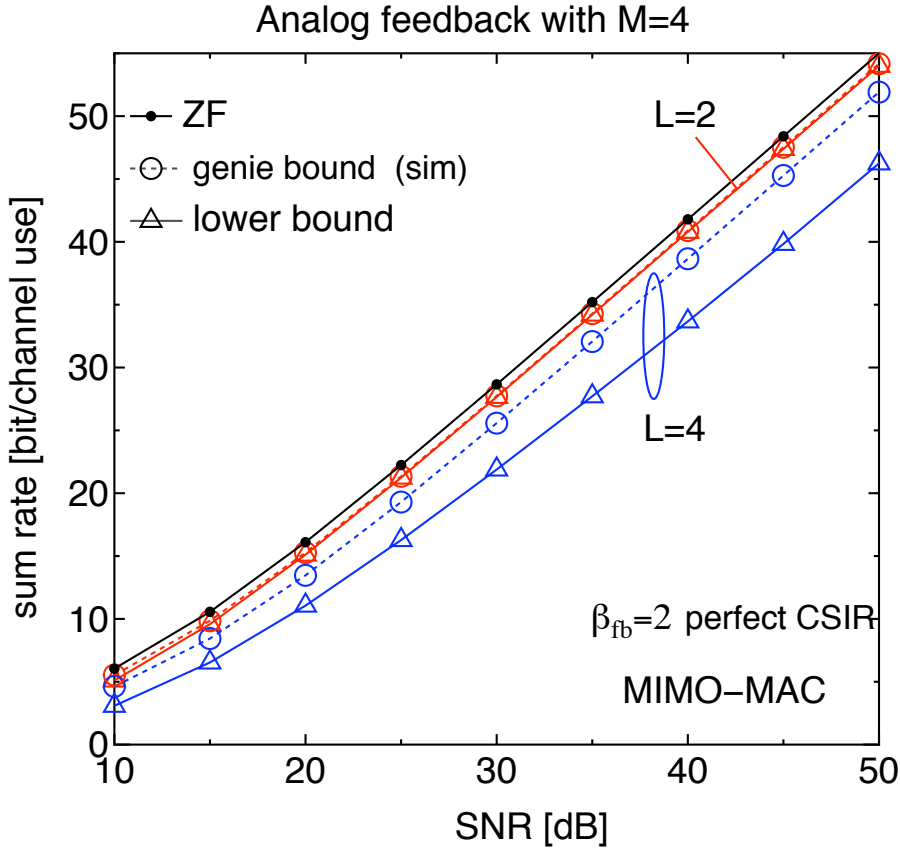


Fig. 7. Impact of L with analog feedback over MIMO-MAC

$\log \log(P/N_0)$ yields a surprisingly small gap. The genie-aided bound is able to maintain a constant rate gap even for $L = M$ in accordance with our earlier analysis. Although not shown here, a system using $L = 2$ and $\beta_{fb} = 1$ does outperform $L = 4$, $\beta_{fb} = 2$ (both configurations use a total of $2M$ feedback symbols) in terms of the lower bound and the genie-aided upper bound throughout the SNR range shown; this validates our earlier claim about the optimality of $L = \frac{M}{2}$ whenever at least $2M$ feedback symbols are used.

B. Digital Feedback

In the case of digital feedback, we let $L \leq M$ UTs multiplex their channel state feedback codewords at the same time. The resulting MIMO-MAC channel model is again given by (78), but now the vector \mathbf{b}_j contains the L feedback codewords (rather than the scaled UT estimates of the channel coefficients) of the L UTs sharing the same feedback slot. As in Section V, we assume that feedback messages of $\alpha(M-1) \log_2 \frac{P}{N_0}$ bits are sent in $\beta_{fb}(M-1)$ channel uses. Hence, the feedback symbols transmitted by the L UT's can be grouped in a $L \times \beta_{fb}(M-1)$ matrix, while the BS has an $M \times \beta_{fb}(M-1)$ observation upon which to estimate the transmitted symbols. We again assume each feedback symbol has average energy P .

Suppose that the BS receiver operates optimally, by using a bank of ML decoders for all the simultaneously transmitting UTs. The high-SNR error probability performance of the MIMO-MAC channel has been characterized in terms of diversity-multiplexing tradeoff in [67]. In particular, in a MIMO-MAC with i.i.d. channel fading (as defined here) and users transmitting with *multiplexing gain* r , i.e., with rate $r \log_2 \frac{P}{N_0}$ bits/symbol, the optimal ML decoder achieves an individual user average error probability

$$P_{e,fb} \doteq \left(\frac{P}{N_0} \right)^{-d^*(r)}$$

The “dot-equality” notation, introduced in [68], [67], indicates that $\lim_{P/N_0 \rightarrow \infty} \frac{-\log P_{e,fb}}{\log P/N_0} = d^*(r)$. The error probability SNR exponent $d^*(r)$ is referred to as the optimal *diversity gain*. Particularizing the results of [67]

to the case of $L \leq M$ users with 1 antenna each, transmitting to a receiver with M antennas, we have that the optimal diversity gain is given by

$$d^*(r) = \begin{cases} M(1-r) & \text{for } 0 \leq r \leq 1 \\ 0 & \text{otherwise} \end{cases} \quad (100)$$

This is the same exponent of a channel with a single user with a single antenna, transmitting to a receiver with M antennas (single-input multiple-output with receiver antenna diversity).⁹ In other words, under our system parameters, each UT achieves an error probability that decays with SNR as if TDMA on the feedback link was used (as if the UT transmitted its feedback message alone on the MIMO uplink channel). From what is said above, we have that the multiplexing gain of all UTs is given by $r = \frac{\alpha}{\beta_{fb}}$. Furthermore, from the derivation of Section VII, we require that $1 < \alpha < \beta_{fb}$. It follows that the average feedback error message probability in the MIMO-MAC fading channel is given by

$$P_{e,fb} = \left(\frac{P}{N_0} \right)^{-M(1-\alpha/\beta_{fb})} \times g \left(\frac{P}{N_0} \right) \quad (101)$$

where $g(x)$ is some sub-polynomial function, such that $\lim_{x \rightarrow \infty} x^{-\epsilon} g(x) = 0$ for all fixed $\epsilon > 0$.

If we examine the rate-gap expression with digital feedback (72) or (73), we see that we require $P_{e,fb}$ to go to zero at least as $\left(\frac{P}{N_0} \right)^{-1}$ in order to achieve a bounded rate gap. From (101) we see that for all $1 < \alpha < \beta_{fb}$ such that $M(1 - \alpha/\beta_{fb})$ is strictly larger than 1, the resulting rate gap is bounded and the effect of feedback errors vanishes. This imposes the condition $\beta_{fb} > \frac{M}{M-1}$ and $\alpha < \frac{M-1}{M} \beta_{fb}$, which is stricter than the condition $\beta_{fb} > 1$ and $\alpha < \beta_{fb}$ needed in the case of TDMA an unfaded feedback channel previously analyzed in Section VII.

We conclude that by using optimal coding over the MIMO-MAC feedback channel and by using an optimal ML decoder at the BS, a bounded rate gap can also be achieved with digital feedback. In this way, a system that uses a number of feedback channel uses that scales linearly with the number of the BS antennas M is achievable also with digital feedback.

At this point, we would like to notice that achieving the optimal diversity gain $d^*(r)$ on the MIMO-MAC is not easy in terms of system implementation. First, optimal coding for the MIMO-MAC is still at an early stage. The achievability result in [67] is obtained using a Gaussian random coding argument and requires coding block length not smaller than $L + M - 1$ (in our case, this imposes the additional, not very stringent, constraint $\beta_{bf} \geq 1 + \frac{L}{M-1}$). Clearly, random codes are not suited for efficient ML decoding. Therefore, lattice and other structured codes for the MIMO-MAC have been investigated in some recent works [69]. Nevertheless, these code constructions are not straightforward. Furthermore, the required ML decoder typically makes use of some lattice-based tree search, as the class of decoders presented in [70]. Although simpler than exhaustive search, these decoders are still considered quite prohibitive for practical implementation.

Driven by these considerations, we investigate a very simple scheme directly related to the uncoded QAM digital feedback approach analyzed in Section VII. Perhaps surprisingly, we shall see that the main conclusions hold unchanged even for this simple scheme, although the conditions on α and β_{bf} are more stringent.

In the proposed suboptimal scheme, each group of L simultaneously transmitting UTs sends its feedback message by using plain uncoded QAM modulation. The receiver is based on a spatial ZF linear filter, that separates the L codewords, followed by independent symbol-by-symbol detectors. The diversity-multiplexing gain tradeoff of this type of architecture was recently investigated in [71], where both ZF and MMSE linear receivers are analyzed. It is shown that both receivers achieve the same diversity gain, although at fixed rate and finite SNR the MMSE receiver achieves much better performance. Nevertheless, we investigate here the ZF receiver since its analysis with QAM modulation can be given in closed form for non-asymptotically large SNR. This provides an upper bound on the rate gap performance of schemes based on linear detection and independent decoding of the feedback messages.

⁹In [67] it is shown that each user can achieve its single-user diversity gain whenever the systems is in the lightly-loaded regime (i.e., whenever r is sufficiently small), but a smaller diversity gain is generally achieved when in the heavily-loaded regime (large r). In the case when $L < M$, the MAC is in the lightly-loaded regime for any $0 \leq r \leq 1$ and thus it easily follows that each user achieves diversity gain $M(1-r)$. When $L = M$, the lightly-loaded regime only corresponds to $0 \leq r \leq \frac{M}{M+1}$. However, it can easily be confirmed that the optimal diversity gain while in the heavily-loaded regime ($\frac{M}{M+1} \leq r \leq 1$) is also equal to the single-user diversity $M(1-r)$ in the case when each transmitter (UT) has one antenna and the number of transmitters is equal to the number of receive antennas.

Consider the channel model (78) where $b_{i,j}$ is the j -th QAM symbol (with energy per symbol equal to P) transmitted by UT i . The BS receiver multiplies the received signal by the channel pseudo-inverse matrix, $\mathbf{A}^+ = (\mathbf{A}^\mathsf{H} \mathbf{A})^{-1} \mathbf{A}^\mathsf{H}$, which exists in this form with probability 1 since $L \leq M$. The resulting observation at the input of the QAM detector for UT k , symbol ℓ , is given by

$$g_{k,\ell} = b_{k,\ell} + [\mathbf{A}^+ \tilde{\mathbf{w}}_\ell]_k \quad (102)$$

where $b_{k,\ell}$ is the QAM symbol, $\tilde{\mathbf{w}}_\ell$ is the ℓ -th column of $\tilde{\mathbf{W}}$ and $[\cdot]_k$ selects the k -th component of the vector inside the square brackets. It is well-known [72] that the noise term $[\mathbf{A}^+ \tilde{\mathbf{w}}_\ell]_k$ is Gaussian for given \mathbf{A} , with conditional distribution $\mathcal{CN}(0, N_0/\chi)$, where $\chi = \frac{1}{[(\mathbf{A}^\mathsf{H} \mathbf{A})^{-1}]_{k,k}}$ denotes a central chi-squared random variable with $2(M-L+1)$ degrees of freedom and mean $M-L+1$. Thus, each UTs effectively sees a feedback channel with a per-symbol SNR given by $\chi \left(\frac{P}{N_0} \right)$. The QAM symbol error probability, conditioned with respect to the channel gain χ , is upperbounded by

$$P_s(\chi) \leq 2 \exp \left(-\frac{3}{2} \chi \left(\frac{P}{N_0} \right)^{1-\alpha/\beta_{\text{fb}}} \right).$$

The conditional probability of feedback message error is

$$P_{e,fb}(\chi) = 1 - (1 - P_s(\chi))^{\beta_{\text{fb}}(M-1)} \leq \beta_{\text{fb}}(M-1)P_s(\chi)$$

Finally, using the characteristic function of χ , we obtain the Chernoff union bound for the average probability of feedback error in the form:

$$\begin{aligned} P_{e,fb} &= \mathbb{E}[P_{e,fb}(\chi)] \\ &\leq 2\beta_{\text{fb}}(M-1)\mathbb{E} \left[\exp \left(-\frac{3}{2} \chi \left(\frac{P}{N_0} \right)^{1-\alpha/\beta_{\text{fb}}} \right) \right] \\ &= \frac{2\beta_{\text{fb}}(M-1)}{\left[1 + \frac{3}{2} \left(\frac{P}{N_0} \right)^{1-\alpha/\beta_{\text{fb}}} \right]^{M-L+1}} \\ &= O \left(\left(\frac{P}{N_0} \right)^{-(1-\alpha/\beta_{\text{fb}})(M-L+1)} \right). \end{aligned} \quad (103)$$

The key difference from the AWGN case studied in Section VII is that the probability of feedback error now vanishes only polynomially rather than exponentially with (average SNR) $\frac{P}{N_0}$. Notice also the suboptimality of this simple approach with respect to an optimal MIMO-MAC strategy: before we obtained the optimal diversity gain of $M(1-\alpha/\beta_{\text{fb}})$ while this simple strategy achieves a diversity gain only equal to $(M-L+1)(1-\alpha/\beta_{\text{fb}})$. The interpretation for the achieved diversity is straightforward: the spatial ZF filter creates a separate $1 \times (M-L+1)$ (single-input, multiple-output) feedback channel for each UT, for which the optimal diversity order [68] is indeed equal to $(M-L+1)(1-r)$, with $r = \alpha/\beta_{\text{fb}}$ in our case.

Using (103) in the rate gap expressions (72) or (73), we can characterize the achievable rate under this simple MIMO-MAC strategy. It follows from direct inspection of the bounds that the rate gap is bounded if $\alpha > 1$ and $(M-L+1)(1-\alpha/\beta_{\text{fb}}) > 1$. These conditions can be satisfied only if $L < M$ and $\beta_{\text{fb}} > \frac{M-L+1}{M-L}$, and α is chosen to satisfy

$$\alpha < \beta_{\text{fb}} \frac{M-L}{M-L+1} \quad (104)$$

which is more restrictive than both the AWGN case and the optimal MIMO-MAC case.

Furthermore, while in the AWGN case the term $\frac{P}{N_0} P_{e,fb}$ in the rate gap expression vanishes rapidly (faster than polynomially, in P/N_0), in this case it vanishes only polynomially, as $(P/N_0)^{1-(1-\alpha/\beta_{\text{fb}})(M-L+1)}$. Thus, for finite SNR the rate gap may be significantly larger than in the case of unfaded feedback channel. Finally, the same observations about detecting feedback errors at the UTs and discarding the corresponding slots done at the end of Section VII apply here. For example, a rate lower bound identical to (74) applies by replacing the appropriate expression for the average feedback message error probability $P_{e,fb}$.

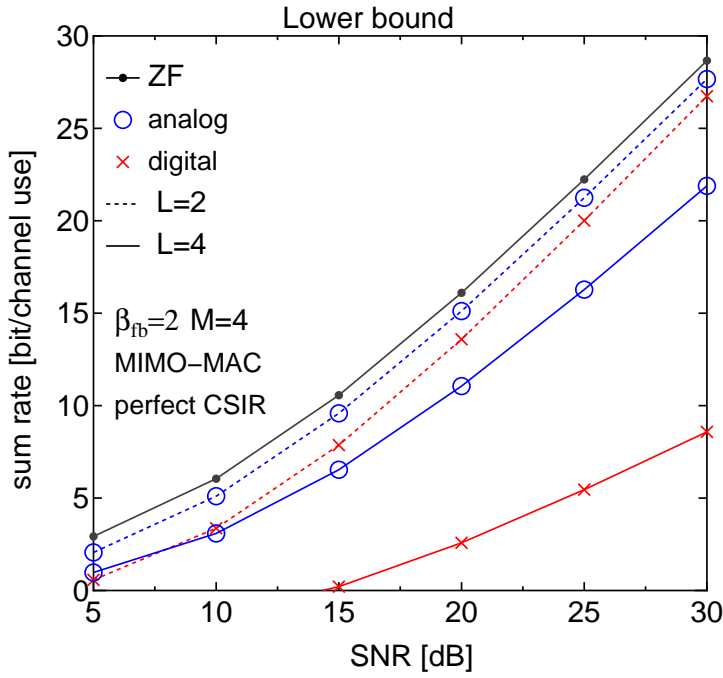


Fig. 8. Lower bound over MIMO-MAC with $M = 4$ and $L = 2, 4$

Fig. 8 and 9 show the lower bound and the genie-aided upper bound, respectively, for analog and digital feedback over the MIMO-MAC. We consider $M = 4$, $L = 2, 4$, $\beta_{fb} = 2$ and assume perfect CSIR. For digital feedback, the values of α are numerically optimized. The lower bounds are evaluated by (90) for analog feedback and (73) with the average feedback error probability (103) for digital feedback, respectively, where for the latter case the error probability resulting from the ZF detector and QAM modulation in the feedback channel was used.

From Fig. 8 we notice that the lower bound for digital feedback does not achieve a bounded rate gap when $L = M = 4$, as expected by our analysis (analog feedback also does not achieve a bounded rate gap for $L = 4$, as described in Section VIII-A). In this case, each UT is feeding its information back over a 1×1 Rayleigh channel (after the ZF spatial filter), for which average probability of error cannot be made to decrease with SNR sufficiently fast. For $L = 2$ the rate gap for both analog and digital feedback are bounded. Although the lower bound for digital feedback will converge to perfect CSI throughput at asymptotically large SNR (because $\beta_{fb} > \frac{M-L+1}{M-L} = \frac{3}{2}$ and $L < M$), digital performs worse than analog throughout the SNR range plotted here. On the contrary, the genie-aided upper bounds plotted in Fig. 9 display very good performance even when $L = M = 4$, and also an approximate equivalence between analog and digital. The substantial gap between the lower and genie-aided bounds can again be explained by the impulsive nature of the multi-user interference in the presence of feedback errors, as in Section VII.

Fig. 10 compares analog feedback and digital feedback with QAM modulation over MIMO-MAC with $M = 4$, $L = 2$ as a function of β_{fb} under perfect CSIR. For each feedback scheme, we plot both the achievable rates and the genie-aided upper bound of Theorem 3 along with ZF with perfect CSIT. For digital feedback, we plot also the achievable rates with ideal feedback error detection (74) with the average feedback error probability (103). Moreover, the values of α with digital feedback are optimized numerically. It is interesting to compare this figure with Fig. 6 for the AWGN case. On one hand, these results confirm that analog feedback achieves nearly the performance of ZF with perfect CSIT over all ranges of β_{fb} and performs slightly better than the AWGN case. On the other hand, we see clearly that digital feedback is very sensitive to the feedback redundancy β_{fb} and requires significantly higher value than AWGN case to achieve the performance of analog feedback. In other words, the advantage of analog feedback becomes evident over MIMO-MAC for small and moderate values of β_{fb} . A thorough investigation of the digital feedback scheme with optimal MIMO-MAC coding and decoding is out of the scope of the present paper and it is left for future investigation.

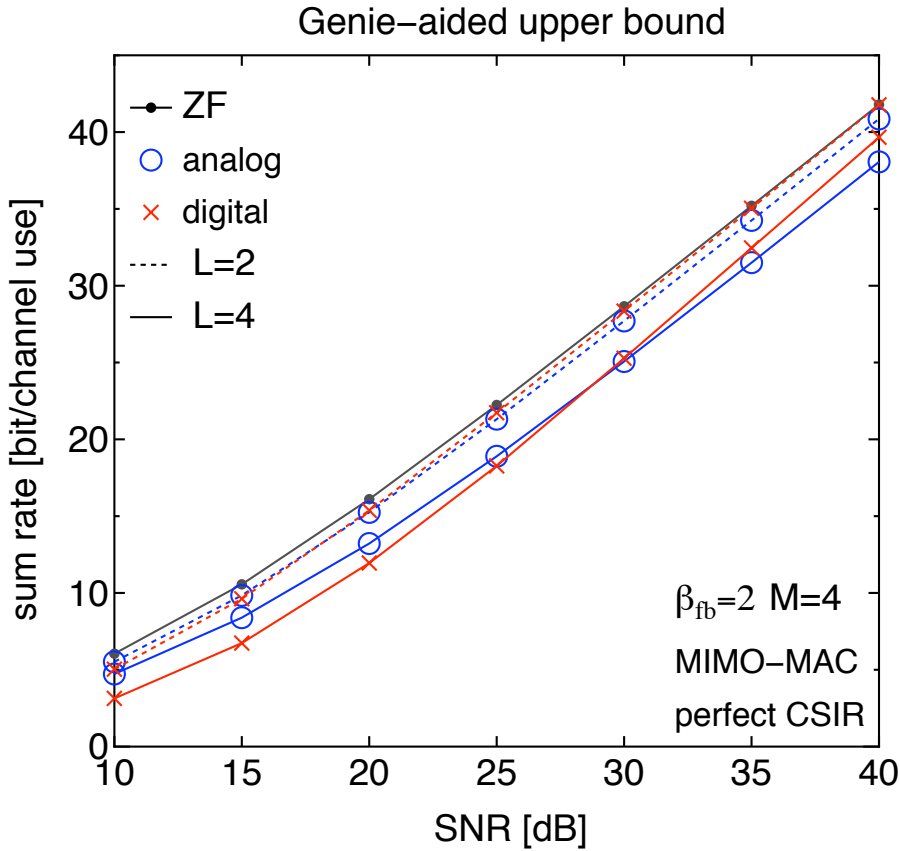


Fig. 9. Genie-aided bound over MIMO-MAC with $M = 4$ and $L = 2, 4$

IX. EFFECTS OF CSIT FEEDBACK DELAY

So far we have restricted our treatment to the case of block-fading, where each transmission round, formed by common training, feedback, dedicated training and data transmission (see baseline system of Section II) takes place in the same frame, where the channel coefficients are random but constant in time.

In this section we wish to take into account the effect of a delay in the channel state feedback: we assume that the block-fading channel changes from frame to frame according to a given stationary correlation model, defined the fading process Doppler spectrum [73]. In particular, assuming spatial independence, each entry of \mathbf{h}_k evolves independently according to the same complex circularly symmetric Gaussian stationary ergodic random process, denoted by $\{h(t)\}$, with mean zero, variance 1 and power spectral density (Doppler spectrum) denoted by $S_h(\xi)$, $\xi \in [-1/2, 1/2]$. Notice that with the assumed block-fading model, the discrete-time process $\{h(t)\}$ has time that ticks at the frame rate, i.e., we have a new fading value $h(t)$ at each frame, that stays constant for the frame duration.

Because of symmetry and spatial independence, we can neglect the UT index k and the antenna index and consider scalar rather than vector processes. Generalizing (4), the observation available at each UT at time $t - d$ from the common training phase takes on the form

$$\left\{ s(t - \tau) = \sqrt{\beta_1 P} h(t - \tau) + z(t - \tau) : \tau = d, d + 1, d + 2, \dots, \infty \right\} \quad (105)$$

where d indicates the feedback delay in slots. This means that the channel state feedback to be used by the BS at slot time t is formed from noisy observations of the channel up to time $t - d$. The case considered so far corresponds to $d = 0$. Furthermore, we have only considered the case where the UT channel estimator neglects all past measurements but the current one, i.e., a block-by-block channel estimation. As we shall see in the sequel, for $d = 0$ only a very little to gain can be achieved by taking into account the past channel measurements and the channel correlation in time. On the contrary, for $d > 0$, making use of the channel time correlation is essential.

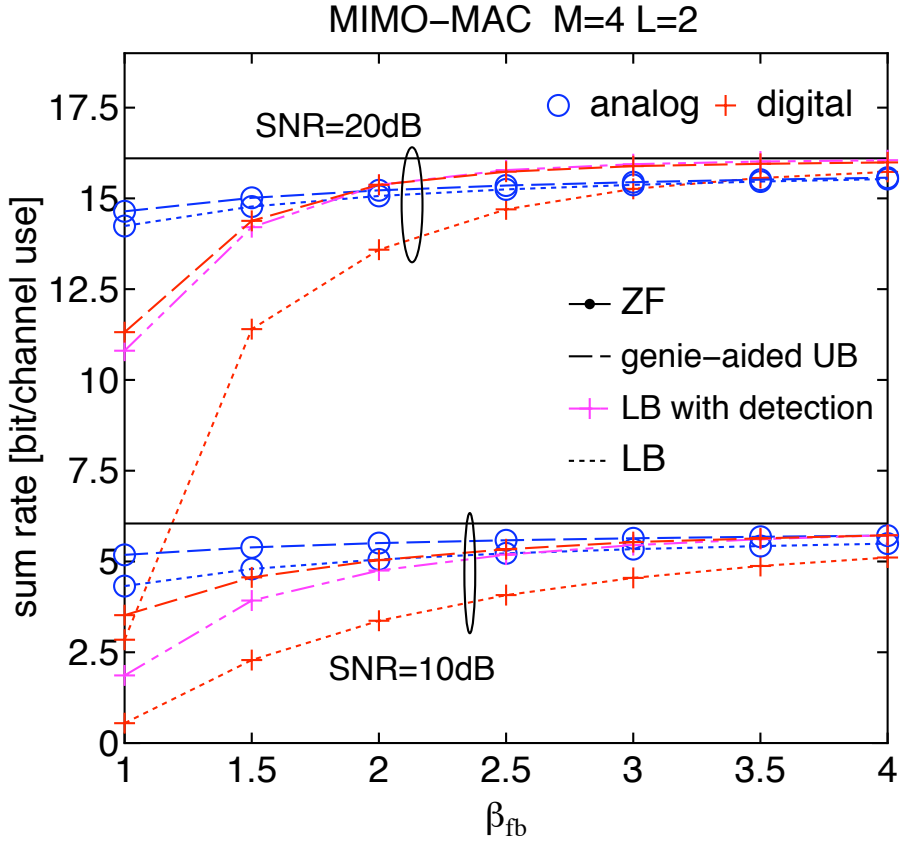


Fig. 10. Comparison as a function of β_{fb} over MIMO-MAC with $M = 4$ and $L = 2$

In this section we focus on the case $d = 1$, which is the most relevant in practical applications¹⁰ and it allows an elegant closed-form analysis.

A. Analog feedback

For simplicity of analysis we assume that the channel state feedback link is unfaded AWGN with orthogonal access (as in Section (IV)). We consider a scheme where each UT at time $t - d$ produces the MMSE estimate of its channel at time t , and sends it via the analog feedback link to the BS. On the practical side, the proposed scheme is attractive since it allows any arbitrary large number of UTs (even much larger than M) to track and predict their own channel from the common training broadcasted by the BS. For example, in scheduling algorithms based on user selection [74], [44], [58], [59] the UTs may decide to send their channel state feedback message together with a request to be served in a given slot based on their predicted channel state. However, the analysis of this section is restricted to the case of M active users, as done previously. In this case, with analog feedback, having the UT predict its channel or just feeding back its noisy channel observation and letting the BS perform channel prediction yields essentially equivalent results.

Let $\tilde{h}(t)$ denote the MMSE estimate of $h(t)$ given the observation in (105). Given the joint Gaussianity of h and s , we can write

$$h(t) = \tilde{h}(t) + n(t) \quad (106)$$

where $\mathbb{E}[|n(t)|^2] = \sigma_1^2$ is the estimation MMSE, that depends on the common training SNR $\beta_1 P/N_0$, on the prediction order d and on the channel second-order statistics (i.e., the Doppler spectrum $S_h(\xi)$). This term will be characterized later, depending on the case $d = 0$ or $d = 1$. Also, $\tilde{h}(t)$ and $n(t)$ are independent, and $\mathbb{E}[|\tilde{h}(t)|^2] =$

¹⁰It should be noticed here that high-data rate downlink systems such as 1xEv-Do [74] already implement a very fast channel state feedback with at most one slot delay.

$1 - \sigma_1^2$. The analog feedback signal is given by

$$g(t) = \frac{\sqrt{\beta_{\text{fb}} P}}{\sqrt{1 - \sigma_1^2}} \tilde{h}(t) + \tilde{w}(t)$$

Finally, the BS obtains the MMSE estimate of $h(t)$ from $g(t)$ as follows

$$\hat{h}(t) = \frac{\mathbb{E}[h(t)g(t)^*]}{\mathbb{E}[|g(t)|^2]} g(t) = \frac{\sqrt{\beta_{\text{fb}} P (1 - \sigma_1^2)}}{N_0 + \beta_{\text{fb}} P} g(t) \quad (107)$$

After some simple algebra, we find the resulting estimation error at the BS is given by

$$\sigma_e^2 = \frac{1}{1 + \beta_{\text{fb}} \frac{P}{N_0}} + \frac{\beta_{\text{fb}} \frac{P}{N_0}}{1 + \beta_{\text{fb}} \frac{P}{N_0}} \sigma_1^2 \quad (108)$$

Notice that for the memoryless case with $d = 0$ we have that $\sigma_1^2 = (1 + \beta_1 P/N_0)^{-1}$ and (108) coincides with (41).

From classical Wiener filtering theory [50], one-step prediction ($d = 1$) MMSE error is given by

$$\epsilon_1(\delta) = \exp \left(\int_{-1/2}^{1/2} \log(\delta + S_h(\xi)) d\xi \right) - \delta \quad (109)$$

where in (109) we assume a unit-power process, $\int_{-1/2}^{1/2} S_h(\xi) d\xi = 1$, observed in background white noise with per-component variance δ . The filtering MMSE ($d = 0$) is easily related to the prediction MMSE as

$$\epsilon_0(\delta) = \frac{\delta \epsilon_1(\delta)}{\delta + \epsilon_1(\delta)}. \quad (110)$$

In our case, we have $\delta = N_0/(\beta_1 P)$. Notice that if $\epsilon_1(\delta) = 1$ (i.e., the channel process is i.i.d. so that the past observations are useless), then

$$\epsilon_0(\delta) = \frac{\delta}{1 + \delta} = \frac{1}{1 + \beta_1 \frac{P}{N_0}} \quad (111)$$

which coincides with (7), consistent with the baseline model presented in Section II.

We shall discuss the rate gap bound achieved by analog feedback in the case of channel time-correlation and feedback delay by letting $\sigma_1^2 = \epsilon_d(\delta)$ in (108) for $d = 0, 1$, and then using the resulting σ_e^2 in the rate gap bound expression. Since the dedicated training symbols are multiplexed with the data, dedicated training estimation error σ_2^2 is the same as discussed before and shall not be rediscussed here. For simplicity and in order to isolate the effects of channel correlation and feedback delay, we shall assume ideal dedicated training and let $\sigma_2^2 = 0$.

It is apparent from the proof of Theorem 4 that the rate gap is dominated by the behavior of the term $\frac{P}{N_0} \sigma_e^2$. We distinguish two cases of channel fading statistics: *Doppler process* and *regular process*:

- We say that $\{h(t)\}$ is a Doppler process if $S_h(\xi)$ is strictly band-limited in $[-F, F]$, where $F < 1/2$ is the maximum Doppler frequency shift, given by $F = \frac{vf_c}{c} T_f$, where v is the mobile terminal speed (m/s), f_c is the carrier frequency (Hz), c is light speed (m/s) and T_f is the frame duration (s). Furthermore, a Doppler process satisfies $\int_{-F}^F \log S_h(\xi) d\xi > -\infty$. This condition holds for most (if not all) channel models usually adopted in the wireless mobile communication literature (see [73] and references therein), where typically the Doppler spectrum has no spectral nulls within the support $[-F, F]$. A Doppler process has prediction error¹¹

$$\epsilon_1(\delta) = \delta^{1-2F} \exp \left(\int_{-F}^F \log(\delta + S_h(\xi)) d\xi \right) - \delta \quad (112)$$

Therefore, $\lim_{\delta \rightarrow 0} \epsilon_1(\delta) = 0$.

- We say that $\{h(t)\}$ is a regular process if $\epsilon_1(0) > 0$ (see [75] and references therein). In particular, a process satisfying the Paley-Wiener condition [50] $\int_{-1/2}^{1/2} \log S_h(\xi) d\xi > -\infty$ is regular.

We now analyze the cases of no delay and one-step delay for both types of processes.

¹¹As in [75], the same result holds for a wider class of processes such that the Lebesgue measure of the set $\{\xi \in [-1/2, 1/2] : S_h(\xi) = 0\}$ is equal to $1 - 2F$, and such that $\int_{\mathcal{D}} \log(S_h(\xi)) d\xi > -\infty$ where \mathcal{D} is the support of $S_h(\xi)$.

a) *No feedback delay* ($d = 0$): In this case, we have

$$\frac{P}{N_0}\sigma_e^2 = \frac{P}{N_0} \left[\frac{1}{1 + \beta_{\text{fb}} \frac{P}{N_0}} + \frac{\beta_{\text{fb}} \frac{P}{N_0}}{1 + \beta_{\text{fb}} \frac{P}{N_0}} \frac{\delta \epsilon_1(\delta)}{\delta + \epsilon_1(\delta)} \right] \quad (113)$$

$$\begin{aligned} &\leq \frac{1}{\beta_{\text{fb}}} + \frac{1}{\beta_1} \frac{\epsilon_1(\delta)}{\delta + \epsilon_1(\delta)} \\ &\leq \frac{1}{\beta_{\text{fb}}} + \frac{1}{\beta_1} \end{aligned} \quad (114)$$

It follows that for both Doppler and regular processes the rate gap is bounded. Furthermore, by comparing the term $\frac{P}{N_0}\sigma_e^2$ when the channel has memory with the block-by-block estimation (see for example (42)), we observe that the gain obtained by exploiting the channel memory and using optimal filtering is generally rather limited in the high-SNR region.

b) *Feedback delay* ($d = 1$): In this case, we have

$$\frac{P}{N_0}\sigma_e^2 = \frac{P}{N_0} \left[\frac{1}{1 + \beta_{\text{fb}} \frac{P}{N_0}} + \frac{\beta_{\text{fb}} \frac{P}{N_0}}{1 + \beta_{\text{fb}} \frac{P}{N_0}} \epsilon_1(\delta) \right] \quad (115)$$

$$\leq \frac{1}{\beta_{\text{fb}}} + \frac{1}{\beta_1} \frac{\epsilon_1(\delta)}{\delta} \quad (116)$$

Using (109) and recalling that $\delta^{-1} = \beta_1 P/N_0$, we have

$$\frac{1}{\beta_1} \frac{\epsilon_1(\delta)}{\delta} = \frac{P}{N_0} \exp \left(\int_{-1/2}^{1/2} \log(N_0/(\beta_1 P) + S_h(\xi)) d\xi \right) - \frac{1}{\beta_1} \quad (117)$$

For a regular fading process, since $\epsilon_1(0) > 0$, we have that (117) increases linearly with $\frac{P}{N_0}$ even in the case of perfect CSIR (i.e., letting $\beta_1 \rightarrow \infty$). This shows that even though the channels are perfectly known at the UTs, because of the fact that the feedback link has a delay, a system that makes use of zero-forcing naive beamforming to M users would be interference limited (the rate gap grows like $\log \frac{P}{N_0}$).¹²

Fortunately, physically meaningful fading processes belong to the class of Doppler processes, at least over a time-span where they can be considered stationary. For a practical relative speed between BS and UT, such time span is much larger than any reasonable coding block length. Hence, we may say that Doppler processes are more the rule than the exception. In this case, the system behavior is radically different. We have the following result that characterizes the rate at which noisy prediction error goes to zero for Doppler processes:

Lemma 2: The noisy prediction error of a Doppler process satisfies

$$\epsilon_1(\delta) = \kappa \delta^{1-2F} + O(\delta) \quad (118)$$

for $\delta \downarrow 0$, where κ is a constant term independent of δ .

Proof: Applying Jensen's inequality to (112) from the fact that $\int S_h(\xi) d\xi = 1$, we obtain the upper bound

$$\epsilon_1(\delta) \leq \delta^{1-2F} \left[\left(\frac{1}{2F} + \delta \right)^{2F} - \delta^{2F} \right] \quad (119)$$

Using the fact that \log is increasing, we arrive at the lower bound

$$\epsilon_1(\delta) \geq \delta^{1-2F} \left[\exp \left(\int_{-F}^F \log S_h(\xi) d\xi \right) - \delta^{2F} \right] \quad (120)$$

Combining these bounds we obtain the result. \square

Using Lemma 2, we can rewrite (117) as

$$\frac{1}{\beta_1} \frac{\epsilon_1(\delta)}{\delta} = \frac{1}{\beta_1} \left[\kappa \left(\frac{\beta_1 P}{N_0} \right)^{2F} + O(1) \right] \quad (121)$$

¹²Of course, in order to have a non-interference limited system we can always use TDMA and serve one user at a time. However, in this case the sum-rate would grow like $\log(P/N_0)$ instead of $M \log(P/N_0)$ as promised by the MIMO downlink with perfect CSIT.

For non-perfect CSIR (fixed and finite β_1), the term in (121) grows like $\left(\frac{P}{N_0}\right)^{2F}$. It follows that multi-user interference grows as $\left(\frac{P}{N_0}\right)^{2F}$, and thus the rate gap grows like $2F \log \frac{P}{N_0}$. Using this in the rate lower bound of Corollary (3.1), and considering the pre-log factor in high-SNR, we have that the system sum-rate is lowerbounded by

$$\sum_{k=1}^M R_k \geq M(1 - 2F) \log \frac{P}{N_0} + O(1) \quad (122)$$

This shows that a multiplexing gain of $M(1 - 2F)$ is achievable.

In the case of perfect common training (i.e., $\beta_1 \rightarrow \infty$), an interesting singularity is observed. Since $2F < 1$, it is clear that (121) vanishes as $\beta_1 \rightarrow \infty$. Hence, with perfect common training, the effect of a feedback delay becomes irrelevant and the system can preserve full multiplexing gain (because the rate gap is bounded). Under the assumption of perfect common training, each UT is able to perform *perfect prediction* of its channel state on the basis of its past noiseless observations of the channel state, by the definition of a Doppler process. Thus, it is as if there is no delay and the only inaccuracy in the CSI provided to the BS is due to the distortion introduced on the feedback link. Note that this behavior is not exhibited if the prediction is performed at the BS rather than the UT: assuming imperfect feedback, the BS is provided with noisy delayed channel observations (due to the imperfect feedback channel) even if each UT has noiseless observations.

Remark 9.1: It is interesting to notice here the parallel with the results of [75] on the high-SNR capacity of the single-user scalar ergodic stationary fading channel with no CSIR and no CSIT, where it is shown that for a class of *non-regular* processes that includes the Doppler processes defined here, the high-SNR capacity grows like $\mathcal{L} \log(P/N_0)$, where \mathcal{L} is the Lebesgue measure of the set $\{\xi \in [-1/2, 1/2] : S_h(\xi) = 0\}$. In our case, it is clear that $\mathcal{L} = 1 - 2F$. These results, as ours, rely on the behavior of the noisy prediction error $\epsilon_1(\delta)$ for small δ . \diamond

B. Digital feedback

Digital feedback can be used within the very same framework if, again, each UT predicts its current channel vector $\mathbf{h}(t)$ from the sequence of common training outputs (105) and then quantizes its prediction (using RVQ) to $\hat{\mathbf{h}}(t)$ and feeds back the quantization index using B bits over $\beta_{fb}(M-1)$ channel uses, as in Section V. Notice that the channel estimation and prediction at the UTs is identical to what was already discussed for analog feedback. In order to isolate the effect of feedback delay, we do not consider digital feedback errors, although putting together the results of this section with the uncoded QAM feedback transmission of Section VII is a routine exercise.

Using (106), we have that each UT has a channel vector MMSE estimate $\hat{\mathbf{h}}_k(t)$, such that $\mathbf{h}_k(t) = \hat{\mathbf{h}}_k(t) + \mathbf{n}_k(t)$, with estimation error σ_1^2 equal to $\epsilon_0(\delta)$ or to $\epsilon_1(\delta)$, for delay $d = 0, 1$, respectively, and where $\delta = \frac{\beta_1 P}{N_0}$. By replicating the steps in (56) we arrive at the interference variance

$$\begin{aligned} \mathbb{E}[|I_k|^2] &= P(1 - \sigma_1^2) 2^B \beta \left(2^B, \frac{M}{M-1} \right) + \frac{M-1}{M} P \sigma_1^2 \\ &\leq P(1 - \sigma_1^2) 2^{-\frac{B}{M-1}} + \frac{M-1}{M} P \sigma_1^2 \end{aligned} \quad (123)$$

Using this into the rate gap bound expression (22) we notice that, by choosing B as discussed in the previous sections, the rate gap behavior is dominated by the product $\frac{P}{N_0} \sigma_1^2$. This is the term that we have already discussed for the analog feedback case. Hence, the same conclusions obtained for the analog feedback case apply here.¹³

C. Examples

Fig. 11 compares the achievable rates of analog and digital feedback over a temporally-correlated channel with a feedback delay of $d = 0$ or $d = 1$. We consider a Gauss-Markov model (or auto regressive model of order 1),

¹³Here we have considered only the case where each UT predicts its current channel state and then quantizes its prediction and feeds back the quantization index. An alternative to quantizing the new prediction during each frame is to, intuitively, quantize only the innovation in the channel process and for the BS to update its channel estimate according to the quantized innovation. This approach has been considered in the context of point-to-point MIMO systems [76], [77] and may also be appropriate for the MIMO downlink channel, although we do not pursue that avenue here.

which is a typical example of a regular process widely used in the literature. Under this model the channel evolves in time as:

$$h(\tau) = rh(\tau - 1) + \sqrt{1 - r^2}\Delta(\tau) \quad (124)$$

where r is the correlation coefficient ($0 < r < 1$) and the innovation process $\Delta(\tau)$ is complex Gaussian with unit variance and is i.i.d. in time. The Gauss-Markov model allows a closed-form expression for the one-step prediction error variance as a function of $\delta = \frac{N_0}{\beta_1 P}$ and r , given by (see for example [31])

$$\epsilon_1(\delta) = (1 - r^2) \left[1 + \frac{-(1 + \delta) + \sqrt{1 + \delta^2 + 2\delta\frac{1+r^2}{1-r^2}}}{2} \right] \quad (125)$$

To isolate the effect of a delayed feedback, we assume perfect CSIR ($\beta_1, \beta_2 \rightarrow \infty$) in which case the prediction error variance coincides with the innovation variance, $\epsilon_1(0) = 1 - r^2$. In our examples, we considered $M = 4$, $\beta_{fb} = 2$ and $r = 0.9$, $r = 0.99$, and $r = 0.999$.

Recall that the rate gap with analog and digital feedback under perfect CSIR is given respectively by

$$\Delta R^{\text{AF}} = \log \left(1 + \frac{M-1}{M} \frac{P}{N_0} \sigma_e^2 \right) \quad (126)$$

$$\Delta R^{\text{DF}} = \log \left(1 + \left(\frac{P}{N_0} \right)^{1-\beta_{fb}} (1 - \sigma_1^2) + \frac{M-1}{M} \frac{P}{N_0} \sigma_1^2 \right) \quad (127)$$

where σ_e^2 is given in (113) and (115), $B = \beta_{fb}(M-1) \log_2(P/N_0)$, and $\sigma_1^2 = \epsilon_d(\delta)$ for $d = 0, 1$.

For the case of no delay ($d = 0$), as expected from (113), the rate gap is bounded for both analog and digital schemes and performance does not significantly depend on the correlation coefficient. In contrast, for $d = 1$ the system performance depends critically on the fading correlation coefficient. From (126) we note that the rate gap is larger than

$$\log \frac{2M-1}{M} \approx \log 2 = 1 \text{ bit}$$

for $\frac{P}{N_0} \sigma_e^2 > 1$. This threshold may be regarded as the separation of two distinct regimes: a small rate-gap regime and a large rate-gap regime. From (115) we obtain the SNR threshold separating these two regimes in terms of r and β_{fb} as

$$\frac{P}{N_0} > \frac{\beta_{fb} - 1 + \sqrt{(\beta_{fb} + 1)^2 - 4r^2\beta_{fb}}}{2\beta_{fb}(1 - r^2)}$$

In the case of ideal feedback ($\beta_{fb} \rightarrow \infty$), the threshold simplifies to $\frac{P}{N_0} > \frac{1}{1-r^2}$, which sets a very simple relationship between the operating SNR and the fading correlation coefficient.

Indeed, for correlation $r = 0.9$ the channel innovation almost completely eliminates the opportunity to perform naive zero-forcing. For $r = 0.99$ the achieved rates are already quite attractive in practice. For example, a sum rate of 10 bit/s/Hz can be obtained at SNR ≈ 20 dB. For even slower fading (e.g., $r = 0.999$ in the figure) the same target of 10 bit/s/Hz can be achieved at SNR between 15 and 16 dB (depending on the feedback method) and it is very close to what can be achieved in the case of zero delay.

Fig. 12 shows the genie-aided upper bounds for the Gauss-Markov fading with the same parameters of Fig. 11. Even with full side information of about the interference coefficients \mathcal{A}_k , feedback delay yields a sum rate that saturates at high SNR. The asymptotic rate limit for high SNR can be approximated in closed form, as given in (129), obtained here below.

In Fig. 13, we compare analog and digital feedback with the classical Jake's correlation model given by [39], [40]

$$S_h(\xi) = \frac{1}{\pi \sqrt{F^2 - \xi^2}}, \quad -F \leq \xi \leq F \quad (128)$$

where $F = \frac{v f_c}{c} T_f$ with $f_c = 2$ GHz and $T_f = 1$ msec. Notice that $S_h(\xi)$ is strictly bandlimited in $[-F, F]$. Again we assume perfect CSIR to focus on the effect of a feedback delay and let, as before, $M = 4$ and $\beta_{fb} = 2$. We confirm that with a delay $d = 1$ the ZF performs in a radically different way with a Jake's correlation model

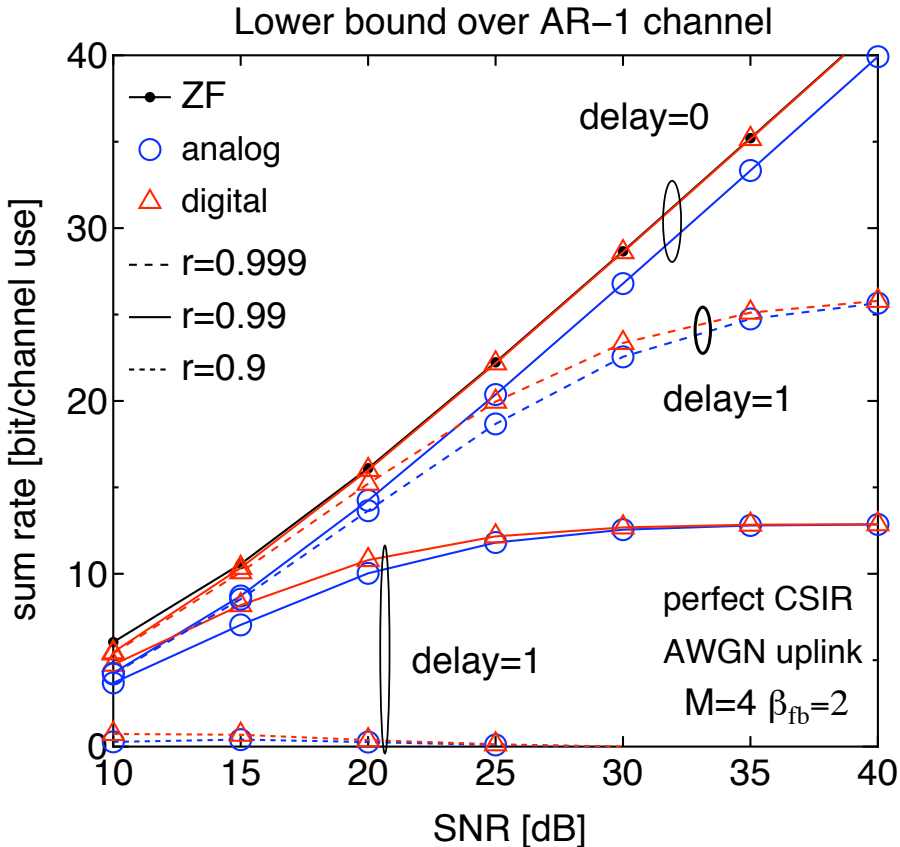


Fig. 11. Lower bounds with Gauss-Markov correlation.

(a Doppler process) compared to the Gauss-Markov process. It is remarkable that with a delay of $d = 1$ and a reasonable mobile speed of $v = 10, 50$ km/h, both analog and digital achieve nearly the sum rate by ZF with ideal CSIT. For example, with $v = 50$ km/h, we have $F = 0.0926$. For $M = 4$, the achieved multiplexing gain is 3.26 instead of 4, yielding a spectral efficiency of 14 bit/s/Hz at SNR of 20 dB. For a slower mobile speed of 10 km/h, the performance with $d = 1$ essentially coincides with that with a delay-free feedback link.

Finally in Fig. 14 we compare a common Gauss-Markov “fit” of the Jakes’ process to the true Jakes process. The auto-correlation for samples separated by one frame (delay $d = 1$) is given by $J_0(2\pi F)$. Since the Jakes’ model is more complicated for analysis and simulation, it is customary to make a maximum-entropy approximation of the fading statistics [78] and replace the Jakes’ model with a Gauss-Markov model with $r = J_0(2\pi F)$. The achievable rate lower bound is plotted for mobile speeds of $v = 3, 10$, and 50 km/h, which correspond to $F = 0.0056, 0.0185$, and 0.0926 and $r = 0.9997, 0.9966$ and 0.9172 , respectively. For simplicity we have plotted only the achievable rates of analog feedback. We note that for $v = 50$ the rates achievable under the first-order model are vastly different than under the true Jakes’ model. On the other hand for $v = 10$ and $v = 3$ (typical pedestrian speed) we see similar performance for both the Jakes’ and Gauss-Markov model until the Gauss-Markov rates hit their respective ceilings.

In conclusion, the most noteworthy result of this analysis is that under common fading models (Doppler processes), both analog and digital feedback scheme achieves a potentially high multiplexing gain even with realistic, noisy and delayed feedback.

Remark 9.2: Interestingly, the unbounded rate gap with a regular process is not due to the looseness of the lower bound. In fact, for the special case of a Gauss-Markov correlation model we are able to prove that the genie-aided upper bound that exploits perfect knowledge of the $\mathcal{A}_k = \{a_{k,j}\}$ yields a saturated rate for asymptotically high SNR. For analytical simplicity, we assume perfect common training, although the result trivially generalizes to imperfect common training. From (33), the genie-aided upper bound of both analog and digital feedback achieves

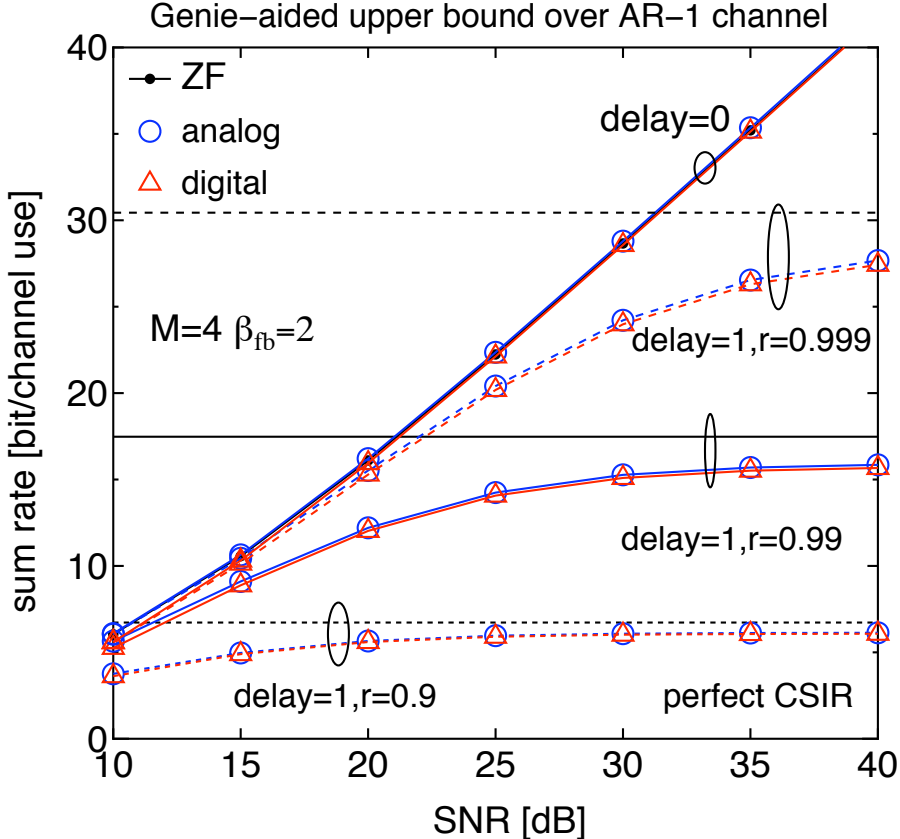


Fig. 12. Genie-aided upper bounds with Gauss-Markov correlation. The horizontal lines show the closed-form approximation of the asymptotic rates for high SNR.

the following rate:

$$R_k^{\text{GM}} = \mathbb{E} \left[\log \left(1 + \frac{P|\mathbf{h}_k^H(t)\hat{\mathbf{v}}_k(t)|^2}{N_0M + P \sum_{j \neq k} |\mathbf{h}_k^H(t)\hat{\mathbf{v}}_j(t)|^2} \right) \right]$$

where $\hat{\mathbf{v}}_j(t)$ is orthogonal to $\tilde{\mathbf{h}}_k(t) = r\mathbf{h}_k(t-1)$, i.e., we have $\mathbf{h}_k^H(t)\hat{\mathbf{v}}_j(t) = (1-r^2)\Delta_k(t)^H\hat{\mathbf{v}}_k(t)$ for $j \neq k$ from (124). In the following, we show that the above rate converges to a constant as $P \rightarrow \infty$.

$$\begin{aligned} \lim_{P/N_0 \rightarrow \infty} R_k^{\text{GM}} &= \mathbb{E} \left[\log \left(|\mathbf{h}_k^H(t)\hat{\mathbf{v}}_k(t)|^2 + \sum_{j \neq k} |\mathbf{h}_k^H(t)\hat{\mathbf{v}}_j(t)|^2 \right) \right] - \mathbb{E} \left[\log \left(\sum_{j \neq k} |\mathbf{h}_k^H(t)\hat{\mathbf{v}}_j(t)|^2 \right) \right] \\ &\stackrel{(a)}{\leq} \log \left(1 + (1-r^2)(M-1) \right) - \mathbb{E} \left[\log \left((1-r^2) \sum_{j \neq k} |\Delta_k^H(t)\hat{\mathbf{v}}_j(t)|^2 \right) \right] \\ &\stackrel{(b)}{=} \log \left(\frac{1}{1-r^2} + M-1 \right) - \mathbb{E}[\log(\|\Delta_k(t)\|^2)] - \mathbb{E} \left[\log \left(\sum_{j \neq k} \frac{|\Delta_k^H(t)\hat{\mathbf{v}}_j(t)|^2}{\|\Delta_k(t)\|^2} \right) \right] \\ &\stackrel{(c)}{=} \log \left(\frac{1}{1-r^2} + M-1 \right) - \psi(M) + \frac{1}{2M-1} + \frac{1}{2M-2} \end{aligned} \quad (129)$$

where (a) follows by applying Jensen's inequality to the first term and noticing $\mathbf{h}_k^H(t)\hat{\mathbf{v}}_k(t) \sim \mathcal{N}(0, 1)$ and $\Delta_k^H(t)\hat{\mathbf{v}}_j(t) \sim \mathcal{N}(0, 1)$, (b) follows by expressing $|\Delta_k^H(t)\hat{\mathbf{v}}_j(t)|^2 = \|\Delta_k^H(t)\|^2 \frac{|\Delta_k^H(t)\hat{\mathbf{v}}_j(t)|^2}{\|\Delta_k^H(t)\|^2}$, (c) is obtained by identifying that $\|\Delta_k(\tau)\|^2$ is complex chi-square distributed with M degrees of freedom, $\sum_{j \neq k} \frac{|\Delta_k^H(t)\hat{\mathbf{v}}_j(t)|^2}{\|\Delta_k(t)\|^2}$ is beta distributed with $(M-1, 1)$, and finally $\psi(M)$ is the Euler-Digamma function. \diamond

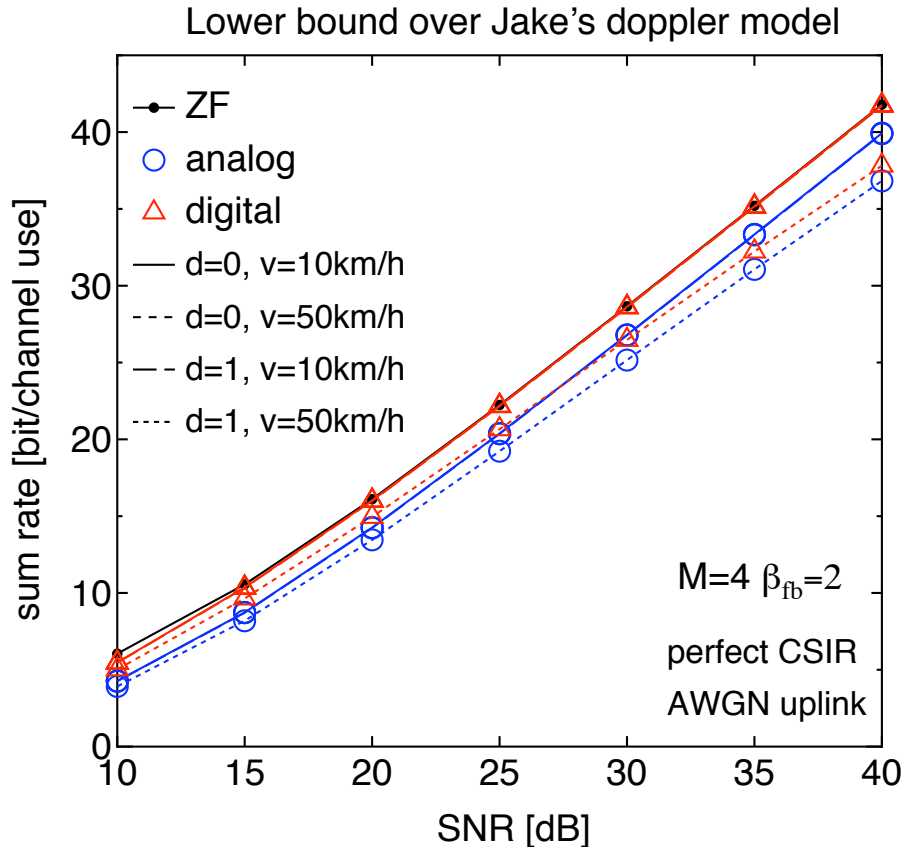


Fig. 13. Lower bounds with Jakes' correlation.

X. CONCLUSIONS

We have presented a comprehensive analysis of the achievable performance of ZF beamforming under realistic, pilot-based, channel estimation and channel state feedback. We considered what we believe are the most relevant system aspects. In particular, the often neglected effect of explicit channel estimation at the UTs. Both the vector channel state estimation for the purpose of channel state feedback (common training phase) and the dedicated channel state estimation once the beamforming vectors have been computed was considered. As for the feedback, we provided a comprehensive comparison of analog and digital feedback schemes, including the effect of the MIMO-MAC fading channel, of feedback errors for the case of digital feedback and of feedback delay.

Our results build on prior work, but generalize many results and models, and provide a comprehensive analysis, based on firm bounds on the ergodic achievable rate with Gaussian inputs. We focused on the case of FDD in order to make the comparison between analog and digital feedback meaningful. With TDD, assuming channel reciprocity, CSIT comes "for free", as a byproduct of uplink channel estimation, which is in any case necessary in order to enable coherent detection. However, our analysis of analog feedback easily particularize to the case of TDD. Also, as pointed out in the paper, the choice of TDD versus FDD is based on many other system design considerations, such that every choice has its own merits and drawbacks. It is perhaps important to point out here that our results show that, even in the case of FDD, a system with explicit CSIT feedback can be implemented, where the number of training and feedback channel uses scales linearly with the number of BS antennas, and eventually with the downlink throughput.

Of course, the throughput of the system analyzed here can be considerably improved via the use of combined beamforming and user selection/scheduling. Simulation results show that a system with $K = 10$ and $M = 4$, with a greedy scheduling as proposed in [44], [31], achieves a very small gap with respect to the optimal dirty-paper coding and perfect CSIT case with the same parameters. Although a full analytical characterization of a system with beamforming and user selection based on imperfect CSI appears difficult, there are results indicating that the dependence on CSIT quality when user selection is performed is roughly the same as the equal-power/no selection

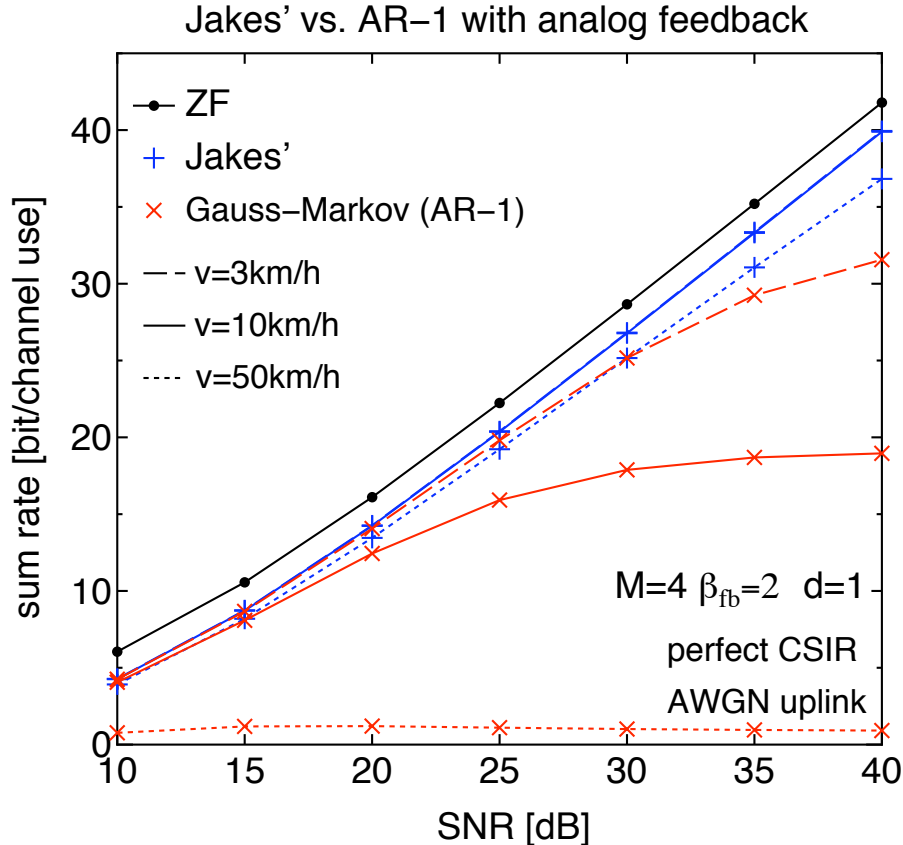


Fig. 14. Achievable rate bounds for Jakes' correlation model and its maximum-entropy Gauss-Markov approximation of order 1, for different mobile speeds.

scenario analyzed here [58], [38]. However, a careful analysis of such a system is left for future work.

Acknowledgment

The work of G. Caire was partially supported by NSF Grant CCF-0635326.

REFERENCES

- [1] G. J. Foschini and M. J. Gans, "On limits of wireless communications in a fading environment when using multiple antennas," *Wireless Personal Commun. : Kluwer Academic Press*, no. 6, pp. 311–335, 1998.
- [2] I. Telatar, "Capacity of multi-antenna Gaussian channels," *European Transactions on Telecommunications*, vol. 10, no. 6, pp. 585–595, 1999.
- [3] G. Caire and S. Shamai, "On the achievable throughput of a multiantenna Gaussian broadcast channel," *IEEE Trans. on Inform. Theory*, vol. 49, no. 7, pp. 1691–1706, 2003.
- [4] S. Vishwanath, N. Jindal, and A. Goldsmith, "Duality, achievable rates, and sum-rate capacity of Gaussian MIMO broadcast channels," *IEEE Trans. on Inform. Theory*, vol. 49, no. 10, pp. 2658–2668, 2003.
- [5] P. Viswanath and D. Tse, "Sum capacity of the vector Gaussian broadcast channel and uplink-downlink duality," *IEEE Trans. on Inform. Theory*, vol. 49, no. 8, pp. 1912–1921, 2003.
- [6] W. Yu and J. Cioffi, "Sum capacity of Gaussian vector broadcast channels," *IEEE Trans. on Inform. Theory*, vol. 50, no. 9, pp. 1875–1892, 2004.
- [7] H. Weingarten, Y. Steinberg, and S. Shamai, "The capacity region of the gaussian multiple-input multiple-output broadcast channel," *IEEE Trans. on Inform. Theory*, vol. 52, no. 9, pp. 3936–3964, 2006.
- [8] N. Jindal and A. Goldsmith, "Dirty paper coding vs. TDMA for MIMO broadcast channels," *IEEE Trans. Inform. Theory*, vol. 51, no. 5, pp. 1783–1794, May 2005.
- [9] D. Gesbert, M. Kountouris, J. R. W. Heath, C. B. Chae, and T. Salzer, "From Single user to Multiuser Communications: Shifting the MIMO paradigm," *IEEE Sig. Proc. Magazine*, 2007.
- [10] U. Erez and S. Ten Brink, "A close-to-capacity dirty paper coding scheme," *IEEE Trans. on Inform. Theory*, vol. 51, no. 10, pp. 3417 – 3432, October 2005.
- [11] A. Bennatan, D. Burshtein, G. Caire, and S. Shamai, "Superposition coding for side-information channels," *IEEE Trans. on Inform. Theory*, vol. 52, no. 5, pp. 1872 – 1889, May 2006.
- [12] Y. Sun, A. Liveris, V. Stankovic, and Zixiang Xiong, "Near-capacity dirty-paper code designs based on TCQ and IRA codes," in *proceedings of IEEE Int. Symp. on Inform. Theory, ISIT*, Adelaide, Australia, September 2005, pp. 184 – 188.
- [13] F. Boccardi, F. Tosato, and G. Caire, "Precoding Schemes for the MIMO-GBC," in *Int. Zurich Seminar on Communications*, February 2006, pp. 10 – 13.
- [14] R. Fischer, C. Windpassinger, A. Lampe, and J. Huber, "MIMO precoding for decentralized receivers," in *proceedings of IEEE Int. Symp. on Inform. Theory, ISIT*, Lausanne, Switzerland, 2002, p. 496.
- [15] B. Hochwald, C. Peel, and A. Swindlehurst, "A vector-perturbation technique for near-capacity multiantenna multiuser communication-Part II: perturbation," *IEEE Trans. on Communications*, vol. 53, no. 3, pp. 537–544, 2005.
- [16] C. Windpassinger, R. Fischer, T. Vencel, and J. Huber, "Precoding in multiantenna and multiuser communications," *IEEE Trans. on Commun.*, vol. 3, no. 4, pp. 1305–1316, 2004.
- [17] T. Yoo and A. Goldsmith, "On the optimality of multiantenna broadcast scheduling using zero-forcing beamforming," *IEEE Journal on Selected Areas in Communications*, vol. 24, no. 3, pp. 528–541, 2006.
- [18] A. Narula, M. J. Lopez, M. D. Trott, and G. W. Wornell, "Effcient use of side information in mulitiple-antenna data transmission over fading channels," *IEEE Jour. Select. Areas in Commun.*, vol. 16, no. 8, pp. 1423–1436, October 1998.
- [19] D. Love, R. Heath Jr, and T. Strohmer, "Grassmannian beamforming for multiple-input multiple-output wireless systems," *IEEE Trans. on Inform. Theory*, vol. 49, no. 10, pp. 2735–2747, 2003.
- [20] K. Mukkavilli, A. Sabharwal, E. Erkip, and B. Aazhang, "On beamforming with finite rate feedback in multiple-antenna systems," *IEEE Trans. on Inform. Theory*, vol. 49, no. 10, pp. 2562–2579, 2003.
- [21] S. Srinivasa and S. A. Jafar, "The optimality of transmit beamforming: a unified view," *IEEE Trans. on Inform. Theory*, vol. 53, no. 4, pp. 1558–1564, April 2007.
- [22] S. A. Jafar and S. Srinivasa, "On the optimality of beamforming with quantized feedback," *To appear in the IEEE Trans. on Comm.*, 2007.
- [23] C. K. Au-Yeung and D. J. Love, "On the performance of random vector quantization limited feedback beamforming in a MISO system," *IEEE Trans. Wireless Comm.*, vol. 6, pp. 458 – 462, 2007.
- [24] A. D. Dabbagh and D. J. Love, "Feedback rate-capacity loss tradeoff for limited feedback MIMO systems," *IEEE Trans. on Inform. Theory*, vol. 52, no. 5, pp. 2190–2202, May 2006.
- [25] N. Jindal, "MIMO broadcast channels with finite rate feedback," *IEEE Trans. on Inform. Theory*, vol. 52, no. 11, pp. 5045–5059, November 2006.
- [26] T. Marzetta, "How Much Training is Required for Multiuser MIMO ?" *Signals, Systems and Computers, 2006. ACSSC'06. Fortieth Asilomar Conference on*, pp. 359–363, 2006.
- [27] T.L.Marzetta and B.M.Hochwald, "Fast Transfer of Channel State Information in Wireless Systems," *Submitted to "IEEE Transactions on Signal Processing"*, June 2004.
- [28] P. Ding, D. J. Love, and M. D. Zoltowski, "On the Sum Rate of Multi-Antenna Broadcast Channels with Channel Estimation Error," *Asilomar*, October 2005.
- [29] P. Ding, D. Love, and M. Zoltowski, "Multiple antenna broadcast channels with shape feedback and limited feedback," *IEEE Trans. on Sig. Proc.*, vol. 55, no. 7 Part 1, pp. 3417–3428, 2007.
- [30] A. Dana, M. Sharif, and B. Hassibi, "On the capacity region of multi-antenna gaussian broadcast channels with estimation error," in *IEEE Int. Symp. on Inform. Theory*, July 2006.
- [31] M. Kobayashi and G. Caire, "Joint Beamforming and Scheduling for a Multi-Antenna Downlink with Imperfect Transmitter Channel Knowledge," *IEEE J. Select. Areas Commun.*, vol. 25, no. 7, 2007.
- [32] A. Lapidoth, S. S. (Shitz), and M. . A. Wigger, "On the Capacity of Fading MIMO Broadcast Channels with Imperfect Transmitter side-Information," *Annual Allerton Conference on Communication, Control, and Computing*, September 2005.

- [33] S. Shamai, G. Caire, and N. Jindal, "On the Required Accuracy of Transmitter Channel State Information in Multiple-Antenna Broadcast Channels," *Asilomar Conference on Signals, Systems and Computers*, 2007.
- [34] S. Shamai, S. Verdu, and R. Zamir, "Systematic lossy source/channel coding," *IEEE Trans. on Inform. Theory*, vol. 44, no. 2, pp. 564 – 579, 1998.
- [35] K. Narayanan, G. Caire, and M. Wilson, "Duality between broadcasting with bandwidth expansion and bandwidth compression," in *proceedings of IEEE Int. Symp. on Inform. theory, ISIT*, Nice, France, 2007.
- [36] P.Viswanath, D.N.C.Tse, and R.Laroia, "Opportunistic Beamforming Using Dumb Antennas," *IEEE Trans. on Inform. Theory*, vol. 48, no. 6, June 2002.
- [37] M. Sharif and B. Hassibi, "On the capacity of a mimo broadcast channel with partial side information," *IEEE Trans. Inform. Theory*, vol. 51, no. 2, pp. 506–522, February 2005.
- [38] N. Ravindran and N. Jindal, "Multi-User Diversity vs. Accurate Channel Feedback for MIMO Broadcast Channels," *Arxiv preprint cs.IT/0710.1336*.
- [39] D. Tse and P. Viswanath, *Fundamentals of Wireless Communication*. Cambridge University Press, 2005.
- [40] A. Goldsmith, *Wireless Communications*. Cambridge University Press, 2005.
- [41] B. Hassibi and B. Hochwald, "How much training is needed in multiple-antenna wireless links?" *IEEE Trans. on Inform. Theory*, vol. 49, no. 4, pp. 951–963, 2003.
- [42] H. Weingarten, Y. Steinberg, and S. Shamai, "The capacity region of the Gaussian multiple-input multiple-output broadcast channel," *IEEE Trans. on Inform. Theory*, vol. 52, no. 9, pp. 3936 – 3964, September 2006.
- [43] T. Yoo and A. Goldsmith, "On the optimality of Multiantenna Broadcast Scheduling using Zero-Forcing Beamforming," *IEEE J. Select. Areas Commun.*, vol. 24, no. 3, pp. 528–541, 2006.
- [44] G. Dimic and N. Sidiropoulos, "On Downlink Beamforming with Greedy User Selection: Performance Analysis and Simple New Algorithm," *IEEE Trans. on Sig. Proc.*, vol. 53, no. 10, pp. 3857–3868, October 2005.
- [45] A. Bayesteh and A.K. Khandani, "An Efficient Method for User Selection in MIMO Broadcast Channels," *Proceeding of CISS'2005*, March 2005.
- [46] S. Jafar and A. Goldsmith, "Isotropic Fading Vector Broadcast Channels: The Scalar Upper Bound and Loss in Degrees of Freedom," *IEEE Trans. on Inform. Theory*, vol. 51, no. 3, 2005.
- [47] J. Jose, A. Ashikhmin, P. Whiting, and S. Vishwanath, "Scheduling and Pre-Conditioning in Multi-User MIMO TDD Systems," *Arxiv preprint cs.IT/0709.4513*.
- [48] <http://www.ieee802.org/11/>.
- [49] T. Rappaport, *Wireless Communications: Principles and Practice*. IEEE Press Piscataway, NJ, USA, 1996.
- [50] H. Poor, *An introduction to signal detection and estimation*. Springer-Verlag New York, Inc. New York, NY, USA, 1994.
- [51] R. Prasad, W. Mohr, and W. Konhauser, *Third Generation Mobile Communication Systems*. Artech House, Inc. Norwood, MA, USA, 2000.
- [52] "Pilots for MIMO communication systems," Patent EP 1556985/US 2004179627/WO 2004038988.
- [53] M. Médard, "Channel Capacity in Wireless Communications of Perfect and Imperfect Knowledge of the Channel," *IEEE Trans. on Inform. Theory*, vol. 46, no. 3, pp. 933–946, May 2000.
- [54] A. Lapidot and S. Shamai, "Fading channels: how perfect need" perfect side information" be?" *IEEE Trans. on Inform. Theory*, vol. 48, no. 5, pp. 1118–1134, 2002.
- [55] S. Boyd and L. Vandenberghe, *Convex Optimization*. Cambridge University Press, 2004.
- [56] M. Alouini and A. Goldsmith, "Capacity of Rayleigh fading channels under different adaptivetransmission and diversity-combining techniques," *IEEE Trans. on Vehic. Tech.*, vol. 48, no. 4, pp. 1165–1181, 1999.
- [57] M. Abramowitz and I. A. Stegun, *Handbook of Mathematical Functions with Formulas, Graphs, and Mathematical Tables*. New York: Dover, 1964.
- [58] T. Yoo, N. Jindal, and A. Goldsmith, "Multi-Antenna Downlink Channels with Limited Feedback and User Selection," *IEEE J. Select. Areas Commun.*, vol. 25, pp. 1478–1491, 2007.
- [59] C. Swannack, G. W. Wornell, and E. Uysal-Biyikoglu, "MIMO Broadcast Scheduling with Quantized Channel State Information," in *Proceedings of the IEEE Int. Symp. on Inform. Theory, ISIT*, Seattle, WA, 2006.
- [60] T. Thomas, K. Baum, and P. Sartori, "Obtaining channel knowledge for closed-loop multi-stream broadband MIMO-OFDM communications using direct channel feedback," in *IEEE Global Telecommunications Conference, 2005. GLOBECOM '05*, vol. 6, November 2005.
- [61] D. Samardzija and N. Mandayam, "Unquantized and Uncoded Channel State Information Feedback on Wireless Channels," *Proceeding of IEEE WCNC'2005*, pp. New Orleans, LA, USA, March 2005.
- [62] G. Caire, N. Jindal, M. Kobayashi, and N. Ravindran, "Optimal Tradeoff between Training and Feedback Phases in MIMO Broadcast Channels with Zero-Forcing," *in preparation*.
- [63] N. Jindal, "Antenna combining for the MIMO downlink channel," *To appear IEEE Trans. Wireless Commun.*, 2007.
- [64] M. Gastpar, B. Rimoldi, and M. Vetterli, "To code, or not to code : Lossy source-channel communication revisited," *IEEE Trans. on Inform. Theory*, vol. 49, May 2003.
- [65] H. Shin and J. Lee, "Capacity of multiple-antenna fading channels: spatial fading correlation, double scattering, and keyhole," *Information Theory, IEEE Transactions on*, vol. 49, no. 10, pp. 2636–2647, 2003.
- [66] A. Edelman, "Eigenvalues and Condition Numbers of Random Matrices," 1989, MIT PhD Dissertation.
- [67] D. N. C. Tse, P. Viswanath, and L. Zheng, "Diversity-multiplexing tradeoff in multiple-access channels," *IEEE Trans. on Inform. Theory*, vol. 50, no. 9, pp. 1859–1874, 2004.
- [68] L. Zheng and D. Tse, "Diversity and multiplexing: a fundamental tradeoff in multiple-antenna channels," *IEEE Trans. on Inform. Theory*, vol. 49, no. 5, pp. 1073–1096, 2003.
- [69] P. Elia, K. Kumar, S. Pawar, P. Kumar, and H. Lu, "Explicit Space-Time Codes Achieving The Diversity-Multiplexing Gain Tradeoff," *Arxiv preprint cs.IT/0602054*, 2006.

- [70] A. Murugan, H. Gamal, M. Damen, and G. Caire, "A unified framework for tree search decoding: rediscovering the sequential decoder," *Information Theory, IEEE Transactions on*, vol. 52, no. 3, pp. 933–953, 2006.
- [71] K. R. Kumar, G. Caire, and A. Moustakas, "The Diversity-Multiplexing Tradeoff of Linear MIMO Receivers," in *proceedings of the IEEE Information Theory Workshop, ITW*, Lake Tahoe, CA, 2007.
- [72] D. Gore, R. Heath Jr, and A. Paulraj, "On performance of the zero forcing receiver in presence of transmit correlation," *Information Theory, 2002. Proceedings. 2002 IEEE International Symposium on*, 2002.
- [73] E. Biglieri, J. Proakis, S. Shamai, and D. di Elettronica, "Fading channels: information-theoretic and communications aspects," *IEEE Trans. on Inform. Theory*, vol. 44, no. 6, pp. 2619–2692, 1998.
- [74] P.Bender, P.Black, M.Grob, R.Padovani, N.Sindhushayana, and A.Viterbi, "CDMA/HDR: A bandwidth-efficient high-speed wireless data service for nomadic users," *IEEE Commun. Mag.*, vol. 38, pp. 70–77, July 2000.
- [75] A. Lapidoth, "On the Asymptotic Capacity of Stationary Gaussian Fading Channels," *IEEE Trans. on Inform. Theory*, vol. 51, no. 2, p. 437, 2005.
- [76] B. Banister and J. Zeidler, "Feedback assisted stochastic gradient adaptation of multiantenna transmission," *IEEE Trans. on Wireless Commun.*, vol. 4, pp. 1121–1135, 2005.
- [77] J. Roh and B. Rao, "Efficient feedback methods for mimo channels based on parameterization," *IEEE Trans. on Wireless Commun.*, vol. 6, pp. 282–292, 2007.
- [78] T. Cover and J. Thomas, *Elements of Information Theory*. John Wiley, New York, 2005.